Vol. 295, No. 3, September 20, 1994
Completing Volume 295

ISSN 0003-2670

ANALYTICA CHIMICA ACTA

An international journal devoted to all branches of analytical chemistry

ELSEVIER

ANALYTICA CHIMICA ACTA

Scope. *Analytica Chimica Acta* publishes original papers, rapid publication letters and reviews dealing with every aspect of modern analytical chemistry. Reviews are normally written by invitation of the editors, who welcome suggestions for subjects. Letters can be published within **four months** of submission. For information on the Letters section, see inside back cover.

Submission of Papers

Americas

Prof. Harry L. Pardue
Department of Chemistry
1393 BRWN Bldg, Purdue University
West Lafayette, IN 47907–1393
USA

Tel:(+1-317) 494 5320
Fax:(+1-317) 496 1200

Computer Techniques

Prof. J.T. Clerc
Universität Bern
Pharmazeutisches Institut
Baltzerstrasse 5, CH-3012 Bern
Switzerland

Tel:(+41-31) 6314191
Fax:(+41-31) 6314198

Prof. Sarah C. Rutan
Department of Chemistry
Virginia Commonwealth University
P.O. Box 2006
Richmond, VA 23284-2006
USA
Tel:(+1-804) 367 7517
Fax:(+1-804) 367 8599

Other Papers

Prof. Alan Townshend
Department of Chemistry
The University
Hull HU6 7RX
Great Britain

Tel:(+44-482) 465027
Fax:(+44-482) 466410

Prof. Willem E. van der Linden
Laboratory for Chemical Analysis
Department of Chemical Technology
Twente University of Technology
P.O. Box 217, 7500 AE Enschede
The Netherlands
Tel:(+31-53) 892629
Fax:(+31-53) 356024

Prof. Paul Worsfold
Dept. of Environmental Sciences
University of Plymouth
Plymouth PL4 8AA
Great Britain

Tel:(+44-752) 233006
Fax:(+44-752) 233009

Submission of an article is understood to imply that the article is original and unpublished and is not being considered for publication elsewhere. *Anal. Chim. Acta* accepts papers in English only. There are no page charges. Manuscripts should conform in layout and style to the papers published in this issue. See inside back cover for "Information for Authors".

Publication. *Analytica Chimica Acta* appears in 16 volumes in 1994 (Vols. 281–296). *Vibrational Spectroscopy* appears in 2 volumes in 1994 (Vols. 6 and 7). Subscriptions are accepted on a prepaid basis only, unless different terms have been previously agreed upon. It is possible to order a combined subscription (*Anal. Chim. Acta* **and** *Vib. Spectrosc.*).
Our p.p.h. (postage, packing and handling) charge includes surface delivery of all issues, except to subscribers in the U.S.A., Canada, Australia, New Zealand, China, India, Israel, South Africa, Malaysia, Thailand, Singapore, South Korea, Taiwan, Pakistan, Hong Kong, Brazil, Argentina and Mexico, who receive all issues by air delivery (S.A.L.–Surface Air Lifted) at no extra cost. For Japan, air delivery requires 25% additional charge of the normal postage and handling charge; for all other countries airmail and S.A.L. charges are available upon request.

Subscription orders. Subscription prices are available upon request from the publisher. Subscription orders can be entered only by calendar year and should be sent to: Elsevier Science B.V., Journals Department, P.O. Box 211, 1000 AE Amsterdam, The Netherlands. Tel: (+31-20) 5803 642, Telex: 18582, Telefax: (+31-20) 5803598, to which requests for sample copies can also be sent. Claims for issues not received should be made within six months of publication of the issues. If not they cannot be honoured free of charge. Readers in the U.S.A. and Canada can contact the following address: Elsevier Science Inc., Journal Information Center, 655 Avenue of the Americas, New York, NY 10010, U.S.A. Tel: (+1-212) 633 3750, Telefax: (+1-212) 633 3990, for further information, or a free sample copy of this or any other Elsevier Science journal.
Advertisements. Advertisement rates are available from the publisher on request.

US mailing notice – Analytica Chimica Acta (ISSN 0003-2670) is published 3 times a month (total 48 issues) by Elsevier Science B.V. (Molenwerf 1, Postbus 211, 1000 AE Amsterdam). Annual subscription price in the USA US$ 3035.75 (valid in North, Central and South America), including air speed delivery. Second class postage paid at Jamaica, NY 11431. *USA Postmasters*: Send address changes to Anal. Chim. Acta, Publications Expediting, Inc., 200 Meacham Av., Elmont, NY 11003. Airfreight and mailing in the USA by Publication Expediting.

ANALYTICA CHIMICA ACTA

An international journal devoted to all branches of analytical chemistry

(Full texts are incorporated in CJELSEVIER, a file in the Chemical Journals Online database available on STN International; Abstracted, indexed in: Aluminum Abstracts; Anal. Abstr.; Biol. Abstr.; BIOSIS; Chem. Abstr.; Curr. Contents Phys. Chem. Earth Sci.; Engineered Materials Abstracts; Excerpta Medica; Index Med.; Life Sci.; Mass Spectrom. Bull.; Material Business Alerts; Metals Abstracts; Sci. Citation Index)

VOL. 295 NO. 3 CONTENTS SEPTEMBER 20, 1994

ELSEVIER

Analytica Chimica Acta 295 (1994) 221–231

ANALYTICA CHIMICA ACTA

Simulation of ^{13}C nuclear magnetic resonance spectra of tetrahydropyrans using regression analysis and neural networks

Deborah L. Clouser, Peter C. Jurs *

Department of Chemistry, The Pennsylvania State University, 152 Davey Laboratory, University Park, PA 16802, USA

Received 10 January 1994; revised manuscript received 13 April 1994

Abstract

The ^{13}C NMR spectra of tetrahydropyrans are simulated directly from their molecular structures. A set of 29 tetrahydropyrans is used as a training set to generate regression equations and to train neural networks, and three additional compounds are used as a cross-validation set. The results of simulations done by regression analysis are found to be extremely sensitive to molecular geometries. To account for this, two different methods of descriptor manipulation, an averaging method and a Boltzmann-weighted averaging method, are introduced, and the models generated from the descriptor sets are compared. The results for the Boltzmann-weighted averaging method are found to be better than those based on descriptors derived from only the lowest energy conformation.

Keywords: Nuclear magnetic resonance spectrometry; Neural networks; Simulation spectra; Tetrahydropyrans

1. Introduction

Tetrahydropyrans are an interesting group of compounds which are present in carbohydrates, as well as many other naturally occurring compounds [1]. By simulating the ^{13}C NMR spectra of these compounds, their spectra can be constructed and compared to the observed spectra.

One method of simulating ^{13}C NMR spectra is through the use of empirical modeling. This method utilizes linear models derived from a set of compounds whose chemical shifts are known. These models relate the chemical shift of a carbon atom to a set of atom-based descriptors through the following equation

$$S = b_0 + b_1X_1 + b_2X_2 + \cdots + b_nX_n$$

where S is the chemical shift of a carbon atom, b_n is the coefficient determined by multiple linear regression, and X_n is the value of the descriptor. Once these models have been developed, they can be used to predict chemical shifts for carbon atoms not used in their development.

Computational neural networks can also be used to predict the shifts of the individual carbon atoms. This work uses fully-connected, feed-forward neural networks. Such networks are usually trained by the back-propagation method [2], but here we use a quasi-Newton training method based on the work of Broyden [3,4], Fletcher

* Corresponding author.

SSDI 0003-2670(94)00191-N

[5,6], Goldfarb [7] and Shanno [8] because previous comparisons have shown this method to be faster and to provide superior results. The neural networks used here have one output neuron to predict the ^{13}C NMR shift of a carbon atom quantitatively. Such networks implement a model-free non-linear fitting process with some similarities to traditional non-linear regression. The networks used here are model-free because descriptors used in linear regression are used as inputs to determine the shifts with neural networks. This method does not require that a model be chosen beforehand. Neural networks as described here and trained with the quasi-Newton algorithm will be called neural networks in the remainder of this paper.

In previous empirical modeling studies of ^{13}C NMR chemical shifts, descriptors for each carbon atom in the data set have been calculated solely from the molecular conformation with the lowest strain energy. This paper presents results obtained by using more accurate encoding of the structural environment of the carbons by calculating the descriptors for more than one molecular conformation, and using one of two new methods to manipulate the resulting descriptors. These two new methods are a simple averaging method and a Boltzmann-weighted averaging method. The descriptors thus generated represent the carbon atom's structural environment more accurately, and they lead to superior ^{13}C NMR spectral simulation models.

2. Experimental

The ^{13}C NMR spectra for the 32 tetrahydropyran compounds were obtained from the Chemical Concepts database (Weinheim, Germany). The spectra for all of these compounds can be found in Ref. [9]. The software used was incorporated as part of the ADAPT software system [10,11]. This software is installed on a Sun 4/110 workstation operating at the Pennsylvania State University. The neural network software used consisted of the neural network described above, including a quasi-Newton algorithm, all run on a DEC 3000 AXP 500 workstation with field test software.

3. Results and discussion

3.1. Data set characterization

The 32 tetrahydropyrans compounds used for this study are listed in Table 1. Compounds 1–29 were used as a training set, and 30–32 were used as an external prediction set to test the external predictive ability of the equations generated by regression analysis. The three compounds in the cross-validation set were randomly chosen. One notable feature of this data set is that the shifts

Table 1
Tetrahydropyrans used in the study

Number	Compound
1	2-Methyltetrahydropyran
2	4-Methyltetrahydropyran
3	Tetrahydropyran
4	*cis*-3,5-Dimethyltetrahydropyran
5	3,3-Dimethyltetrahydropyran
6	*trans*-2,4-Dimethyltetrahydropyran
7	*cis*-2,4-Dimethyltetrahydropyran
8	3-Methyltetrahydropyran
9	*cis*-2,3-Dimethyltetrahydropyran
10	*cis*-2,5-Dimethyltetrahydropyran
11	*cis*-3,4-Dimethyltetrahydropyran
12	*trans*-2-Ethyl-6-methyltetrahydropyran
13	*trans*-2,3-Dimethyltetrahydropyran
14	*trans*-2,5-Dimethyltetrahydropyran
15	*trans*-3,4-Dimethyltetrahydropyran
16	*cis*-2,6-Dimethyltetrahydropyran
17	*trans*-2,6-Dimethyltetrahydropyran
18	2,2-Dimethyltetrahydropyran
19	4,4-Dimethyltetrahydropyran
20	3,3,5-Trimethyltetrahydropyran
21	*R*-2,*cis*-3,*trans*-5-Trimethyltetrahydropyran
22	*R*-2,*trans*-3,*trans*-5-Trimethyltetrahydropyran
23	*R*-2,*trans*-3,*cis*-5-Trimethyltetrahydropyran
24	*R*-3,*cis*-4,*cis*-5-Trimethyltetrahydropyran
25	*R*-3,*trans*-4,*cis*-5-Trimethyltetrahydropyran
26	*R*-3,*cis*-4,*trans*-5-Trimethyltetrahydropyran
27	*trans*-2-Ethylmethyltetrahydropyran
28	*cis*-2-Ethyl-5-methyltetrahydropyran
29	*cis*-2-Ethyl-6-methyltetrahydropyran
30	*trans*-3,5-Dimethyltetrahydropyran
31	2,2,6-Trimethyltetrahydropyran
32	2-Ethyltetrahydropyran

fall into two groups. One group, the atoms not bonded directly to an oxygen, has shifts ranging from 5.07 ppm to 46.06 ppm. The second group, the atoms that are bonded directly to an oxygen, has shifts ranging from 63.43 ppm to 80.21 ppm. Even though the spread of the shifts is large at 75 ppm, the whole set of carbon atoms was treated as one data set, and it was not necessary to divide them into subsets in this work.

3.2. Structure entry

Two-dimensional coordinates were provided by the Chemical Concepts database for each compound. These coordinates were read into ADAPT, and then the structures were placed in their lowest strain energy three-dimensional conformation with most large groups being equatorial. The strain energy for each compound was minimized using standard molecular mechanics techniques as implemented in MM2 [12,13].

3.3. Unique carbon atom perception

Once the compounds had been entered and modeled, the unique carbon atoms from each compound were identified. This is done to avoid biasing the data for a certain type of carbon. In this study, the training set is comprised of the 182 unique carbon atoms of compounds 1–29, and the cross-validation set is comprised of the 19 unique carbon atoms of compounds 30–32.

3.4. Descriptor calculation

Descriptors are numerical representations of the environment surrounding each carbon atom and are calculated directly from the molecular structures. Using only the 201 unique atoms, more than 180 descriptors were calculated to encode the various topological, geometrical and electronic features found within the data set. To insure that only meaningful descriptors were used in regression analysis, descriptors with a high pairwise correlation, $r > 0.95$, were removed, as were descriptors whose values were more than 80% identical. Only 65 descriptors remained after this screening process.

3.5. Multiple regression analysis

The remaining descriptors were analyzed using leaps-and-bounds regression [14], and a 9-descriptor equation was found to yield the best results. The descriptors, statistics, and coefficients of this model are reported in the top section of Table 2. The standard error for this model is 1.37 ppm. This is somewhat above the 1.00 ppm that is typically desired in order to generate quality spectra. The 19 carbon atoms of the external prediction set were predicted with a standard error of 2.49 ppm. This value is larger than desirable, and it has been influenced by several substantial outliers.

One measure of the quality of the simulated spectra is to use the spectra as queries for library searching. When this was done against a large library, the spectra generated by this model were accurate enough that number one matches were found for all compounds. That is, the authentic spectra were retrieved as best matches to the query spectra. However, the scores, which are a measure of the quality of the spectra, were poor.

Of the 9 descriptors in the equation, ICON and TCON are topological, TOCG, MPCG, and CHCG are electronic, and HHI3, COEL, and COET are geometrical. The definitions for these descriptors are presented in Table 2. CHCG, which is the extended Hückel charge on the carbon center, is the descriptor that provides the most information about the atoms in the data set. This is because in this data set, the factor that has the most influence on the chemical shift is the distance from the oxygen atom, which is a strong deshielding atom. This distance is reflected by the value of the descriptor.

This model produces one badly fit shift, the methyl substituent at the three position of compound **24**, which has a reported shift of 5.07 ppm. There are other similar compounds in the data set, but the shift of the methyl carbon at the three position in these similar compounds is higher by almost 10 ppm. Many of the earlier models had tremendous difficulty in predicting this shift accurately. The shift is correct as reported, but the value is just different enough from the atoms in similar environments that the

model had problems predicting it. This model predicts the shift at 7.88 ppm, which was the best result for any regression model. The residual error for this atom is one of the largest, and contributes to the overall error of this model being higher than 1.00 ppm.

The presence of geometrical descriptors in the model indicates that the geometry of the molecule is an important determinant of the chemical shift for these tetrahydropyrans. This led to testing of the sensitivity of this model to the different conformations that tetrahydropyrans can assume. A similar test had been performed with a set of cyclopentanones, which is another set of compounds that can assume more than one conformation [15]. To perform the test for the tetrahy-

Table 2
Regression equations, statistics and results

Descriptor [a]	Mean	S.D. [b]	Coefficient	Mean effect [c] (ppm)
Low regression model				
ICON 1	0.956	0.307	−4.70 ± 0.64	−4.49 ± 0.61
TCON3	3.32	0.609	3.71 ± 0.34	12.3 ± 1.1
TOCG3	0.193	0.133	−12.1 ± 1.7	−2.33 ± 0.32
MPCG 1	0.00347	0.0478	−32.6 ± 6.4	−0.113 ± 0.022
HHI3 2	0.132	0.0809	44.2 ± 2.9	5.83 ± 0.38
CHVD 1	0.172	0.201	10.7 ± 1.0	1.84 ± 0.17
CHCG 1	0.107	0.230	87.8 ± 0.94	9.39 ± 0.10
COEL 1	0.0441	0.106	8.30 ± 1.5	0.366 ± 0.066
COET 1	0.873	1.05	4.67 ± 0.33	4.08 ± 0.29
Intercept			11.6	
	$n = 182$		$s = 1.37$ ppm	$r = 0.998$
	$n = 19$		$s = 2.49$ ppm	$r = 0.997$
Average regression model				
ACNC 2	0.0397	0.0504	−62.6 ± 9.9	−24.8 ± 3.9
ICON 1	0.956	0.0307	−35.7 ± 1.8	−34.1 ± 1.7
ACON 2	0.448	0.0459	55.1 ± 10.6	24.6 ± 4.7
NTCG 1	0.139	0.161	−88.1 ± 3.9	122 ± 0.5
WAC2 1	0.264	0.138	−96.6 ± 6.8	25.5 ± 1.8
HHI3 2	0.122	0.0754	65.8 ± 5.0	8.02 ± 0.61
TTBS 1	2.59	2.16	−1.14 ± 0.22	−2.99 ± 0.57
LTBS 1	0.922	0.606	6.38 ± 0.65	5.88 ± 0.60
TOTA 1	0.412	0.737	4.06 ± 0.47	1.67 ± 0.19
COET 1	0.00908	0.0424	28.8 ± 7.3	0.261 ± 0.066
Intercept			23.3	
	$n = 182$		$s = 1.91$ ppm	$r = 0.996$
	$n = 19$		$s = 4.14$ ppm	$r = 0.992$
Boltzmann regression model				
MNAC3	−0.133	0.118	622 ± 1.8	−0.83 ± 0.23
MPCG 1	−0.00347	0.0478	−23.4 ± 7.0	0.0812 ± 0.024
HHI3 2	0.131	0.0804	66.5 ± 2.8	8.71 ± 1.14
CHVD 1	0.171	0.196	9.23 ± 1.5	1.58 ± 0.25
CXVD 1	0.280	0.228	5.92 ± 0.97	1.66 ± 0.27
STAS 1	0.487	0.353	−1.32 ± 0.41	−0.642 ± 0.20
STBS 1	0.286	0.384	1.45 ± 0.35	0.358 ± 0.10
TOTB 1	0.630	0.618	−1.13 ± 0.37	−0.712 ± 0.23
CHCG 1	0.108	0.232	87.1 ± 1.1	9.41 ± 0.12
COET 1	0.873	0.232	4.79 ± 0.38	4.18 ± 0.33
Intercept			14.7	
	$n = 182$		$s = 1.53$ ppm	$r = 0.998$
	$n = 19$		$s = 3.53$ ppm	$r = 0.994$

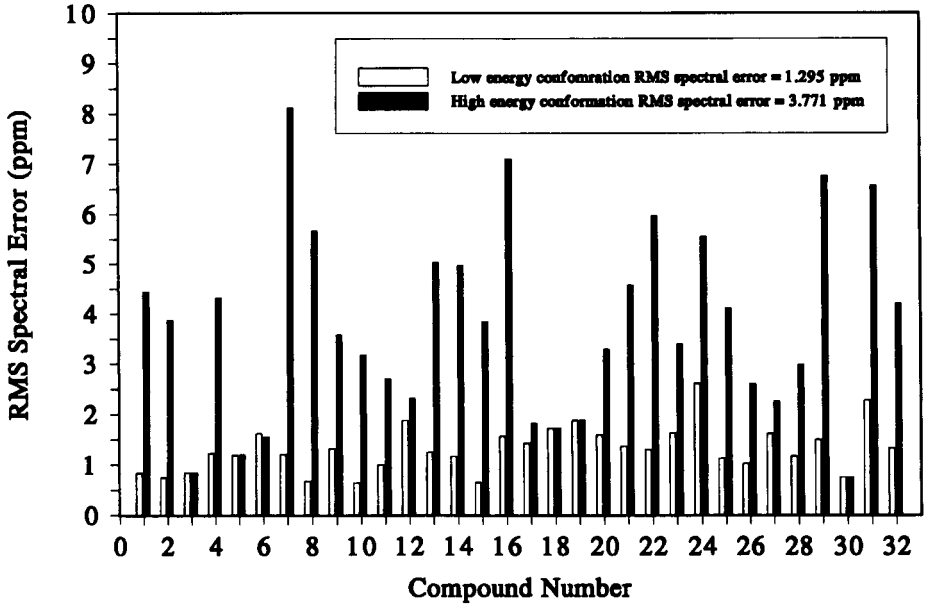

Fig. 1. Results of the test performed to determine the sensitivity of the low energy regression equation to different geometries.

dropyrans, all of the molecules that were originally entered in the lowest strain energy conformation needed to be generated in their ring-flipped, or high strain energy, conformations. This was done by drawing a six-membered ring that was inverted compared to the low energy conformation and then adding the side chains in their appropriate positions. These rings were then energy minimized in their new conformations using MM2. Once these conformations were minimized, the descriptors that appeared in the best regression equation were calculated for these conformations. These new descriptor values were then used with the regression equation and the

Notes to table 2:

[a] Descriptor definition ("heavy atom" denotes all non-hydrogen atoms). ICON 1, the connectivity index over bonds one bond away from the carbon center; TCON 3, the total connectivity index over bonds three bonds away from the carbon center; TOCG 3, the sum of the absolute values of the sigma charges for carbons three bonds away from the carbon center; MPCG 1, the most positive sigma charge among heavy atoms 1 bond away from the carbon center; HHI3 2, the sum of the inverse cubed through-space distance from the hydrogens attached to the carbon center to other hydrogens four bonds away; CHVD 1, the van der Waals energy due to interactions between the carbon center and hydrogens in the molecule; CHCG 1, the extended Htickel charge on the carbon center; COEL 1, the van der Waals energy due to interactions between the carbon center and all oxygens three or more bonds away; COET 1, the van der Waals energy between the carbon center and all oxygens two or more bonds away; ACNC 2, the averaged corrected connectivity index over bonds two bonds away from the carbon center; ACON 2, the average connectivity index over bonds two bonds away from the carbon center; NTCG 1, the sum of the sigma charges one bond away from the carbon center; WAC2 1, the weighted sum of atomic charges on heavy atoms located within two bonds of the carbon center; TTBS 1, the sum of the strain associated with torsional bonds involving the carbon center; LTBS 1, the largest strain associated with a torsional bond with the carbon center, TOTA 1, the sum of the strain associated with torsional bonds involving oxygen atoms and the carbon center; MNAC 1, the most negative charge due to all heavy atoms one bond from the carbon center; CXVD 1, the van der Waals energy due to the interactions between the carbon center and other heavy atoms; STAS 1, the smallest strain associated with a torsional angle involving the carbon center; STBS 1, the smallest strain associated with a torsional bond involving the carbon center.

[b] S.D. = Standard deviation.

[c] Mean effect = the average shielding and deshielding contribution of each descriptor on the predicted chemical shift.

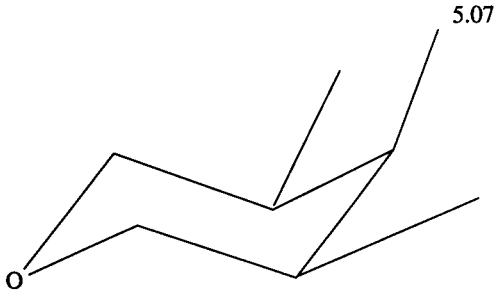

24

previous coefficients. The results of this test are found in Fig. 1. If the descriptor values were similar for both conformations, the results of the predictions would be similar. As can be seen, there is a large difference in the results obtained when using the descriptors derived from the two conformations. The low strain energy compounds had an RMS spectral error of 1.30 ppm, while the high strain energy compounds had an RMS spectral error of 3.77 ppm. This shows that the descriptor values and the regression models derived from them produce shift predictions that are very sensitive to conformational changes.

After this test was performed, the strain energies were analyzed. The strain energies were found for each compound in the low and the high energy conformation using MM2, and they are presented in Fig. 2. The difference in strain energy between the two conformations averaged 3.99 kcal/mol, with some differences as small as 0.59 kcal/mol and others as large as 25.0 kcal/mol. The strain energy value for most of the compounds in the low energy conformation is between 9 and 10 kcal/mol. Since the barrier for ring inversion is 10.3 kcal/mol [16], it can be assumed that many of these compounds were undergoing ring inversion while the ^{13}C NMR spectra were recorded. As shown by Fig. 2, the shift predictions are sensitive to different geometries, and since more than one geometry may have been present when the spectra were recorded, the regression models will not be able to give excellent results unless the different geometries are taken into account. Two methods were developed in an attempt to encode other conformations in order to improve results. These

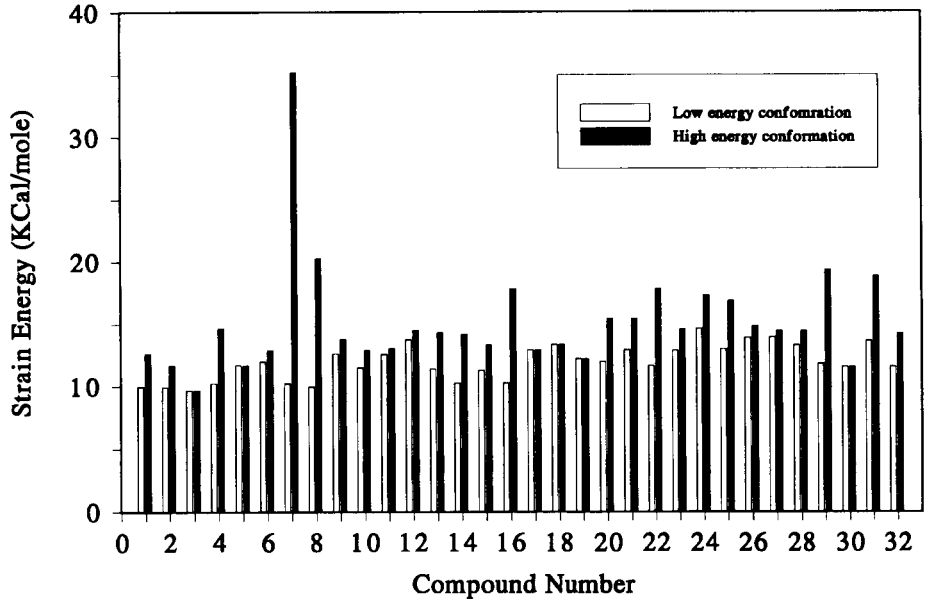

Fig. 2. Strain energies for compounds **1–32** as determined by MM2.

methods were an averaging method and a Boltzmann-weighted averaging method.

3.6. Descriptor averaging

To create descriptors that were averaged for the two conformations, geometric and electronic descriptors were calculated for both energy conformations, and these values were averaged. The topological descriptors for both conformations were the same, so only one set of those descriptor values was needed. Once calculated, all of the descriptors, including topological, were screened in a similar manner to the low energy conformation descriptors. The screening process was redone because the averaging method may have changed the descriptor values enough so that different values may be eliminated or retained as compared to the low energy conformation descriptor screening process. Even though different descriptors could have been required to predict the shifts using the averaging method, similar descriptors were found to be important.

From the remaining set of descriptors, a 10-descriptor model was found using leaps-and bounds-regression analysis. This model is shown in the center section of Table 2 along with its statistics. The model has three descriptors that are the same as the low energy conformation model: TCON, HHI3 and COET. Three additional descriptors are similar: ACNC, ACON and NTCG. One type of descriptor that appears in this model that is not present in the low energy conformation model is a descriptor that encodes torsional strain. This model contains three strain energy descriptors: TTBS, LTBS and TOTA. Since one factor that distinguishes the high energy conformation from the low energy conformation is the strain energies, these types of descriptors are expected to appear in the model. The results achieved with this method were not as good as those achieved by assuming only the low energy conformation is present, even though a number of the same descriptors are present. The low energy conformation training set yielded a standard error of 1.37 ppm, while the averaged conformation training set standard error was 1.91 ppm. The difference in error may be due to the fact that many of these compounds favor the low energy conformation, and even though they can flip into the high energy conformation, they are not in that conformation half of the time. Therefore, the averaging method used is allowing for a larger contribution from the high energy conformation than is actually present. Since three of the descriptors are the same in the low energy conformation model and averaged conformation model, but have different values, and three others are similar, it would appear that this is indeed the case. The error for the external prediction set carbon atoms has also increased for this model compared to the model developed with the descriptors for the low energy conformation.

3.7. Boltzmann-weighted averaging

The second method that was used in the attempt to more accurately encode the environments of the carbon atoms in the tetrahydropyrans was to assume a Boltzmann distribution between the high and low energy conformations. The equation used to calculate the descriptors' values comes from the Boltzmann equation

$$N_2 = N_1 e^{-\Delta E/RT}$$

In order to use the values of the descriptors in both the high and low energy conformation, the following equation is used

$$D = LEC\frac{N_1}{N_1 + N_2} + HEC\frac{N_2}{N_1 + N_2}$$

with LEC being the value of the descriptor for the low energy conformation, HEC being the value of the descriptor for the high energy conformation and D being the new value of the descriptor. Substituting for N_1 and N_2 yields the following equation

$$D = \frac{LEC}{1 + e^{-\Delta E/RT}} + \frac{HEC e^{-\Delta E/RT}}{1 + e^{-\Delta E/RT}}$$

The values of the strain energy used to determine ΔE are shown in Fig. 1. The descriptors derived with the Boltzmann-weighted scheme were screened in a similar manner to the averaged method descriptors, and for the same reasons.

From the remaining set of descriptors, a 10-descriptor model was found. This model is shown in the lower section of Table 2 along with its statistics. Of these 10 variables, HHI3, CHVD, CXVD, STAS, STBS, TOTB, and COET are geometrical. The geometry was shown to be important before, but it appears to be even more important for the Boltzmann-weighted descriptor method since a large number of geometrical descriptors are present. This may be due to the fact that the geometry determines the strain energy of the molecule, and it is the strain energy that determines the amount of time spent in the low energy conformation versus the high energy conformation. Once again, CHCG is the descriptor which appears to encode the most information about the data set. The results are not as good as the low energy conformation results, with the Boltzmann-weighted averaging method giving a standard error of 1.53 ppm. It is not immediately clear why this is so. This may be because the descriptors that were important for the model could not predict as well as the low energy conformation descriptors. The Boltzmann method does give better results than the averaged conformation method. The error for the external prediction set carbon atoms is also intermediate between those for the other two models.

3.8. Neural networks

Once regression analysis had been performed, and the best descriptors for the data set had been determined, neural networks were trained using the same data. Neural networks using quasi-Newton training were utilized for this work. The operation of these neural networks has been explained in detail elsewhere [17] so only a brief description is given here.

During training, the descriptors for each atom are presented to the network, and the network generates a predicted chemical shift for that atom. The difference between the predicted chemical shift and the known chemical shift, the error, is used to alter the adjustable weights within the network. An epoch of training has occurred when each atom in the training set has been presented to the network once. Quasi-Newton networks train faster than back propagation networks because of the way in which the weights are determined. In back propagation training, the step size is constant and is determined by the learning rate

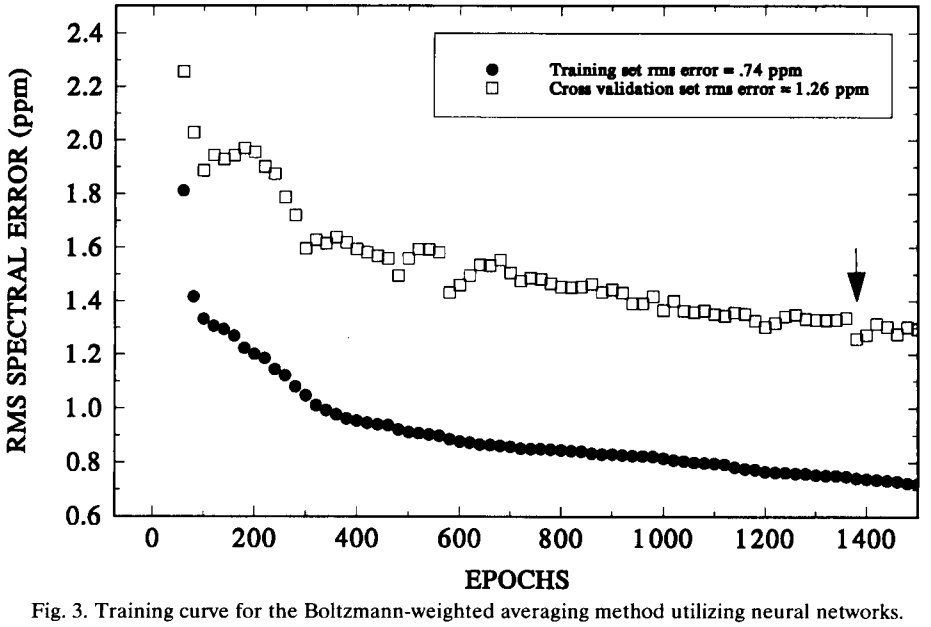

Fig. 3. Training curve for the Boltzmann-weighted averaging method utilizing neural networks.

term. This term is not present in the quasi-Newton training method. Instead, the step size is variable and is dependent on the shape of the error function for each weight. This allows the minimum error to be found much more quickly and cuts down on the training time required for quasi-Newton networks as compared to back-propagation networks. Coupling the faster algorithm with the DEC 3000 AXP 500 workstation allowed more experiments to be performed for each set of data since the training time of the networks was so small as to be negligible. The weights for the quasi-Newton method are initialized randomly (as with back propagation), but being able to train more networks means that a much larger set of random starting weights can be used, increasing the chances of finding a network with a low error.

For the low energy conformation dataset, a neural network with the architecture 9:5:1 (5 hidden layer neurons) was found to be optimum. The nine descriptors were presented to the networks in two groups: a training set and cross-validation set. This cross-validation set is comprised of the same atoms that are present in the external prediction set for linear regression. Instead of determining the external predictive ability of the model, the cross-validation set was used to help eliminate the problem of overfitting the data. When the RMS error for the cross-validation set fails to improve, the network is no longer giving results that are applicable to atoms not found in the data set, and the training is stopped. A visual example of how this is done using a training curve is shown in Fig. 3.

Neural networks have some advantages over linear regression. First the output of the network need not be linearly related to the input descriptors, so if any non-linear relationships exist in the data, these will be accounted for. Second, neural networks are model free; the data are not fit to a function that was chosen beforehand. These two advantages often lead to better results as compared to linear regression. Regression analysis continues to play a role in these studies, however. Stepwise regression and leaps-and-bounds regression provide effective means for finding informative descriptors for these studies, even though

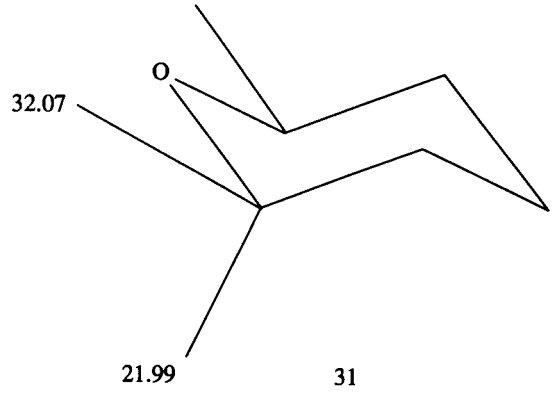

they are linear techniques. Often, the descriptors found through regression analysis, when presented to neural networks, support the development of excellent model. Using neural networks, the RMS error for the training set for the descriptors derived from low energy conformations was 0.92 ppm, with the cross-validation set RMS error being 1.21 ppm. The overall error improved, but the cross-validation set error was still above the goal of 1.00 ppm. This may be due to two shifts the neural network was unable to predict accurately.

In compound **31**, there are two atoms that at room temperature should have similar shifts but are reported as being 21.99 ppm and 32.07 ppm. Since the neural networks developed using descriptors derived from low energy conformations is reporting them as 25.07 and 31.81, the cross-validation set error is inflated somewhat due to one of these shifts.

The results from both of the alternative methods of descriptor calculation also improved. The averaged conformation results are not as accurate as the low energy conformation results, however, with the RMS error for the training set being 1.11 ppm. The results obtained with the Boltzmann-weighted averaging method, however, did improve. Recall that the error for the regression analysis using a training set of 182 atoms was 1.53 ppm and the RMS error for prediction of the 19 atoms (3 compounds) of the external prediction set was 3.53 ppm. For direct comparison, a neural network trained with this same 182-atom training

set gave an RMS error of 0.74 ppm and a cross-validation set RMS error of 1.26 ppm.

To insure that this result was not due to chance, a number of tests were run with neural networks using different, randomly-chosen training sets of 163 atoms and cross-validation sets of 19 atoms (totalling the same 182 atoms as above), with the final 19 atoms forming the prediction set. The RMS errors for the training sets ranged from 0.72 to 0.89 ppm, and the RMS errors for the cross-validation sets ranged from 0.81 to 1.31 ppm. Predictions were done on the same 19 atoms (3 compounds: **30**, **31**, **32**) with RMS errors for these true predictions ranging from 1.26 to 1.78 ppm.

Unlike regression analysis, the neural network was able to utilize the information provided by the descriptors derived from the Boltzmann-weighted averaging method. This may be because the descriptors that were found by linear regression analysis may have contained more information for non-linear relationships than for linear relationships. This effect could arise from using a linear method to determine input descriptors for a non-linear method. A plot of the predicted versus observed shifts is shown in Fig. 4. All of the shifts are predicted well, with a lone exception. This is the atom in compound **31** that is reported as being 21.99 ppm. This network predicts the shift at 26.25 ppm. The factors influencing the shift of this atom were not accurately encoded by this neural network, so the atom appears to be an outlier. However, since one of the goals of this work is to be able to simulate the entire spectrum of compound **31**, this one point cannot be disregarded.

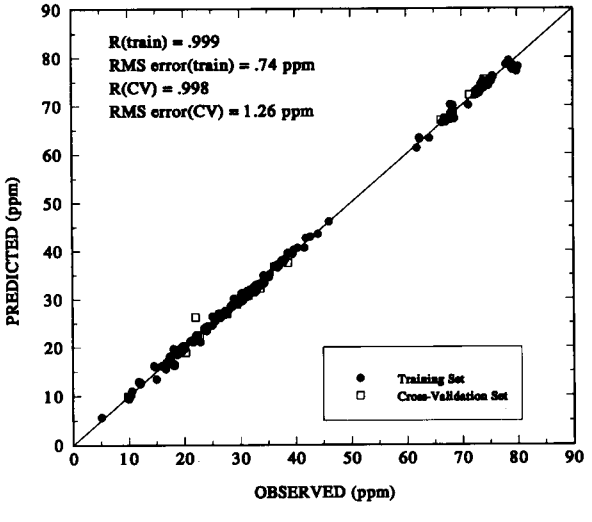

Fig. 4. Observed versus predicted shifts for the descriptors obtained by the Boltzmann-weighted averaging method utilizing neural networks.

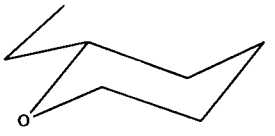

2-ethyl-tetrahydropyran

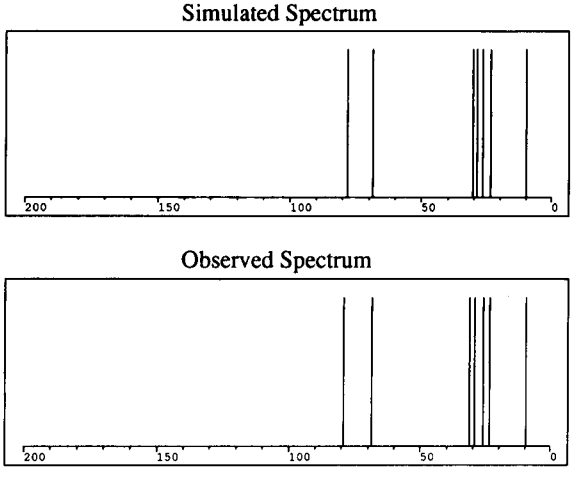

Fig. 5. Simulated and observed spectra for compound **32**.

The training curve for this method is shown in Fig. 3. The large jump at 1400 epochs is simply due to an adjustment in the weights and biases that caused a large decrease in the error of the prediction. An example of the accuracy of the neural network is shown by the comparison of an entire predicted spectrum to an observed spectrum in Fig. 5. This is compound **32**, one of the cross-validation set members. The Boltzmann-weighted averaging method with a neural network gives a predicted spectrum that is almost identical to the observed spectrum with an RMS error of only 0.68 ppm. The visual similarity be-

tween the simulated and observed spectra is striking.

Based on the improved results obtained by the Boltzmann-weighted averaging method, it is apparent that in using only the low energy conformation, the shift prediction may not always be accurate. This method may be one way of improving results; however, better methods may exist. One drawback of this method is that the assumption being made is that these compounds exist only in two conformations, specifically the ring-flipped conformations. Not taken into account are the intermediate structures. These structures may be present for only very short periods of time while the ring is flipping from one conformation to another, but they may contribute to the overall chemical shift. By not incorporating these structures, this method is not as complete as it could be, but for this data set, it gives better results than the conventional method.

4. Conclusions

Multiple linear regression analysis and quasi-Newton neural networks were used to accurately predict the chemical shifts of tetrahydropyrans. In addition, two new methods of descriptor calculation were developed and their predictive ability was demonstrated. These two new methods show that for some data sets, alternative means of descriptor calculation could be used to give better results. Though not entirely complete, the Boltzmann method could give researchers another tool to aid in the prediction of ^{13}C NMR shifts of compounds whose shifts were found to be extraordinarily sensitive to their geometries.

Acknowledgments

The authors would like to thank S.L. Dixon and J.W. Ball for their help with this project.

References

[1] P.J. Brogden, C.D. Gabbutt and D.D. Hepworth, in A.J. Boulton and A. McKillop (Eds.), Comprehensive Heterocyclic Chemistry, Vol. 4, Pergamon, New York, 1984, p. 574.
[2] J.W. Ball and P.C. Jurs, Anal. Chem., 65 (1993) 3615.
[3] C.G. Broyden, J. Inst. Maths. Appl., 6 (1970) 76.
[4] C.G. Broyden, J. Inst. Maths. Appl., 6 (1970) 222.
[5] R. Fletcher, Comput. J., 13 (1970) 317.
[6] R. Fletcher, Practical Methods of Optimization, Vol. 1, Wiley, New York, 1980.
[7] D. Goldfarb, Math. Comp., 24 (1970) 23.
[8] D.F. Shanno, Math. Comp., 24 (1970) 647.
[9] E.L. Eliel, M. Manoharan, K.M. Pietrusiewicz and K.D. Hargrave, Org. Magn. Reson., 21 (1983) 94.
[10] A.J. Stupper, W.E. Brugger and P.C. Jurs, in Computer-Assisted Studies of Chemical Structure and Biological Function, Wiley-Interscience, New York, 1979, pp. 83–90.
[11] P.C. Jurs, J.T. Cou and M. Yuan, in E.C. Olsen and R.E. Christoffersen (Eds.), Computer-Assisted Drug Design, American Chemical Society, Washington, DC, 1979, pp. 103–129.
[12] U. Burkert and N.L. Allinger, Molecular Mechanics, ACS Monograph 177, American Chemical Society, Washington, DC, 1982.
[13] T.A. Clark, A Handbook of Computational Chemistry: A Practical Guide to Chemical Structure and Energy Calculations, Wiley-Interscience, New York, New York, 1985.
[14] G.M. Furnival and R.W. Wilson, Jr., Technometrics, 16 (1971) 499.
[15] D.S. Egolf and P.C. Jurs, Anal. Chem., 59 (1987) 1586.
[16] F.G. Riddell, in The Conformational Analysis of Heterocyclic Compounds, Academic Press, New York, 1980, p. 67.
[17] L. Xu, J.W. Ball, S.L. Dixon and P.C. Jurs, Environ. Toxicol. Chem., 13 (1994) 841.

ELSEVIER

Analytica Chimica Acta 295 (1994) 233–241

ANALYTICA CHIMICA ACTA

Study of the secondary structure of proteins in aqueous solutions by attenuated total reflection Fourier transform infrared spectrometry

Jean-Marc Millot, Nadia Allam, Michel Manfait *

Laboratoire de Spectroscopie Biomoléculaire, GIBSA, UFR de Pharmacie, 51096 Reims Cedex, France

Received 17th December 1993; revised manuscript received 13th April 1994

Abstract

An approach to the determination of secondary structure content in proteins in aqueous solutions based on attenuated total reflection (ATR) Fourier transform infrared (FT-IR) spectrometry is proposed. ATR-FT-IR spectra of eleven proteins with known crystal structures were recorded. An algorithm for careful subtraction of the solvent background was developed and the reproducibility of the spectra was established for a wide range of protein concentrations in aqueous solutions. Two techniques were compared for the determination of secondary structure content [classical least-squares analysis (CLS) and partial least-squares analysis (PLS)] and optimum conditions for their utilization were suggested. The best correlation between the ATR-FT-IR approach and X-ray diffraction data was obtained with the PLS analysis and the distinction of four types of secondary structures (ordered and disordered α-helix, β-sheet and undefined conformation). The averages of the differences in the percentage content between X-ray and IR secondary structures predicted in the ATR mode are 7.1% and 2.8% for the ordered and disordered α-helix, respectively, 6.5% for the β-sheet and 4.7% for the undefined structure.

Keywords: Infrared spectrometry; Attenuated total reflection; Proteins; Secondary structure

1. Introduction

The knowledge of protein conformation has been one of the major goals in biochemistry since the importance of a structure–function relationship was postulated. However, simple experimental methods providing reliable information on protein secondary or tertiary structures and on protein conformational changes induced by internal and/or external factors are still required. Among the spectroscopic methods currently used for the determination of secondary structures of proteins and peptides (x-ray diffraction analysis, NMR, circular dichroism, Raman spectrometry), infrared spectrometry, and more particularly Fourier transform infrared (FT-IR) spectrometry, has become a prominent approach owing to the relative simplicity of this technique [1–7].

* Corresponding author.

SSDI 0003-2670(94)00181-K

However, during the last few years, the application of FT-IR spectrometry for studying protein conformation has been discussed for different reasons. These include the limitations of its application to the study of proteins in solution owing to the inherent problem of working with aqueous solutions. Subtraction of the water background is a serious problem even when using the FT-IR technique, which is much more powerful than the conventional IR method. Any imperfection in the subtraction of the very strong OH bending mode will leave a residual water spectrum (or will create negative features in the spectrum), leading to irreproducibility of the results.

The study of proteins in aqueous solutions, between two windows separated by a spacer, has proved difficult because of the reproducibility of protein spectra, particularly for protein concentrations below 20 mg ml^{-1}. Deuterium oxide has often been used as the solvent to allow the observation of the amide I and II bands of proteins [3,4,8]. However, the hydrogen–deuterium exchange, which occurs rapidly when proteins are placed in D_2O, causes spectroscopic changes and probably also conformational changes as well [9].

The above problems can be avoided by employing the FT-IR technique in combination with the attenuated total reflection (ATR) approach. There are several advantages of this method, e.g., it requires small (1 mg) amounts of materials and a reproducible path-length can be achieved. The technique has recently been applied to the study of some water-soluble and membrane-bound proteins [10]. The authors reported the ATR-FT-IR spectra and quantitative calculations of the secondary structures for some dried proteins and of the deuterated films containing these species.

In this study, the ATR technique was applied for studying the secondary structures of proteins in aqueous solution. A subtraction procedure is proposed that decreases the contribution from water without perturbing the real shape of the amide I bands. Two techniques for the determination of secondary structure content [classical least-squares analysis (CLS) and partial least-squares analysis (PLS)] were compared and optimum conditions of their utilization were established.

2. Experimental

2.1. Calibration set of water-soluble proteins

The proteins were purchased from Sigma: lysozyme (LZM) from chicken egg white, myoglobin (MGB) from horse skeletal muscle, chymotrypsinogen A (CTG) from bovine pancreas, ribonuclease A (RIB) from bovine pancreas, α-chymotrypsin (ACT) from bovine pancreas, concanavalin A (CNA) from jack bean, papain (PPN) from papaya latex, trypsin inhibitor (TPI) from soyabean, cytochrome *c* (CTC) from horse heart, avidin (AVN) from egg white and alcohol dehydrogenase (ADH) from equine liver. This set of proteins was chosen for the ATR-FT-IR experiments for the following reasons: well defined amounts of canonical types of secondary structures have been identified for all of them according to the classification of Levitt and Greer [11]; all of them have high solubility in water, enabling experiments to be carried out over a wide range of concentrations; and this set includes proteins with a high relative contribution of some of the preferential canonical types of secondary structures (e.g., myoglobin 77% of α-helix, concanavalin A 64% of β-sheet).

All proteins were of the highest purity and without excess of the salts. Stock solutions were prepared by dissolving lyophilized samples in sodium phosphate buffer (0.01 M, pH 7.2) up to a concentration of 50 mg ml^{-1} and were diluted up to the desired concentration and pH before each experiment.

2.2. Infrared spectrometry and sample preparation

ATR-FT-IR spectra were obtained using a Bomem MB100 FT-IR spectrometer equipped with a liquid nitrogen-cooled mercury cadmium telluride detector at a resolution of 4 cm^{-1}. One hundred interferograms were averaged. The spectrometer was continuously purged with dry air (Balston dry air generator) to eliminate water vapour absorption. The ATR supply was used as described [12,13]. The internal reflection element was a ZnSe ATR plate (50 × 10 × 1.5 mm; Specac GB) with aperture angle of 45°, yielding six inter-

nal reflections and maintained at a constant temperature (20 ± 0.1°C). The ZnSe crystal was chosen because there is no protein absorption on its surface [12,14], in contrast to the germanium crystals traditionally used in ATR experiments, which induce fairly strong protein–surface interactions [15].

Aqueous solutions of proteins (ca. 80 μl) with concentrations ranging from 5 to 50 mg ml^{-1} were dropped on a horizontal surface of the crystal. The solution was spread uniformly on the crystal and covered with a glass slide. With this set-up it was possible to work with aqueous solutions of proteins, whereas in some previous studies the use of dried preparations, deuterium oxide solutions or hydrated films was necessary [8,10,16].

2.3. Buffer spectrum subtraction

The following procedure for subtraction of the water and buffer background was developed and was found not to perturb the shape of the amide I band of the proteins. An absorbance $P(\nu)$ of the pure protein moiety at the wavenumber ν, without a contribution of the absorption of buffer solution $S(\nu)$, can be expected:

$$P(\nu) = T(\nu) - \alpha S(\nu) - \beta \quad (1)$$

where $T(\nu)$ are experimental values of absorbances in the ATR-FT-IR spectrum of an aqueous protein solution at the wavenumber ν and α and β are parameters of minimization. The parameters α and β were determined by the minimization of the following term:

$$\sum_{i=1720\,cm^{-1}}^{2250\,cm^{-1}} \{T(\nu_i) - [\alpha S(\nu_i) + \beta]\}^2 = \min. \quad (2)$$

The absorption of pure protein at each spectral point ν was calculated from Eq. 1 after the calculation of parameters α and β from the Eq. 2.

2.4. Secondary structure calculations

Prior to secondary structure calculations, a straight baseline passing through the ordinates at 1720 and 1480 cm^{-1} was subtracted. Spectra were then normalized to a total area of 1 in the spectral range 1480–1720 cm^{-1}.

The secondary structure calculations were performed using two algorithms, one based on the classical least-squares analysis (CLS) [17] and the other on partial least-squares analysis (PLS) [17]. Both methods required the availability of calibration sets of known compositions that consist of proteins whose x-ray structure is known.

For the CLS method, it is assumed that the protein spectra are linear combinations of p pure-structure spectra, i.e., α-helix, β-sheet, and undefined conformation:

$$\mathbf{A} = (\mathbf{C} \cdot \mathbf{K}) + \mathbf{E} \quad (3)$$

where $\mathbf{A}$ is the (m, n) matrix of the m spectra of the calibration proteins, $\mathbf{C}$ is the (m, p) matrix of the conformation fractions of the calibration proteins, $\mathbf{K}$ is the (p, n) matrix in which rows are the (p) pure-structure spectra and $\mathbf{E}$ is the (m, n) matrix of spectral errors. The calibration step of CLS analysis gives the least-squares solution of Eq. 3 that corresponds to the calculated $\hat{\mathbf{K}}$ matrix:

$$\hat{\mathbf{K}} = [\mathbf{C}' \cdot \mathbf{C}]^{-1} \cdot \mathbf{C}' \cdot \mathbf{A} \quad (4)$$

For predictions, the least-squares solution for the vector of unknown conformations $\hat{\mathbf{c}}$ is

$$\hat{\mathbf{c}} = \left[\hat{\mathbf{K}} \cdot \hat{\mathbf{K}}'\right]^{-1} \cdot \hat{\mathbf{K}} \cdot \mathbf{a} \quad (5)$$

where $\mathbf{a}$ is the spectrum of the protein to be analysed.

For the PLS method, the base vectors ($\mathbf{B}$ matrix, Eq. 6) are not the pure-component spectra, as for CLS, but loading vectors which are linear combinations of the original calibration spectra. After generation of these loading vectors, the PLS method decomposed the calibration spectra into two matrices $\mathbf{B}$ and $\mathbf{T}$:

$$\mathbf{A} = (\mathbf{T} \cdot \mathbf{B}) + \mathbf{E} \quad (6)$$

where $\mathbf{B}$ is an (h, n) matrix in which the rows represent the new base set of h full-spectrum vectors (loading vectors), $\mathbf{T}$ is an (m, h) matrix of intensities in the coordinate system of the h loading vectors and $\mathbf{E}$ is an (m, n) matrix of spectral residuals, not fitted by the PLS model. The fractions of a given conformation can be related to

the spectral intensities (T) in the new coordinate system (for more details on the mathematical procedures, see [17]).

2.5. CLS and PLS validation

To validate the calculation methods, secondary structure predictions were compared with x-ray secondary structure contents. Thus, the standard error of prediction (SEP) was estimated for each type of canonical secondary structure taken into account during the calculations:

$$SEP = \sqrt{\sum_{i=1}^{n} (y_i - y_i')^2 / n} \qquad (7)$$

where n is the number of proteins studied, y_i is the percentage content of some canonical secondary structure in the protein i calculated from the infrared data and y_i' is the percentage of the same structure determined from x-ray diffraction data for the same protein i.

3. Results and discussion

3.1. ATR-FT-IR technique and the problem of water subtraction

When IR spectrometry is used, the problem of interference between the relatively weak amide I band of proteins and the very strong O–H deformation band of water appears. To obtain a satisfactory water subtraction, a rigorous instrumental set-up is required: high signal-to-noise ratio, no changes in the characteristic line shapes, no changes in the instrumental purge flow-rate between scans and constant path-length of the IR beam through the sample during an experiment.

The path-length of the beam is the most important factor for quantitative IR studies. An uncontrolled path-length can introduce sufficient errors in calculations of secondary structure of proteins in thin layers and films. One way to solve this problem is to employ the ATR approach. An

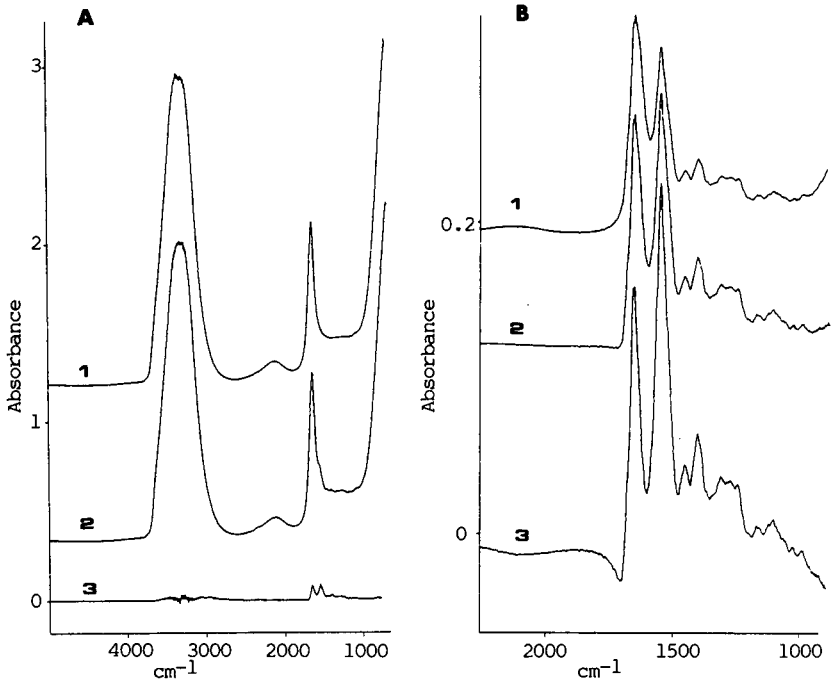

Fig. 1. (A) Subtraction process of a buffer spectrum from a protein solution spectrum. 1 = buffered solution spectrum; 2 = cytochrome c solution spectrum (50 mg ml^{-1}); 3 = cytochrome c after solvent subtraction (spectrum 2 − 0.98 × spectrum 1). (B) Influence of the subtraction coefficient α. α = (1) 0.93; (2) 0.98 (exact coefficient); (3) 1.01.

accurate path-length matching can be obtained, as the path-length in this system is defined by the number of internal reflections in the ATR crystal multiplied by the depth of penetration of the IR radiation [12,13]. When a ZnSe crystal with six internal reflections and a 0.152λ depth of penetration was used in these experiments, a highly reproducible path-length of 0.912λ (5.7 μm at 1600 cm^{-1}) could be achieved. This permits careful subtraction of the water background when the internal standard of intensity of the 2100 cm^{-1} absorption band of the water is used.

Fig. 1A shows the result (spectrum 3) of subtracting the buffer spectrum (1) from the spectrum of protein solution (2). The protein absorption is very weak compared with the buffer solution. To control the quality of subtraction, two criteria were considered: negative values of absorption must not appear and the intensities for both the 3000 and 600 cm^{-1} regions must not diverge from zero. The ATR device provides very stable experimental conditions for this algorithm of water subtraction. This can be seen from the very weak variations of the coefficient of subtraction ($\alpha = 1 \pm 0.02$), as calculated by the procedure of minimization. When this algorithm of subtraction is employed, a flat baseline between 1720 and 2250 cm^{-1} is achieved (Fig. 1B, spec-

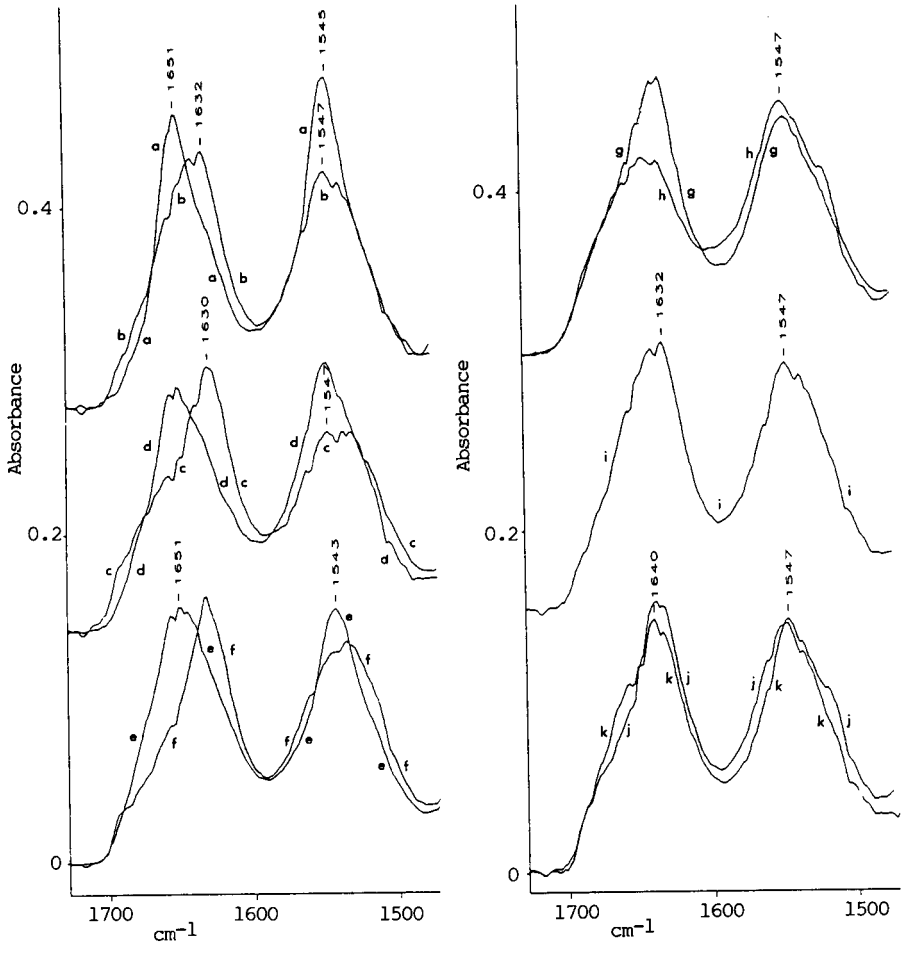

Fig. 2. Amide I and II IR bands of calibration proteins (50 mg ml^{-1}). (a) Myoglobin; (b) α-chymotrypsin; (c) avidin; (d) cytochrome *c*; (e) lysozyme; (f) concanavalin A; (g) chymotrypsinogen A; (h) papain; (i) alcohol dehydrogenase; (j) trypsin inhibitor; (k) ribonuclease A.

Table 1
Secondary structure content (%) as estimated from IR and x-ray data

Protein		Method								
		X	CLS-3	CLS-3B	CLS-4	CLS-4B	PLS-8	PLS-8B	PLS-5B	X
LZM	H	46	45	40	–	–	–	–	–	–
	Ho	–	–	–	33	28	30	30	28	24
	Hd	–	–	–	31	27	16	16	17	22
	S	19	21	22	20	21	19	18	21	19
	U	35	34	38	16	24	35	36	34	35
MGB	H	77	99	100	–	–	–	–	–	–
	Ho	–	–	–	58	58	35	35	37	53
	Hd	–	–	–	25	25	23	26	26	24
	S	0	−4	−5	−2	−1	2	5	6	0
	U	23	5	5	19	18	40	34	31	23
CTG	H	12	22	19	–	–	–	–	–	–
	Ho	–	–	–	12	10	6	6	10	7
	Hd	–	–	–	13	11	12	12	11	5
	S	49	52	51	53	53	50	46	45	49
	U	39	26	30	22	26	32	36	34	39
RIB	H	23	21	27	–	–	–	–	–	–
	Ho	–	–	–	11	16	6	10	9	11
	Hd	–	–	–	10	15	11	11	11	12
	S	46	37	38	37	38	40	40	42	46
	U	31	42	35	42	31	43	39	38	31
ACT	H	8	30	26	–	–	–	–	–	–
	Ho	–	–	–	18	14	17	9	9	3
	Hd	–	–	–	12	10	9	7	7	5
	S	55	56	54	56	53	45	54	53	55
	U	37	14	20	14	23	29	30	31	37
CNA	H	3	2	4	–	–	–	–	–	–
	Ho	–	–	–	−2	−1	8	6	5	0
	Hd	–	–	–	−2	−1	0	0	0	3
	S	64	64	66	60	61	56	55	57	64
	U	33	34	30	44	41	36	39	38	33
PPN	H	25	13	14	–	–	–	–	–	–
	Ho	–	–	–	4	5	10	9	13	13
	Hd	–	–	–	5	6	16	14	11	12
	S	29	28	28	28	28	37	42	38	29
	U	43	59	58	63	61	37	35	38	43
TPI	H	26	24	24	–	–	–	–	–	–
	Ho	–	–	–	14	14	27	27	23	12
	Hd	–	–	–	14	14	8	10	16	14
	S	45	51	51	52	51	27	30	31	45
	U	29	25	25	20	21	38	33	30	29
CTC	H	46	42	44	–	–	–	–	–	–
	Ho	–	–	–	25	26	29	26	27	27
	Hd	–	–	–	17	18	19	18	17	19
	S	15	15	14	15	14	13	16	18	15
	U	39	43	42	43	42	39	40	38	39
AVN	H	10	−2	−4	–	–	–	–	–	–
	Ho	–	–	–	−5	−6	−6	−6	−5	4
	Hd	–	–	–	5	4	6	6	6	6
	S	57	66	66	68	67	62	64	64	57
	U	33	36	38	32	35	38	36	35	33
ADH	H	30	33	32	–	–	–	–	–	–
	Ho	–	–	–	20	19	14	14	15	18
	Hd	–	–	–	15	14	13	12	11	12
	S	38	48	48	49	49	42	44	43	38
	U	32	19	20	16	18	31	30	31	32

Abbreviations: H, total helix; Ho, ordered helix; Hd, disordered helix; S, β-sheets; U, undefined structure. Method X, x-ray data from Levitt and Greer [11]. Infrared methods of prediction are described in Table 2.

trum 2). Spectra 1 and 3 (Fig. 1B) were also obtained by using different subtraction coefficients.

The criteria used in the previous FT-IR studies of proteins were mainly based on the achievement of a flat baseline in the region of 1900–1720 cm^{-1}. The subtraction was judged by eye [2] or by the use of a specially developed algorithms [1,15]. In contrast to the algorithms of subtraction employed previously, that used in this study was applied to reflection spectra from aqueous solutions, and the coefficient of subtraction was calculated in a few seconds by a unique minimization.

3.2. ATR-FT-IR spectra of the calibration set of proteins

All ATR-FT-IR spectra of water-soluble proteins with known crystal structure that were used in this study (Fig. 2) were recorded at least three times and were totally reproducible both in the shape of amide I and II bands and in the values of their absorbances (within a 1% deviation).

The amide I and II regions in the ATR-FT-IR spectra of proteins are very sensitive to their secondary structure. Fig. 2 shows the normalized spectra of aqueous solutions of myoglobin and concanavalin A (spectra a and b, respectively). These proteins have different content of canonical secondary structures. In the spectrum of myoglobin, whose conformation is mainly α-helical with no β-sheet, the Amide I and II bands in water solution are narrow, symmetrical and centered at 1651 and 1545 cm^{-1}, respectively. On the other hand, the preferential secondary structure of concanavalin A is a β-sheet and in this case the amide I and II bands are much broader and are located at ca. 1632 and 1547 cm^{-1}, respectively. Moreover, the amide I band is found to be asymmetric towards high frequencies. These differences in shape and frequencies of the amide I and II bands in aqueous solutions can be particularly used to calculate the conformation of proteins and to elucidate the changes of structure induced by protein interactions.

3.3. Secondary structure calculations for the proteins of the calibration set

To calculate the canonical secondary structure content in the proteins, the choice of the numerical method of analysis of the amide I and II bands has been shown to be very important [7]. Several methods of analysis were used in this study, including different modifications of the classical least-squares algorithm and the partial least-squares technique. For each PLS and CLS method, the secondary structures of each protein were predicted after the elimination of the corresponding spectrum from the spectra calibration set. Differences between the theoretical and pre-

Table 2
Standard errors of predictions (*SEP*, %) for the methods of secondary structure prediction

Parameter	Method						
	CLS-3	CLS – 3B	CLS-4	CLS-4B	PLS-8	PLS-8B	PLS-5B
Secondary structures	3	3	4	4	4	4	4
Baseline subtraction	No	Yes	No	Yes	No	Yes	Yes
Loading vectors (PLS)	–	–	–	–	8	8	5
SEP(%)							
α-Helix	11.2	10.8	–	–	–	–	–
Ordered α-helix	–	–	7.0	5.8	9.6	8.5	7.1
Disordered α-helix	–	–	5.0	3.7	3.9	3.4	2.8
β-Sheet	5.3	5.3	5.9	5.5	7.2	7.4	6.5
Undefined	11.5	9.6	13.4	9.7	7.8	5.8	4.7
Mean	10.0	9.1	8.8	6.8	7.5	6.6	5.6

dicted secondary structures were represented by the *SEP* coefficient in order to validate each method.

First, the amide I and II region was analysed by the CLS method as a linear combination of bands due to only three classes of structure (CLS-3 approach), viz., α-helix, β-sheet and undefined structure, or four (CLS-4) types of conformation, viz., ordered or disordered α-helix, β-sheet and undefined structure. The protocol includes the calculation of the pure-structure spectra from a set of calibration proteins and these pure-structure spectra were then used to determine the secondary structure content of proteins. More precisely, each protein was eliminated in turn from the calibration set, then the secondary structure content of the eliminated protein was predicted (table 1). To compare the accuracy of these methods, standard errors of prediction for each type of secondary structure are presented in Table 2. The best results were achieved with the CLS-4B method where four types of secondary structures were accounted for and a baseline subtraction was carried out. The average standard error of prediction was found to be less then 7%. Moreover, the α-helical content was calculated with an *SEP* of less than 6%.

In order to improve the analysis of ATR-FT-IR data, the PLS approach was also used, three different PLS methods being compared (Table 2). The PLS-8 technique distinguishes four structural types (ordered and disordered α-helix, β-sheet and undefined conformation) and uses eight first loading vectors. PLS-8B is the same technique, but is applied to the spectra after the subtraction of the baseline. PLS-5B, which was applied to baseline-subtracted spectra and used only five first loading vectors, shows the best standard errors of prediction (Table 2).

The effect of the number of loading vectors employed for the calculation of the secondary structure of lysozyme by the PLS technique was studied. Fig. 3 shows that the optimum number of loading vectors employed in this algorithm is five. Spectral data due to protein conformations were concentrated in the first loading vectors, while the last ones mainly included noise and data which are not related to the conformation of

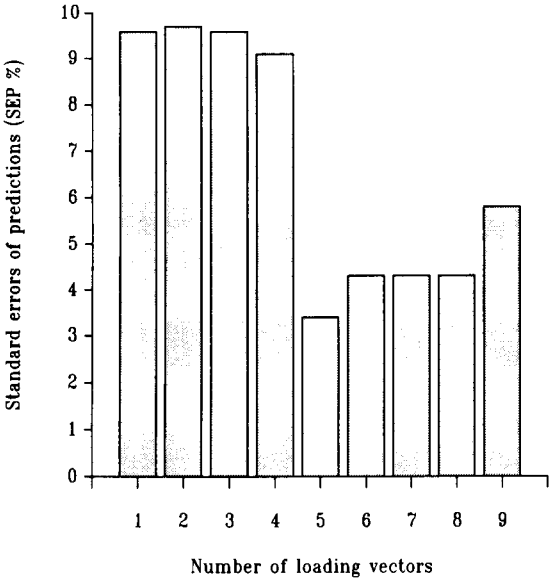

Fig. 3. Standard errors of predictions of lysozyme conformations as a function of the number of loading vectors used in the PLS method.

proteins. The PLS method allows an improvement of the secondary structure calculations as compared with the CLS technique. The standard error of prediction can be decreased from 6.8% to 5.6% when the PLS-5B instead of the CLS-4B algorithm is employed (Table 2). Other workers have described standard deviations of prediction in the same range of 5–6% [1,5]. On the other hand, the standard deviations found by Byler and Susi [3] in the range 2–4%, are better than ours. However, their method was based on the fitting of deconvoluted spectra by Gaussian functions, which required peak assignments and frequency limits of each band and may introduce additional errors.

We tested also the intra-day reproducibility of the PLS-5B secondary structure predictions for different solutions of lysozyme at concentrations of 50, 20 and 5 mg ml^{-1} (Table 3). For that, the spectrum of lysozyme was excluded from the calibration set. For 50 and 20 mg ml^{-1}, the standard deviations between results were found to be ca. 1% for each type of secondary structure. Hence

Table 3
Reproducibility of predictions: analysis of lysozyme spectra by PLS-5B method, expressed as secondary structure content [mean (%) ± standard deviation ($n = 3$)]

Lysozyme concentration (mg ml^{-1})	Ordered α-helix	Disordered α-helix	β-Sheet	Undefined structure
50	27.4 ± 0.5	16.9 ± 0.2	21.9 ± 0.6	33.8 ± 0.1
20	26.1 ± 1.0	15.7 ± 1.1	23.1 ± 0.8	35.1 ± 1.4
5	26.5 ± 2.5	16.7 ± 1.4	20.8 ± 1.8	36.0 ± 2.9

the reproducibility is mostly sufficient to display a variation of the secondary structure content that is induced by a ligand. Moreover, the standard deviations of predictions increased to 3% when ATR-FT-IR spectra from more dilute (5 mg ml^{-1}) protein solutions were recorded. To display a significant variation of the protein conformation at 5 mg ml^{-1}, it would be necessary to repeat the FT-IR measurements.

4. Conclusion

Circular dichroism and Raman spectrometry are other spectroscopic methods that can also be used to determine the secondary structure of proteins. In contrast to IR spectrometry, circular dichroism requires a knowledge of the protein concentration. Moreover, such determinations could be perturbed by aromatic amino acids [6]. Comparable *SEP* values have also been obtained by Raman spectrometry [18–20]. However, the Raman spectrum of a protein–ligand complex was difficult to obtain with a good signal-to-noise ratio, because of interference with the fluorescence emission from the ligand or with the Rayleigh scattered light from a polymerized protein. In contrast, IR spectra are not perturbed by scattering and fluorescence from the sample, and represents a practical method for predicting secondary structures of proteins in interaction with a ligand [21–23]. From the present results, the use of an ATR optical system contributes to obtaining good reproducibility of these predictions, even for more dilute protein solutions.

Acknowledgement

The authors are grateful to Professor I. Nabiev for helpful discussions and for revising the manuscript.

References

[1] F. Dousseau and M. Pezolet, Biochemistry, 29 (1990) 8771.
[2] D.C. Lee, P.I. Haris, D. Chapman and R.C. Mitchell, Biochemistry, 29 (1990) 9185.
[3] D.M. Byler and H. Susi, Biopolymers, 25 (1986) 469.
[4] D.F. Kennedy, A.J. Slotboom, G.H. De Haas and D. Chapman, Biochim. Biophys. Acta, 1040 (1990) 317.
[5] A. Dong, P. Huang and W.S. Caughey, Biochemistry, 29 (1990) 3303.
[6] R.W. Sarver and W.C. Krueger, Anal. Chem., 194 (1991) 89.
[7] J.L.R. Arrondo, A. Muga, J. Castresana and F.M. Goni, Prog. Biophys. Mol. Biol., 59 (1993) 23.
[8] G. Zuber, S.J. Prestrelski and K. Benedek, Anal. Biochem., 207 (1992) 150.
[9] I.R. Nabiev, K.N. Dzhandzhugazyan, R.G. Efremov and N.N. Modyanov, FEBS Lett., 236 (1988) 235.
[10] E. Goormaghtigh, V. Cabiaux and J.M. Ruysschaert, Eur. J. Biochem., 193 (1990) 409.
[11] M. Levitt and J. Greer, J. Mol. Biol., 114 (1977) 181.
[12] K.J. Payne and A. Veis, Biopolymers, 27, 1749 (1988).
[13] P.R. Griffiths and J. Haseth, in P.J. Elving and J.D. Winefordner (Eds.), Fourier Transform Infrared Spectrometry, Chemical Analysis Vol. 83, Wiley, New York, 1986, pp. 191–194.
[14] S.B. Dev, C. Rha and F. Walder, J. Biomol. Struct. Dyn., 2 (1984) 431.
[15] J.R. Powell, F.M. Wasacz and R.J. Jakobsen, Appl. Spectrosc., 40 (1986) 339.
[16] R.J. Jakobsen and F.M. Wasacz, Appl. Spectrosc., 44 (1990) 1478.
[17] D.M. Haaland and D.M. Thomas, Anal. Chem., 60 (1988) 1193.
[18] R.W. Williams, J. Mol. Biol., 166 (1983) 581.
[19] M.B. Bussian and C. Sanders, Biochemistry, 28 (1989) 4271.
[20] M. Berjot, M. Marx and A.J.P. Alix, J. Raman Spectrosc., 18 (1987) 289.
[21] M.C. Levy, S. Lefebvre, M. Rahmouni, M.C. Andry and M. Manfait, J. Pharm. Sci., 80 (1991) 1.
[22] J.M. Le Gal and M. Manfait, Biochim. Biophys. Acta, 1041 (1990) 257.
[23] N. Allam, J.-M. Millot, D. Leynadier, V. Peyrot, C. Briand, F. Breillout and M. Manfait, in T. Theophanides, et al. (Eds.), Fifth International Conference on the Spectroscopy of Biological Molecules, Kluwer, Dordrecht, 1993, pp. 149–150.

ELSEVIER

Analytica Chimica Acta 295 (1994) 243–251

ANALYTICA CHIMICA ACTA

Lactate, glutamate and glutamine biosensors based on rhodinised carbon electrodes

S.F. White [a], A.P.F. Turner [a,*], U. Bilitewski [b], R.D. Schmid [b], J. Bradley [b]

[a] *Cranfield Biotechnology Centre, Cranfield University, Cranfield, Bedford MK43 0AL, UK*
[b] *GBF, Gesellschaft fur Biotechnologische Forschung mbH, Mascheroder Weg 1, D-3300 Braunschweig, FRG*

Received 20th December 1993; revised manuscript received 14th March 1994

Abstract

Amperometric enzyme sensors for lactate, glutamate and glutamine were constructed using rhodinised carbon electrodes. All three sensors operated at a potential of +400 mV (Ag/AgCl). Lactate sensors were constructed using lactate oxidase immobilized in hydroxyethylcellulose, overlaid with a cellulose acetate membrane. Using a flow-injection system, the sensors had a linear range of 0.1 to 1.5 mM. Measurements of lactate concentrations from a mammalian cell culture were compared with results obtained from a commercial instrument. A correlation coefficient of $r = 0.982$ ($n = 15$) was obtained. Glutamate and glutamine sensors were fabricated based on glutaraldehyde immobilization; the former by incorporating glutamate oxidase and the latter based on glutamate oxidase and glutaminase (both had a linear range of 0.1 to 1.5 mM). The feasibility of using these sensors, in conjunction with a previously described glucose sensor, for mammalian cell culture monitoring is discussed

Keywords: Biosensors; Lactate; Glutamate; Glutamine; Rhodinised carbon electrodes

1. Introduction

One versatile approach to the construction of amperometric biosensors has been the use of a Clark oxygen electrode, e.g., [1,2] to detect changes in oxygen concentration resulting from either cellular or enzymatic action. An alternative method has been to monitor the oxidation of enzymatically generated H_2O_2, using either platinum or carbon electrodes, e.g., [3,4]. Despite the widespread use of both methods, there are several drawbacks that impair the efficient operation of biosensors based on these configurations. Principally, the relatively large potential required to detect H_2O_2 can lead to electrochemical interferences from other compounds present in the sample solution. Furthermore, fluctuations in the local oxygen concentration (not occurring as a result of the immobilised biological component) can lead to inaccuracies for sensors based on O_2 detection, and low oxygen tension can impair the operation of both types of sensor.

To overcome the limitation imposed by the requirement for a high potential to detect H_2O_2, metallised carbon electrodes have been investigated [5]. Generally these sensors have operated

* Corresponding author.

SSDI 0003-2670(94)00186-P

at a low potential and have been used to detect several analytes of interest (e.g., H_2O_2, glucose and lactate). For most of these applications, platinum has been the preferred choice of metal.

Lactate sensors were described by Hajizadeh et al. [6], using lactate oxidase immobilised in poly(vinyl alcohol) over platinised carbon electrodes. These sensors were able to detect H_2O_2 at +300 mV vs. Ag/AgCl. The linear range of these electrodes was from 26 μM to 1.7 mM and the sensitivity extended up to 2.94 mM. Mullen [7] described the construction of lactate sensors based on the inclusion of platinised carbon granules, lactate oxidase and hydroxyethylcellulose in an aqueous paste. Using a two electrode cell, a range of lactate concentrations was measured at +400 mV. From the graph shown by the author, the linearity of these sensors appeared to extend up to 20 mM lactate.

Recent reports [8–10] have described the use of rhodium (as a metal catalyst) dispersed over a carbon substrate. Glucose sensors were successfully constructed and operated at a significantly lower potential. We report here the use of rhodinised electrodes in the construction of enzyme sensors (lactate, glutamate and glutamine) for use in mammalian cell culture monitoring.

2. Experimental

2.1. Materials

Spectroscopic graphite rods (6 mm diameter) were obtained from Ringsdorff (Godesberg, Germany). Rhodium (1000 ppm atomic absorption standard solution) was obtained from Aldrich (Steinheim). Cellulose acetate and hydroxyethylcellulose (middle viscosity) were both obtained from Fluka (Neu-Ulm). Glutaraldehyde (25% w/v) and bovine serum albumin (BSA) were both purchased from Sigma (Heindenheim).

Enzymes

Lactate oxidase (EC 1.1.3.2) from *Pedicoccus sp.* (35 units mg^{-1}) and glutaminase (EC 3.5.1.2) grade II from *E. coli* (5.4 units mg^{-1}) were obtained from Sigma. Glutamate oxidase (EC 1.4.3.11) from *Streptomyces sp.* X119-6 (7.7 units mg^{-1}) was a kind gift from Dr. Kusakabe (Yamasa Shoyu Co., Chiba, Japan).

2.2. Methods

All of the electrodes used were cleaned and electroplated according to the method described earlier [9]. For the lactate sensors, lactate oxidase (3 mg) was dissolved in 60 μl of a 1% hydroxyethylcellulose (HEC) solution (prepared in phosphate buffer). An aliquot (15 μl) was applied to the face of each electrode and left to dry for 2 h at room temperature. After drying, an outer cellulose acetate membrane (prepared from a 1% w/v cellulose acetate solution in acetone) was cast by dip-coating 15 μl of the solution over the enzyme layer. The solvent was allowed to evaporate at room temperature and the completed sensors were stored at 4°C until required.

Glutamate sensors were constructed based on the immobilisation of the enzyme using glutaraldehyde. A number of glutamate sensors have been constructed using this method [10–12] and the approach adopted was based on the results of these reports. An enzyme immobilization solution was prepared by dissolving 0.5 mg of glutamate oxidase and 3 mg of BSA in 30 μl of a 0.1 M sodium phosphate buffer solution (pH 7.0). After mixing, 10 μl of a 2.5% glutaraldehyde solution were added. Following a second mixing the solution was left to stand for 30 min at room temperature. An aliquot (15 μl) of this solution was placed on the surface of the rhodinised electrode. After 30 min the sensor face was washed in phosphate buffer to remove any unreacted glutaraldehyde and stored at 4°C until required.

Glutamine sensors were fabricated using a bienzyme membrane incorporating glutamate oxidase and glutaminase. Hydrogen peroxide was generated by the following sequence of reactions:

$$\text{glutamine} + H_2O \xrightarrow{\text{glutaminase}} \text{glutamate} + NH_3$$

$$\text{glutamate} + H_2O \xrightarrow{\text{glutamate oxidase}} \alpha\text{-ketoglutarate} + NH_3 + H_2O_2$$

The sensors were prepared using the method (as described for glutamate sensors) with the ad-

dition of 2 mg glutaminase. All of the experiments were carried out using the flow injection analysis (FIA) system described earlier [9].

All of the working electrodes were poised at +400 mV throughout the experiments and the recorded peak heights were used to ascertain the magnitude of the response.

Lactate sensors

A range of experiments was carried out to determine the optimum operating characteristics of the lactate sensors. The pH optimum was determined by recording the response to a standard (0.5 mM) lactate concentration over a range of values. From pH 5 to 6 a 0.1 M citrate solution was used. Measurements from pH 6 to 8 were made in 0.1 M sodium phosphate and calibrations from pH 8 to 9 were carried out in Tris–HCl buffer. The carrier flow rate optimum was determined by measuring the response from one enzyme electrode to a standard (0.5 mM) lactate solution. A range of flow rates from 0.1 to 0.7 ml min^{-1} was investigated. Consideration was also given to the time required for the chart response to decay from the maximum peak height back to a stable baseline. Operating under optimum conditions, one enzyme electrode was calibrated (using 0.1 M sodium phosphate–0.1 M potassium chloride buffer, pH 7.0) over a range of lactate concentrations. The operating stability of one electrode was determined over a 45 h period. During this time the working electrode potential was maintained at +400 mV and the carrier flow rate at 0.2 ml min^{-1}. The sensor was subjected to periodic (10 h^{-1}) injections of a standard (0.5 mM) lactate solution. Long term storage stability was also determined by measuring the response from one sensor over a 25 day period. Three measurements were made, at intermittent times, of a standard (0.5 mM) lactate solution. Over the 25 days the sensor was stored at 4°C when not in use.

Off-line measurements of lactate concentrations from samples, obtained from a perfusion culture of human hybridoma cells, were made using the FIA system. Initially the sensor was calibrated with 0.5 mM and 1.0 mM lactate solutions. Following calibration, three measurements on each media sample were made. Because the linear range of the sensor did not match the full range of lactate concentrations, the sample solutions were diluted 1:15 with carrier buffer prior to measurement. Results from the biosensor were compared with measurements made using a Model 2000 Yellow Springs Instrument (YSI, Yellow Springs Instrument Co., USA).

Glutamate and glutamine sensors

Experiments were carried out to optimise the performance of glutamate sensors. This included investigations into the effect of pH (using the same buffer concentrations described for the lactate sensors) and flow rate on the sensor response. Following optimisation the sensors were calibrated against a range of glutamate concentrations, in 0.1 M sodium phosphate–0.1 M potassium chloride buffer (pH 7.0). One enzyme electrode was tested continuously over a 24 h period. During this time the working electrode potential was held at a constant +400 mV and the flow rate maintained at 0.2 ml min^{-1}. Periodic injections of a standard (1 mM) glutamate solution were passed through the FIA system at a rate of 10 h^{-1}. The effect of long term storage was also examined by measuring the response from one enzyme sensor, intermittently, over a 20 day period. These measurements were made on a 1 mM glutamate solution, operating under optimum conditions. When not in use the sensor was stored at 4°C. Glutamate concentrations from the mammalian cell cultivation were also determined from undiluted sample solutions, and compared with results obtained using a standard enzyme test kit (Boehringer, Mannheim). All measurements were carried out according to the manufacturers instructions. Prior to the sensor measurements, the electrode was calibrated using 0.5 and 1 mM glutamate solutions (prepared in phosphate buffer). Three measurements were made on each sample.

Likewise, the optimum operating conditions for glutamine sensors were ascertained. Experiments to determine the optimum pH were carried out over the range 4.5 to 6.25 in 0.1 M citrate buffer. Hartman [13] reported that glutaminase was inactivated above pH 5.8, hence the narrow

range investigated. Again the sensors were tested for operational stability over a period of 24 h. During this time a standard 1.5 mM glutamine solution was periodically (10 h^{-1}) injected into the flow stream. Long term storage stability of the glutamine bi-enzyme sensor was examined by measuring, at intermittent times, the response of one sensor to a 1.5 mM glutamine solution over a 12 day period.

3. Results

3.1. Lactate sensors

The effect of pH on the response from lactate sensors is shown in Fig. 1. A maximum response was reached at pH 7.0. Results from experiments carried out to determine the optimum flow rate in terms of maximum peak current and the time required for the response to decline back to a stable baseline are shown in Table 1. When the flow rate was increased the maximum peak current declined. This resulted from a decreased residence time for the substrate at the surface of the sensor. In conjunction with declining peak currents, the time required for the response to decline back to a stable baseline also decreased with increasing flow rate. A flow rate of 0.2 ml min^{-1} was chosen for all subsequent experiments. This permitted a sampling rate of 10 h^{-1} with a high sensitivity.

Table 1
Effect of flow rate on the current response from lactate sensors to a standard (0.5 mM) lactate solution and the base line reversion time

Flow rate (ml min^{-1})	Peak current (nA)	Base reversion time (min)
0.1	180	8.0
0.2	155	5.0
0.3	150	3.25
0.4	140	3.0
0.5	120	3.0
0.6	100	2.5
0.7	90	2.25

Fig. 2 shows a typical response from one lactate sensor to a range of lactate concentrations, operating under optimum conditions. The linear range of these sensors was from 0.1 to 1.0 mM lactate. Overall the precision of these electrodes

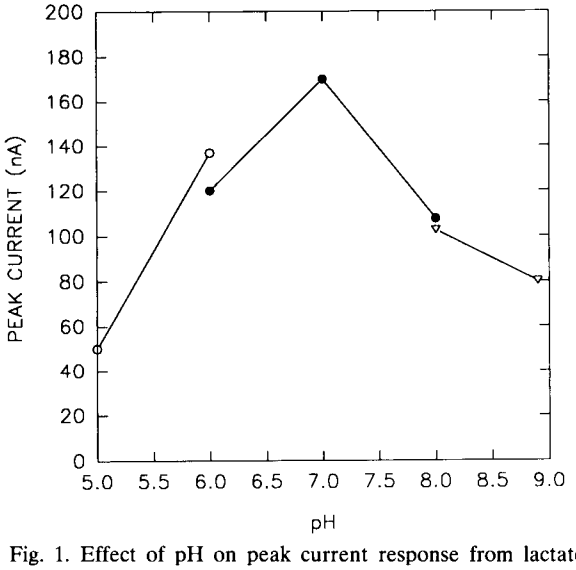

Fig. 1. Effect of pH on peak current response from lactate enzyme sensors. All buffer concentrations were 0.1 M. Key to symbols: ○ = citrate buffer; ● = phosphate buffer; ▽ = Tris–HCl buffer.

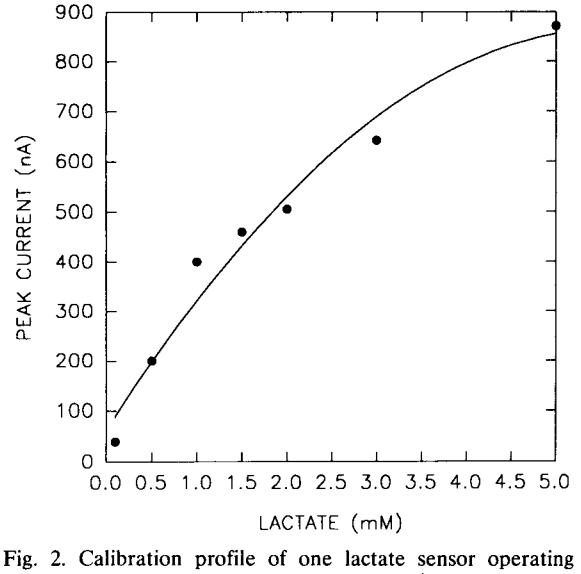

Fig. 2. Calibration profile of one lactate sensor operating under optimum conditions. Each point represents the mean value of three measurements. Generally the coefficient of variation was $< 1\%$.

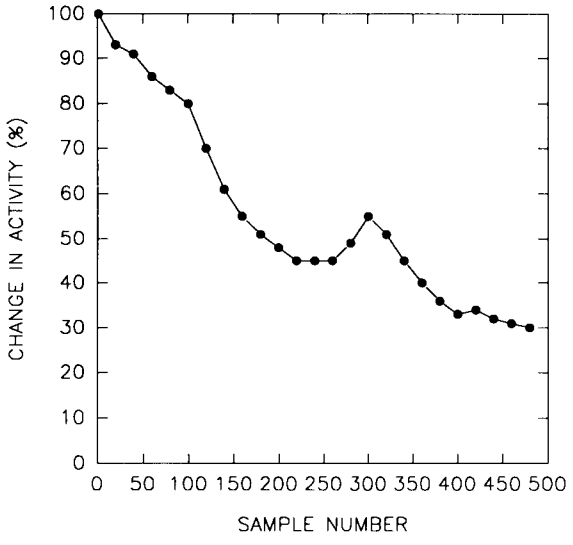

Fig. 3. Operational stability of a lactate sensor over a 45 h period. The sensor was subjected to periodic (10 h^{-1}) injections of a 0.5 mM lactate solution.

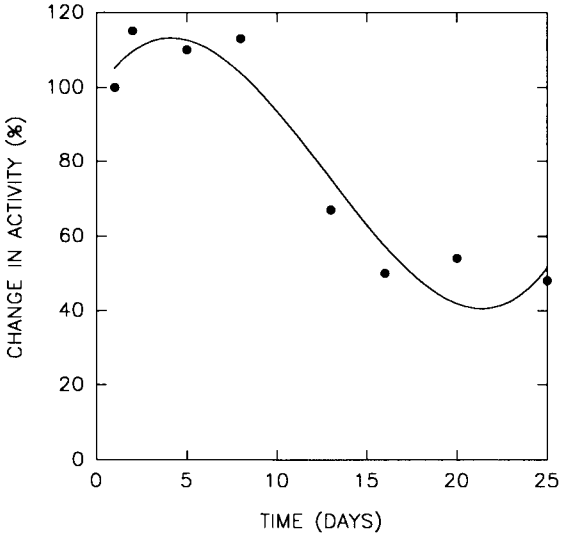

Fig. 4. Effects of long term storage on the activity response of one lactate sensor. Each point represents the mean response of three measurements.

was good with a coefficient of variation $< 1\%$ (3 measurements) at each concentration. Results from experiments to determine the operational and storage stabilities of these sensors are shown in Fig. 3 and Fig. 4, respectively. When one sensor was held at a potential of +400 mV, over a period of 45 h (450 measurements), the activity declined to 30% of its original value. At this point the sensor was still capable of measuring over the initial dynamic range. The graph indicates a steady decline in response, with an increase and subsequent decline between 250 and 350 measurements. The reason for this change in the pattern of response is unclear, but may have been the result of alterations in the porosity of the outer membrane. From Fig. 4 it can be seen that after 25 days storage the sensor activity had declined to 44% of the initial value. When tested at 30 days the sensor produced no response. Over the first 10 days the sensor activity increased before declining steeply between days 11 and 15. These changes and the subsequent loss of activity was attributed to alterations in the structure of the membrane, eventually leading to depletion of the enzyme. Off-line determinations depicting the correlation of lactate measurements for both the enzyme sensor and the YSI instrument are shown in Fig. 5. A correlation coefficient of $r = 0.982$ ($n = 15$) was calculated from these results. Prior to these measurements, several bare rhodinised electrodes were tested against media samples. No

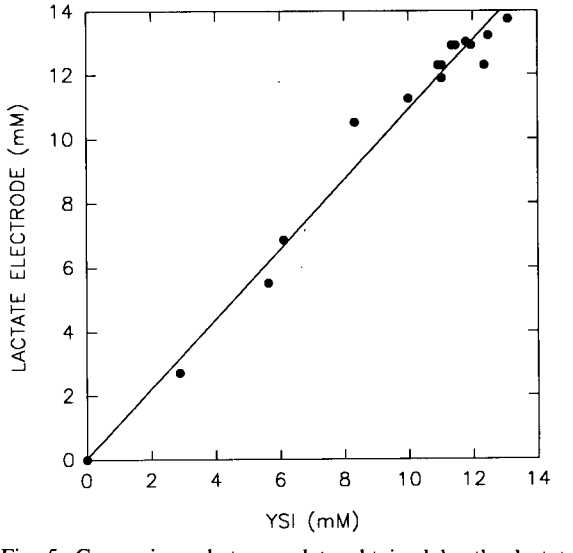

Fig. 5. Comparisons between data obtained by the lactate sensor and the YSI instrument ($r = 0.982$, $n = 15$).

significant signal was observed, indicating the absence of any electrochemically active interferents.

3.2. Glutamate sensors

Glutamate sensors produced their greatest response at pH 7.0 (Fig. 6). Results from the effect of flow rate on sensor response are shown in Table 2. The maximum peak current response and the baseline reversion time both decreased with increasing flow rate. This pattern of results was similar to those observed with lactate sensors. Again, because the choice of flow rate involved a compromise between sensitivity and sample output rate, a flow rate of 0.2 ml min^{-1} was chosen for all subsequent experiments. A typical calibration graph for one glutamate sensor is shown in Fig. 7. The linear range of these sensors was from 0.1 to 1.5 mM, and the sensitivity extended up to at least 3.0 mM. Typically the coefficient of variation at each concentration (3 measurements) was $< 1.5\%$. The overall stability of these sensors is depicted in Fig. 8 and Fig. 9. Over a 24 h period of continuous use, the activity of one sensor declined to 47% of its original value. At this point, a full calibration over the original dynamic range was still possible. Fig. 9 shows the effect of long term storage (20 days) on the response from one sensor. Over this period the sensor response declined to 29% of its original value. Comparisons between the off-line cell culture samples measured with the enzyme sensor and the test-kit, are shown in Fig. 10. A poor correlation ($r = 0.768$, $n = 15$) was observed.

Table 2
Effect of flow rate on the current response from glutamate sensors, to a standard glutamate solution (1 mM) and the baseline reversion time

Flow rate (ml min^{-1})	Peak current (nA)	Base reversion time (min.)
0.1	64	7.3
0.2	57	5.5
0.3	43	5.2
0.4	38	4.5
0.5	32	3.5
0.6	26	3.3
0.7	22	3.2
0.8	21	3.1

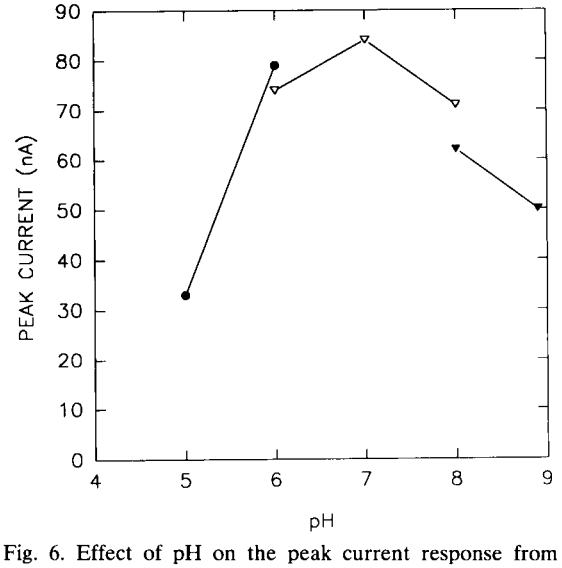

Fig. 6. Effect of pH on the peak current response from a glutamate sensor. All buffer concentrations were 0.1 M. Key to symbols: ● = citrate buffer; ▽ = phosphate buffer; ▼ = Tris–HCl buffer.

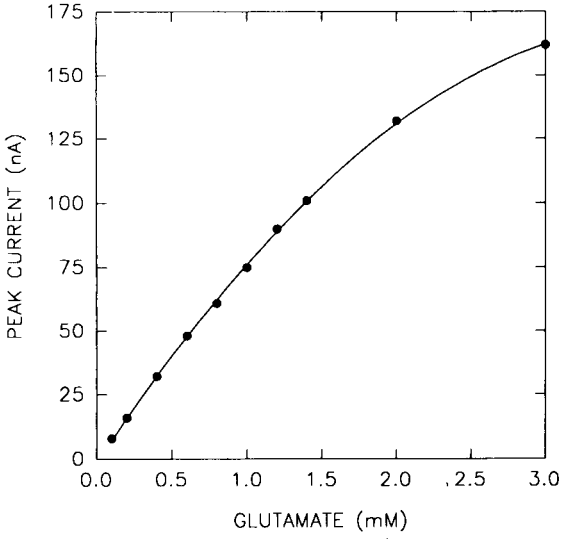

Fig. 7. Calibration profile of one glutamate sensor. Each point represents the mean peak current from three measurements.

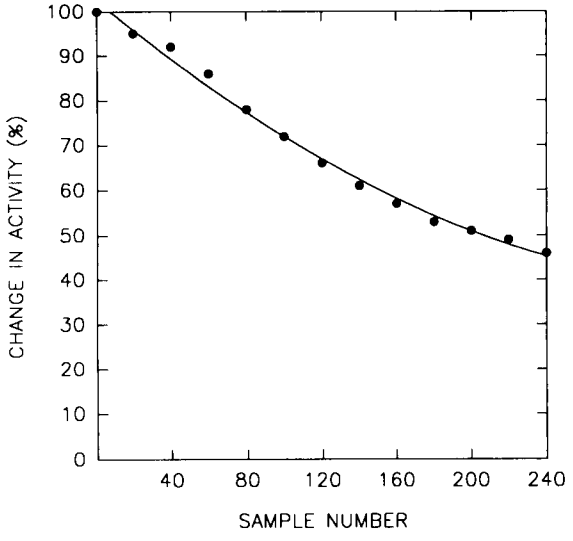

Fig. 8. Operational stability (over 24 h) of a glutamate sensor. The sensor was subjected to periodic (10 h^{-1}) injections of a 1 mM glutamate solution.

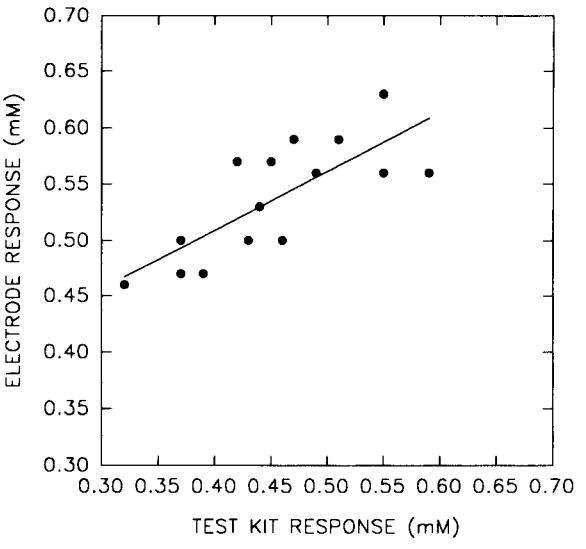

Fig. 10. Comparison between data obtained from a glutamate sensor and the enzyme test kit ($r = 0.768$, $n = 15$).

3.3. Glutamine sensors

The activity response of the bi-enzyme glutamine sensor as a function of pH is shown in Fig. 11. A pH optimum was observed at 5.5; above this value the response declined rapidly. Table 3 depicts the effect of flow rate on maximum peak current and the baseline reversion

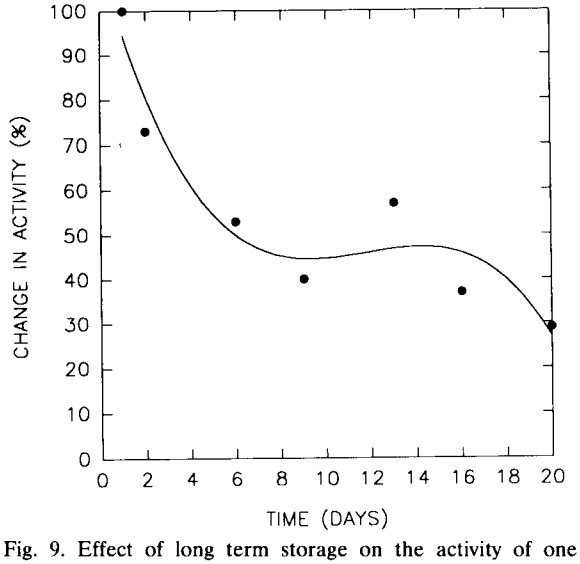

Fig. 9. Effect of long term storage on the activity of one glutamate sensor. Each point represents the mean response of three measurements, taken at intermittent times, over a 20 day period.

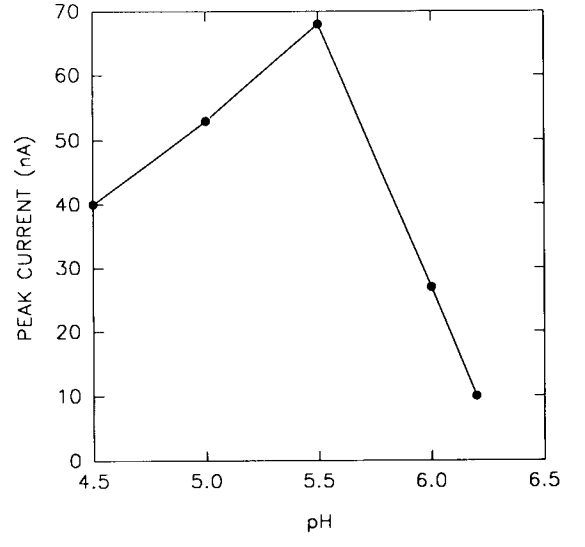

Fig. 11. Effect of pH on the peak current response from glutamine sensors. All measurements were made in 0.1 M citrate buffer.

Table 3
Effect of flow rate on the current response from glutamine sensors to a standard (0.5 mM) glutamine solution and the baseline reversion time

Flow rate (ml min^{-1})	Peak current (nA)	Base reversion time (min)
0.1	85	8.0
0.2	70	6.0
0.3	50	5.3
0.4	45	4.5
0.5	32	4.2
0.6	25	3.6
0.7	23	3.1

time. As before, 0.2 ml min^{-1} was chosen as the optimum flow rate for further experiments. A calibration profile for a typical glutamine sensor is shown in Fig. 12. The linear range of these sensors was again 0.1 to 1.5 mM and the sensitivity extended up to 4.0 mM glutamine. Generally the coefficient of variation between measurements at the same mid-range concentration was < 1.5%. Over a period of 24 h of continuous use, the activity of one sensor declined to 29% of its original value (Fig. 13). Because of the higher activity retained by the glutamate sensor, over the same time period, this increased loss was attributed to glutaminase depletion or loss. Simi-

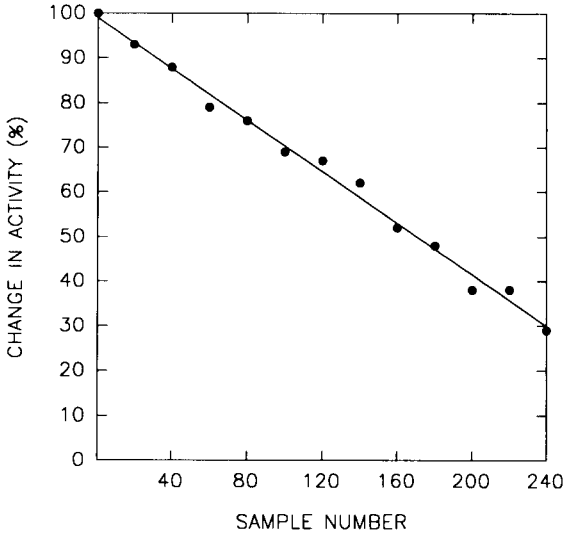

Fig. 13. Operational stability (over 24 h) of one glutamine sensor. The sensor was subjected to periodic (10 h^{-1}) injections of a 1.5 mM glutamine solution.

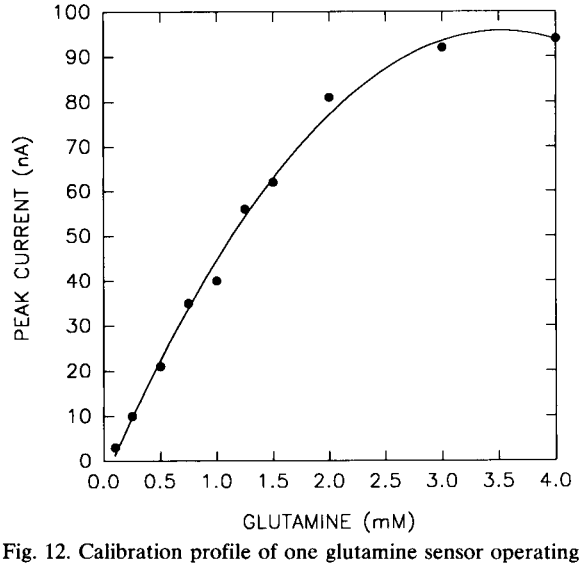

Fig. 12. Calibration profile of one glutamine sensor operating under optimum conditions. Each point represents the mean value of three measurements.

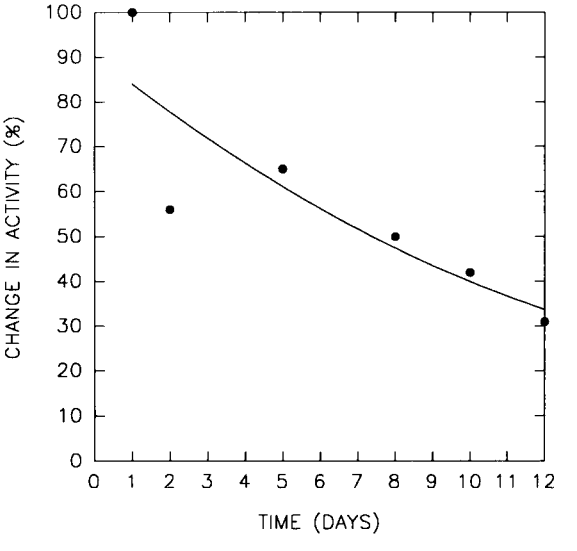

Fig. 14. Effect of long term storage on the response from one glutamine sensor. Over the 12 day period the sensor was measured at intermittent times.

larly, the shorter active life span (12 days) of glutamine sensors (Fig. 14) was probably caused by the loss of glutaminase activity.

4. Conclusions

The use of rhodinised electrodes, as the basis for lactate, glutamate and glutamine enzyme sensors, has been demonstrated. Operating at +400 mV, all of the sensors could measure the desired analyte over a significant range. Initial experiments with authentic media samples showed that lactate and glutamate sensors could measure the respective analyte to a significant degree of accuracy. Utilising these sensors, together with the previously described glucose electrodes, could lead to a method of on-line monitoring of mammalian cell cultures, based on the use of an FIA system.

References

[1] W.J. Aston and A.P.F. Turner, Biotechnol. Genet. Eng. Rev., 1 (1984) 89.
[2] I. Karube, S. Mitsuda and S. Suzuki, Appl. Microbiol. Biotechnol., 7 (1979) 343.
[3] H. Iwai and S. Aikama, Chim. Pharm. Bull., 34 (1986) 3471.
[4] G.M. Delaney, H.P. Bennetto, J.R. Mason, S.D. Roller, J.L. Stirling and C.F. Thurston, Anal. Proc., 23 (1986) 143.
[5] L. Gorton and T. Svensson, J. Mol. Catal., 38 (1986) 49.
[6] K. Hajizadeh, H.B. Halsall and W.R. Heineman, Anal. Chim. Acta, 243 (1991) 23.
[7] W.H. Mullen, Eur. Pat., 0 352 925, 1989.
[8] J. Wang and L. Agnes, Anal. Chim. Acta, 64 (1992) 456.
[9] S.F. White, A.P.F. Turner, U. Bilitewski, R.D. Schmid and J. Bradley, Electroanalysis, (1994) in press.
[10] C.Y. Chien and Y-C Su, Anal. Chim. Acta, 243 (1991) 9.
[11] W. Vahjen, J. Bradley, U. Bilitewski and R.D. Schmid, Anal. Lett., 24 (1991) 1445.
[12] M.V. Cattaneo, J.H.T. Luong and S. Mercille, Biosensors Bioelectron., 7 (1992) 329.
[13] S.C. Hartman, J. Biol. Chem., 243 (1968) 853.

ELSEVIER

Analytica Chimica Acta 295 (1994) 253–262

ANALYTICA CHIMICA ACTA

Optimum composition of neutral carrier based pH electrodes

Eric Bakker *, Aiping Xu, Ernö Pretsch

Swiss Federal Institute of Technology (ETH), Department of Organic Chemistry, Universitätstrasse 16, CH-8092 Zürich, Switzerland

Received 7th January 1994; revised 18th April 1994

Abstract

A simple formalism for the quantitative description of the upper and lower detection limit of pH selective solvent polymeric membrane electrodes containing a neutral carrier and a lipophilic anionic additive is presented, which is based on the consideration of phase transfer equilibria at the sample/membrane interface. It is shown that the lower and upper detection limits are controlled by the activity and lipophilicity of the interfering ions and by the basicity of the ionophore. When interfering cations or anions have completely penetrated the organic phase boundary layer through ion exchange or coextraction equilibria, respectively, the electrode response is expected to be a Nernstian function of the interfering ion activity alone. The measuring range may be shifted by incorporating ionophores of different basicity in the membrane, but cannot be extended with this approach. Instead, a high concentration of ionophore, together with 50 mol-% anionic additive relative to the ionophore, and, most importantly, a more hydrophobic membrane matrix with less cation binding characteristics has to be chosen for achieving a maximum measuring range of the potentiometric sensor.

Keywords: Ion exchange; Potentiometry; Sensors; pH electrodes

1. Introduction

For the determination of pH in various samples, the pH glass electrode is still most widely used. However, there are a number of analytical applications where other sensing materials would be more appropriate. For example, metal/metal oxide electrodes have been shown to be rugged in high temperature applications [1], and neutral carrier based solvent polymeric membranes are more suitable for in vivo blood pH measurements, since very small electrode tip sizes may be realized due to their low membrane resistance and these electrodes can be used in conjunction with other ion-selective solvent polymeric membranes for the determination of ions such as K^+, Na^+, Ca^{2+} and Mg^{2+}. Such membrane materials may also be suitable for applications in food and beverage industry, since glass may break and cause possible health hazards.

The first neutral carrier based solvent polymeric membrane pH electrodes have been developed in Simon's laboratory, where tridodecylamine and other compounds containing basic nitrogen groups have been discovered as selective membrane compounds in pH electrodes [2–8].

* Corresponding author. Department of Chemistry, The University of Michigan, Ann Arbor, MI 48109-1055, USA.

SSDI 0003-2670(94)00188-R

Later, other authors continued this work [9–12]. In recent years, the development of ion-selective optical sensors, where usually also a H^+-selective chromoionophore is incorporated, has led to the discovery of a range of highly lipophilic pH indicators [13], which in addition have been shown to act successfully as H^+ carriers in ion-selective electrodes [14,15]. Furthermore, the study of aminated poly(vinyl chloride) derivatives as membrane material in view of an application in biosensors, where enzymes may be covalently attached to the polymer matrix, has led to extensive investigations of their behavior in pH sensitive membranes [16–22].

However, the interpretation of the response behavior of such pH electrodes have usually only been given qualitatively [6], and there are only few reports about attempts to sufficiently quantify the membrane response. Egorov et al. [9] presented a model which was confirmed with suitable extraction experiments. However, despite its valuable contribution, the resulting electrode function was in its completeness mathematically too cumbersome to allow for straightforward conclusions. Other authors discussed the influence of the diffusion potential within the membrane phase on the membrane response when Donnan failure of the electrode is observed [21]. In that case, no clear distinction was made between effects arising from thermodynamic parameters such as lipophilicity, basicity, or activity of the species involved, and kinetic ones such as mobility of the ions present in the organic phase. The lack of this distinction made it difficult to clarify the experimental findings.

Recently, we have investigated the correlation of the optical signal of thin solvent polymeric films containing H^+-selective chromoionophores with the potentiometric behavior of the respective pH electrode having the same membrane composition [23]. These experiments, along with theoretical considerations on the mechanism of the relevant equilibria involved with optode membranes [13,24], have led to the following simple model for the quantification of the pH response of neutral carrier based solvent polymeric electrode membranes, where only the contribution of the phase transfer equilibrium to the overall response of the electrode is considered. The aim of the present work is to develop a theory which quantifies the upper and lower detection limit as a result from cation and anion interference as the two most important parameters of a pH electrode. Since the model is based on a range of simplifying assumptions, straightforward conclusions are obtained which are well confirmed with experimental results obtained in this and previous works. Especially, the optimum amount of anionic additives, the role of the membrane matrix and of the basicity of the ionophore are elucidated in detail. The results obtained may help in further developing pH electrodes with improved analytical performance.

2. Experimental

2.1. Reagents

All aqueous solutions were prepared in doubly quartz distilled water with salts and acids of highest purity available. The membrane matrix poly(vinyl chloride) (PVC), the anionic additive potassium tetrakis(*p*-chlorophenyl)borate (KTpClPB), the plasticizers bis(2-ethylhexyl)sebacate (DOS) and *ortho*-nitrophenyloctylether (o-NPOE) were purchased from Fluka (Buchs, Switzerland). The plasticizer 1,2,4-tris(2-ethylhexyl)trimellitate (TOTM) was obtained from Scientific Polymer Products (Ontario, NY), chloroparaffin (60 C) from Hüls (Germany), and Mesamoll®, an alkyl sulfonic ester of phenol (techn.), from Bayer (Germany). The ionophore 4-nonadecylpyridine (ETH 1907) was synthesized in our laboratory as described [8].

2.2. Electrode set up and EMF measurements

The electrode membranes containing a specified amount of ionophore and anionic additive in 2 parts plasticizer and 1 part PVC were prepared and assembled as described [25]. The electrodes were measured in the following cell:

$Hg|Hg_2Cl_2|KCl$ (sat.)|3 M KCl sample || membrane || inner filling solution | AgCl | Ag, with a calomel reference electrode of the free-flowing

free-diffusion type [26]. The inner filling solution consisted of 1 M citric acid, 2.73 M NaOH and 0.01 M NaCl, adjusted to pH 5.6. Prior to measurement, the electrodes were conditioned in a solution having the same composition as the inner filling solution for a period of 24 h. The measuring solution was 130 mM NaCl, 10 mM NaOH and 10 mM Tris (2-amino-2-hydroxymethyl-1,3-propanediole, Fluka), which was subsequently titrated with HCl from high to low pH. The sample pH was continuously monitored with a pH glass electrode (Glasbläserei Möller, Zürich), which was measured against the same reference electrode as the solvent polymeric membranes.

3. Results and discussion

3.1. Assumptions

In this paper, we will develop a model for the description of the upper and lower detection limits of neutral carrier based pH electrodes. To simplify the mathematical treatment, and to allow for straightforward results, the theoretical development is based on the following assumptions:

(1) The phase boundary potential at the sample/membrane interface is assumed to govern the membrane response, and the diffusion potential within the membrane phase, which is related to kinetic parameters of the species (e.g., mobilities), is neglected.

(2) The organic phase boundary contacting the sample is in chemical equilibrium with the aqueous sample solution.

(3) Activity coefficients in the membrane phase are constant for all ionic species, and therefore, concentration values are used in the membrane phase.

(4) It is assumed that the ionophore binds strongly to hydrogen ions (i.e., $[LH^+] \gg [H^+]$), and does not form complexes of appreciable strength with interfering ions.

(5) Ion pairs within the membrane phase are neglected.

Assumption (1) may usually hold for mobile neutral carriers [9,22,27,28]. However, for membranes with covalently immobilized ionophores such as aminated poly(vinyl chloride), it might not always be sufficiently valid [21], and deviations from the model presented may be expected. In (2) activity coefficients may be influenced by different parameters such as water uptake of the membrane [29], which however should equally occur at both interfaces of the organic phase and might therefore have a negligible influence on the overall response. Assumption (4) has been shown to be justified for a range of lipophilized pH indicators where no suitable coordinating groups are present [13]. Ionophores being able to complex other ions than H^+ induce a smaller measuring range of the electrode [6] and should be avoided. Assumption (5) might satisfactorily hold for salts of tetraphenylborate derivatives [30], but the activity range where anion extraction occurs may be poorly explained with this assumption. Since the strength of ion pair formation will depend on different parameters such as dielectric behavior of the plasticizer and nature of the extracted anion, this effect is difficult to quantify. However, this assumption allows for very general conclusions, which make the working principle of such electrodes more easily understandable.

3.2. Phase boundary potential

Considering the protonation equilibria of the ionophore in the organic phase, the response of a solvent polymeric membrane containing a neutral pH carrier to hydrogen ion activity steps in the sample solution is described by the phase boundary potential at the sample/membrane interface [31], if the inner filling solution of the electrode is kept constant:

$$E_H = E^0 + \frac{RT}{F} \ln \frac{a_{H^+} \cdot [L]}{[LH^+]} \quad (1)$$

Where a_{H^+} stands for the hydrogen ion activity in the sample, [L] and $[LH^+]$ for the concentration of free and protonated ionophore in the organic phase boundary contacting the sample solution, respectively, R, T and F have their usual significance, and all constant potential contributions are included in E^0.

If [L] and [LH^+] are independent of sample activity changes, they may be included in E^0, and Eq. 1 reduces to the Nernstian equation:

$$E_H = E^{0'} + \frac{RT}{F} \ln a_{H^+} \quad (2)$$

Consequently, no appreciable concentration changes in the organic phase are encountered in the activity range where the electrode response behaves ideally. By inserting the electroneutrality condition in the membrane, [L] is given by the total concentration of ionophore L_T minus the concentration of anionic sites R_T in the membrane ($[L] = L_T - R_T$), and [LH^+] corresponds to R_T. With this information, the ideal electrode response towards pH may described by rearranging Eq. 1:

$$E_H = E^0 + \frac{RT}{F} \ln \frac{a_{H^+} \cdot (L_T - R_T)}{R_T} \quad (3)$$

3.3. Cation interference

For basic samples, interfering cations J^+ may partition into the membrane phase and undergo the following ion-exchange reaction with hydrogen ions:

$$J^+(aq) + LH^+(org) \rightleftharpoons J^+(org) + L(org) + H^+(aq)$$

with the respective ion-exchange constant:

$$K_{exch} = K_a \cdot K_{JH} = \frac{[L] \cdot a_{H^+}}{[LH^+]} \cdot \frac{[J^+]}{a_{J^+}} \quad (4)$$

where K_a is the acidity constant of the ionophore in the membrane phase and K_{JH} is the ion-exchange constant for the free cation between the sample and the organic phase, which is given by the relative lipophilicity of the cations:

$$K_{JH} = \frac{a_{H^+} \cdot [J^+]}{[H^+] \cdot a_{J^+}} \quad (5)$$

The constant K_{exch} is inserted into Eq. 1 to describe the membrane response as a function of interfering ion activity a_{J^+} in the sample:

$$E_J = E^0 + \frac{RT}{F} \ln \left(K_{exch} \frac{a_{J^+}}{[J^+]} \right) \quad (6)$$

Over a certain hydrogen activity range, the electrode responds to both hydrogen and interfering ions and may be equally described with Eqs. 1 and 6. In this case, [J^+] in Eq. 6 will also be a function of the sample pH, and [L] and [LH^+] in Eq. 1 of a_{J^+}, respectively. Eventually, when the interfering ions have completely exchanged the hydrogen ions from the membrane boundary layer, the electrode response will be only a function of a_{J^+} alone. In this case, the concentration of J^+ in the outer phase boundary layer equals the concentration of anionic sites R_T, and one gets from Eq. 6:

$$E_J = E^0 + \frac{RT}{F} \ln \left(K_{exch} \frac{a_{J^+}}{R_T} \right) \quad (7)$$

The lower detection limit according to IUPAC is defined as the cross-section of the two extrapolated linear segments of the calibration curve [32]. Since one segment corresponds to the ideal pH electrode function according to Eq. 3 and the other to the Nernstian electrode response towards the interfering ion activity of the background electrolyte (Eq. 7), the practical detection limit is given where both functions lead to the same membrane potential ($E_H = E_J$). Therefore, the combination of Eq. 3 and 7 yields:

$$a_{H^+}(DL_{cif}) = K_{exch} \cdot \frac{a_{J^+}}{L_T - R_T} \quad (8)$$

Where the symbol DL_{cif} stands for the cation interference induced detection limit. Primarily, the lower detection limit of the electrode is controlled by the basicity of the ionophore and the lipophilicity/activity of the interfering ion. The validity of Eq. 8 has been confirmed with many experimental results obtained previously [6,9]. Accordingly, the cation interference has been found to increase if the basicity of the carrier decreases or interfering cations with decreasing free energy of transfer are present in the aqueous sample. However, the concentration of anionic additive relative to the total ionophore concentration also influences the detection limit. With increasing amount of R_T, the detection limit shifts to higher activity values. For example, the use of carboxylated PVC in ion-selective electrodes

(ISEs) containing highly basic ionophores [18] led to higher detection limits, which suggests that the acidic carboxy groups are being deprotonated by the carrier and then subsequently act as anionic sites.

3.4. Anion interference

With increasing hydrogen ion activity in the sample, interfering anions Y^- may penetrate the membrane through the following coextraction mechanism:

$$Y^-(aq) + H^+(aq) + L(org) \rightleftharpoons Y^-(org) + LH^+(org)$$

with the respective coextraction constant:

$$K_{coex} = \frac{K_{YH}}{K_a} = \frac{[LH^+]}{[L] \cdot a_{H^+}} \cdot \frac{[Y^-]}{a_{Y^-}} \quad (9)$$

Where K_{YH} stands for the coextraction constant of the so called free hydrogen ion and interfering anion from the aqueous phase into the membrane:

$$K_{YH} = \frac{[H^+]}{a_{H^+}} \cdot \frac{[Y^-]}{a_{Y^-}} \quad (10)$$

Again, Eq. 9 is inserted into Eq. 1 to describe the electrode response behavior as a function of interfering anion activity in the sample:

$$E_Y = E^0 + \frac{RT}{F} \ln\left((K_{coex})^{-1} \frac{[Y^-]}{a_{Y^-}} \right) \quad (11)$$

The electrode will then ideally respond to anion activities alone, if all initially unprotonated ionophore in the phase boundary layer is converted into $[LH^+]$ and $[Y^-]$ through coextraction from the sample. Accordingly, $[Y^-]$ in Eq. 11 approaches $L_T - R_T$:

$$E_Y = E^0 + \frac{RT}{F} \ln\left((K_{coex})^{-1} \frac{L_T - R_T}{a_{Y^-}} \right) \quad (12)$$

This result is in clear contrast to the behavior of non-specific ion-exchange membranes, where the coextraction process itself does not lead to a change in the phase boundary potential [33]. In such a case, the mobility of the extracted ions would determine the slope of the resulting electrode function [21]. In neutral carrier based membranes however, the coextraction of electrolyte eventually leads to a saturation of the neutral carrier as shown above, and the membrane composition no longer changes as a function of the electrolyte concentration in the sample. Hence, a Nernstian anionic slope of the electrode, which is not depending on the mobility of the ions involved, is then expected. Indeed, this effect has been found for membranes with both mobile and immobilized ionophores (where the mobility will be significantly different), which has been unexpected in view of the respective theoretical model presented [21].

The upper detection limit is now defined in complete analogy to the lower detection limit by extrapolation of the two linear segments of the calibration curve, which correspond to Nernstian response of the electrode to a_{H^+} and a_{Y^-}, respectively. The upper detection limit is therefore given by combination of Eqs. 3 and 12:

$$a_{H^+}(DL_{aif}) = (K_{coex})^{-1} \frac{R_T}{a_{Y^-}} \quad (13)$$

Where the subscript "aif" stands for anion interference. Again, the upper detection limit is primarily influenced by the basicity of the ionophore and the activity/lipophilicity of the interfering anion Y^-. This relationship has been confirmed with numerous experiments reported previously [6,9,21]. The anion interference always follows the so-called Hofmeister selectivity sequence [34] and therefore indicates that no specific interaction between the extracted anion and the protonated carrier is taking place [35].

3.5. Measuring range

The measuring range of a neutral carrier based pH electrode is given by the activity range between upper (Eq. 8) and lower detection limit (Eq. 13):

$$\frac{a_{H^+}(DL_{aif})}{a_{H^+}(DL_{cif})} = (K_{exch} \cdot K_{coex})^{-1} \cdot \frac{R_T \cdot (L_T - R_T)}{a_{J^+} \cdot a_{Y^-}} \quad (14)$$

Where the constant term $K_{exch} \cdot K_{coex}$ is simplified by inserting Eqs. 4 and 9:

$$K_{exch} \cdot K_{coex} = K_{JH} \cdot K_{HY} = K_{JY} = \frac{[J^+]}{a_{J^+}} \cdot \frac{[Y^-]}{a_{Y^-}} \quad (15)$$

In mixed electrolyte systems, JY represent the one which is extracted the most. The pH response range of the electrode is therefore given by

$$\Delta pH = \log a_{H^+}(DL_{aif}) - \log a_{H^+}(DL_{cif}) = \log \frac{R_T \cdot (L_T - R_T)}{K_{JY} \cdot a_{J^+} \cdot a_{Y^-}} \quad (16)$$

In Figs. 1 and 2, a schematic presentation of the proposed model is presented. Fig. 1 shows the calculated concentration changes of the species $[LH^+]$, $[J^+]$ and $[Y^-]$ for a membrane containing 50 mol-% of a lipophilic anionic additive relative to the ionophore as a function of the sample pH. Since the two activity ranges where the concentration of LH^+ changes may be described with ion exchange and coextraction equilibria, Eqs. 4 and 9, together with the respective mass balances and electroneutrality conditions, were used for the calculation of $[LH^+]$ in the outer phase boundary layer of the organic membrane phase. The corresponding electrode response function with a constant background of interfering electrolyte JY according to Eq. 1 is shown in Fig. 2. The membrane potential follows the Nernstian equation, if no change in the concentration of LH^+ in the organic boundary layer is observed. When J^+ or Y^- have completely penetrated the membrane and either displaced H^+ (in the case of J^+) or fully protonated L by coextraction (in the case of Y^-), the electrode response will be governed by the sample activities of these ions alone. The lower and upper detection limits are given by the two cross-sections of the extrapolated linear segments of the calibration curve.

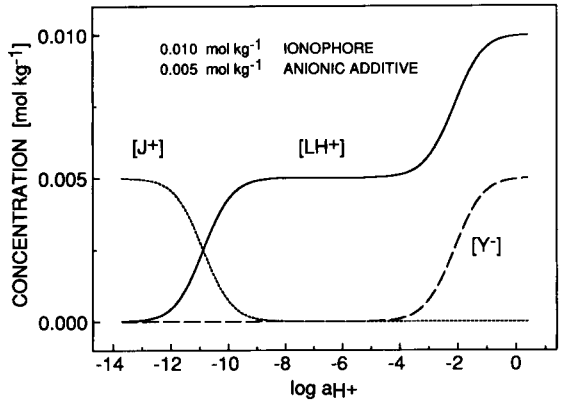

Fig. 1. Calculated equilibrium concentrations of the protonated ionophore ($[LH^+]$) and extracted interfering cations and anions $[J^+]$ and $[Y^-]$, respectively, in the organic phase boundary layer contacting the sample solution as a function of the sample pH. The curves were obtained by using Eqs. 4 and 9 for the respective ion exchange and coextraction equilibrium and inserting appropriate mass balances and electroneutrality conditions with $\log K_{exch} = -4$, $\log K_{coex} = 2$, $a_{J^+} = a_{Y^-} = 0.01$ M. The concentration of ionophore and anionic additive in the membrane were chosen as 0.010 and 0.005 mol kg^{-1}, respectively.

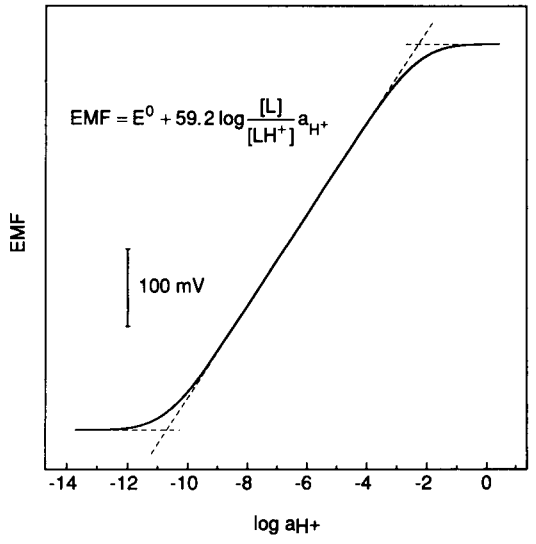

Fig. 2. Calculated pH response function of a H^+-selective solvent polymeric membrane electrode containing 0.010 mol kg^{-1} ionophore and 0.005 mol kg^{-1} anionic additive. The concentrations of free and protonated ionophore in the organic phase boundary layer contacting the sample solution as shown in Fig. 1 were inserted into Eq. 1 to predict the phase boundary potential of the electrode at 25°C. The calculated potential in the range of cation and anion interference reach a horizontal plateau, since a constant ionic background JY was chosen (see Fig. 1).

3.6. Optimum composition of neutral carrier based pH electrodes

According to Eq. 16, the total pH measuring range is not influenced by the basicity of the ionophore, since a change in basicity shifts the upper and lower detection limit simultaneously. Provided that any appreciable complexation of the pH carrier with interfering ions can be neglected, it can hardly be extended by searching ionophores with different structural properties. Obviously, the use of ionophores with two separated pK_a values (dibasic carriers) as reported previously [16] might not lead to an extension of the measuring range according to Eq. 16 as well. However, indirect effects such as a change in the hydrophobicity of the membrane phase or decreased binding characteristics towards interfering ions may have been responsible for beneficial experimental findings. The measuring range is given by the activity and lipophilicity of the interfering electrolyte and by the concentration of the ionophore L_T and anionic site R_T in the membrane. Hence, membrane materials should be carefully evaluated to give a low value of K_{IY}. This could be accomplished with plasticizers or membrane matrices of high hydrophobicity and with low binding characteristics to the interfering ions. The evaluation of a range of plasticizers for pH electrodes have however shown that the activity range of cation interference is usually most heavily influenced by the nature of the plasticizer, whereas the anion interference roughly occurs at about the same pH value (see Fig. 3). This is an indication that the coordination of metal ions through the plasticizer cannot be neglected and usually plays an even more significant role for the membrane selectivity of pH electrodes than its dielectric constant or hydrophobicity. Membranes with high dielectric constant plasticizers, such as o-NPOE, have therefore surprisingly found to induce a larger measuring range than DOS, which carries potentially complexing ester functions. Indeed, the low dielectric constant plasticizer chloroparaffin has no such complexing groups and induces a much larger measuring range of the electrode than DOS (see Fig. 3).

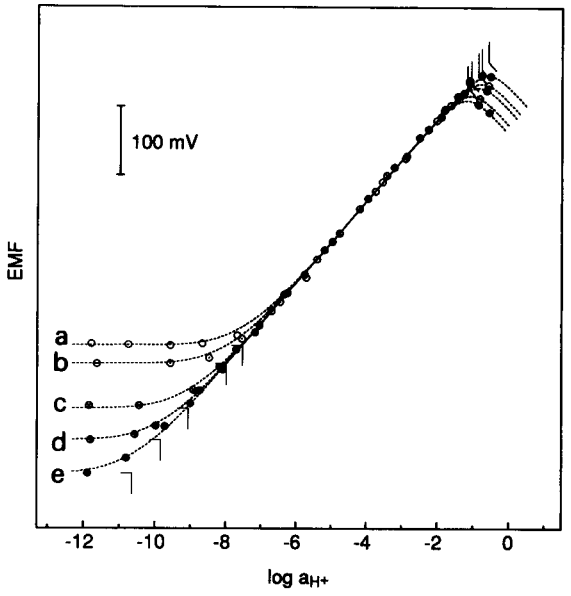

Fig. 3. Potentiometric pH response of ion-selective electrodes based on ETH 1907 (1 wt-%) as neutral carrier and KTpClPB (70 mol-% relative to the ionophore) as anionic additive in plasticized PVC membranes as a function of the plasticizer chosen: (a) DOS (dielectric constant (DK) = 3.9 [41]); (b) TOTM (DK = 4.7 [41]); (c) Mesamoll® (DK = 10.6 [41]); (d) o-NPOE (DK = 23.9 [42]); (e) chloroparaffin (DK = 7.9 [42]). Dotted curves were calculated according to Eqs. 1, 4 and 9 by inserting appropriate mass balances; lower and upper detection limits according to Eqs. 8 and 13, respectively, are indicated by straight vertical lines.

The optimum concentration of anionic sites in the membrane can be evaluated by setting the respective partial differentiation of Eq. 16 to zero:

$$\frac{\delta(\Delta\mathrm{pH})}{\delta R_T} = 04343 \cdot \frac{L_T - 2R_T}{L_T \cdot R_T - (R_T)^2} = 0 \qquad (17)$$

Which leads to:

$$R_T(\max) = \tfrac{1}{2}L_T \qquad (18)$$

Hence, neutral carrier based pH electrodes should ideally contain 50 mol-% anionic additive relative to the total ionophore concentration to ensure a maximum measuring range of the electrode. This novel theoretical result is in agreement with discoveries from different authors who used salts of tetraphenylborate derivatives in the membrane for empirical reasons [21,22,36]. The beneficial effect of tetraphenylborate salts on the

pH electrode response has been initially found to be surprising [36], since this is in contrast to the expected selectivity of ISEs for monovalent towards divalent ions, where a high concentration of free carrier, and therefore a very low concentration of anionic additive has to be chosen [37]. However, membranes without the incorporation of anionic additives showed no Nernstian response to pH at all (data not shown), which is in agreement with findings from other authors [22]. This is unexpected, since PVC is known to contain a substantial amount of anionic impurities [38,39] which usually ensures a cationic response of neutral carrier based membranes. Therefore, the complete failure of the pH response can be understood by the existence of other impurities, which exceed the concentration of the anionic sites in the membrane and therefore deteriorate the electrode response. Consequently, the addition of tetraphenylborate salts will ensure that the electrode response will be governed by the H^+-selective ionophore alone. Comparable effects have been found previously in neutral carrier based electrodes containing no anionic additives [40].

The overall change in the practical measuring range will be only small when using additive concentrations slightly different than 50 mol-%. It is more important to use anionic additives with very weak ion pair formation capabilities, since sites such as sulfonic acid derivatives have been shown to deteriorate the membrane selectivity if the interfering ion exhibits a chemically stronger interaction with the additive than with the ionophore incorporated [40], which is certainly the case with pH carriers [13].

According to Eq. 16, the measuring range will be extended by using a high concentration of neutral ionophore in the membrane. Naturally, this will only be true if all other parameters such as the hydrophobicity of the membrane will remain unaffected by increasing the concentration of carrier and anionic additive. In Fig. 4, the pH response of a membrane containing different amounts of ETH 1907 as ionophore with 70 mol-% KTpClPB in TOTM–PVC (2:1) is shown. Indeed, the practical measuring range increases with increasing ionophore concentration. The solubility of the compound in the membrane phase may however usually limit this optimization approach.

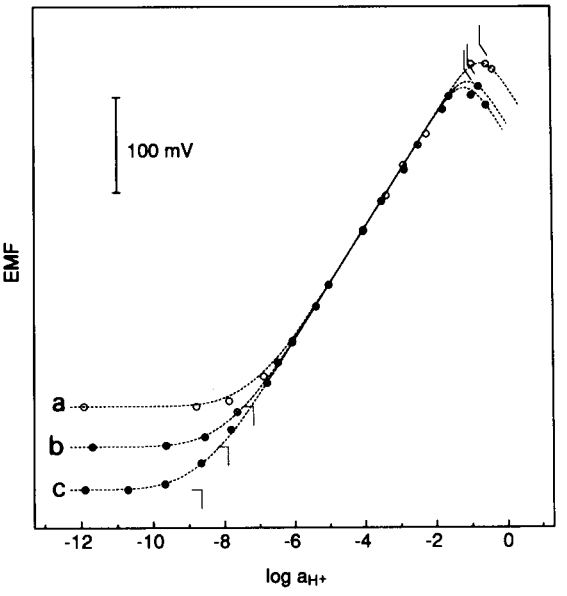

Fig. 4. Measuring range of pH electrodes with KTpClPB (70 mol-% relative to the ionophore) in trioctyltrimellitate/PVC (2:1) as membrane material containing (a) 0.2 wt-%, (b) 1 wt-% and (c) 5 wt-% of ionophore ETH 1907 in the membrane. The measuring ranges are $\Delta pH = 6.4$, 6.8, and 7.5, respectively, and increase with higher ionophore concentration. Dotted curves were calculated according to Eqs. 1, 4 and 9 (see Fig. 3).

4. Conclusions

It has been shown that a simple model, which is considering the boundary potential at the sample/membrane phase only, is adequate to describe various influences of the membrane composition on the performance of neutral carrier based liquid membrane pH electrodes. On the basis of this model, the role of the main parameters influencing the upper and lower detection limits and the working range of such electrodes may be predicted. Accordingly, the following conclusions have been drawn.

(1) The acidity constant of the ionophore incorporated is most heavily determining the lower and upper detection limit of the sensor. The measuring range is shifted, but cannot be ex-

tended by choosing an ionophore with different pK_a.
(2) The overall measuring range cannot be increased by incorporating a dibasic ionophore or two ionophores with different basicities.
(3) Optimum characteristics of the electrode are only achieved by reducing stabilizing interactions between the membrane phase and the interfering ions. Therefore, the ionophore and plasticizer used should contain no coordinating functional groups. Similarly, an anionic additive without strong ion-pair formation capabilities should be chosen. A more hydrophobic membrane material increases the measuring range if other parameters are unchanged. However, a less polar membrane material with ion coordinating capabilities might be less preferable than a more polar one without.
(4) The membrane should contain 50 mol-% anionic additive relative to the total ionophore concentration in order to increase the measuring range to its maximum value. Also, a high ionophore concentration in the membrane is preferable.

Acknowledgments

This work was partly supported by the Swiss Science Foundation.

References

[1] S. Glab, G. Edwall, A. Hulanicki and F. Ingman, Crit. Rev. Anal. Chem., 21 (1989) 29.
[2] D. Erne, D. Ammann and W. Simon, Chimia, 33 (1979) 88.
[3] P. Schulthess, Y. Shijo, H.V. Pham, E. Pretsch, D. Ammann and W. Simon, Anal. Chim. Acta, 131 (1981) 111.
[4] D. Erne, K.V. Schenker, D. Ammann, E. Pretsch and W. Simon, Chimia, 35 (1981) 178.
[5] P. Anker, D. Ammann and W. Simon, Mikrochim. Acta, I (1983) 237.
[6] U. Oesch, Z. Brzózka, A. Xu, B. Rusterholz, G. Suter, H.V. Pham, D.H. Welti, D. Ammann, E. Pretsch and W. Simon, Anal. Chem., 58 (1986) 2285.
[7] U. Oesch, Z. Brzózka, A. Xu and W. Simon, Med. Biol. Eng. Comput., 25 (1987) 414.
[8] P. Chao, D. Ammann, U. Oesch, W. Simon and F. Lang, Pflügers Arch., 411 (1988) 216.
[9] V.V. Egorov and Y.F. Lushchik, Talanta, 37 (1990) 461.
[10] L.T. Jin, Z.L. Shi, J.N. Ye, J.G. Qian and Y.Z. Fang, Anal. Chim. Acta, 244 (1991) 165.
[11] R. Yuan, Y.Y. Chai and R.Q. Yu, Analyst, 117 (1992) 1891.
[12] T.J. Cardwell, R.W. Cattrall, L.W. Deady and K.A. Murphy, Austr. J. Chem., 45 (1992) 435.
[13] E. Bakker, M. Lerchi, T. Rosatzin, B. Rusterholz and W. Simon, Anal. Chim. Acta, 278 (1993) 211.
[14] V.V. Cosofret, T.M. Nahir, E. Lindner and R.P. Buck, J. Electroanal. Chem. Interfacial Electrochem., 327 (1992) 137.
[15] T.M. Nahir and R.P. Buck, Helv. Chim. Acta, 76 (1993) 407.
[16] S.C. Ma, N.A. Chaniotakis and M.E. Meyerhoff, Anal. Chem., 60 (1988) 2293.
[17] S.C. Ma and M.E. Meyerhoff, Mikrochim. Acta, 1 (1990) 197.
[18] E. Lindner, V.V. Cosofret, R.P. Kusy, R.P. Buck, T. Rosatzin, U. Schaller, W. Simon, J. Jeney, K. Tóth and E. Pungor, Talanta, 40 (1993) 957.
[19] V.V. Cosofret, E. Lindner, R.P. Buck, R.P. Kusy and J.Q. Whitley, J. Electroanal. Chem., 345 (1993) 169.
[20] E. Lindner, T. Rosatzin, J. Jeney, V.V. Cosofret, W. Simon and R.P. Buck, J. Electroanal. Chem., 352 (1993) 309.
[21] R.P. Buck, V.V. Cosofret and E. Lindner, Anal. Chim. Acta, 282 (1993) 273.
[22] V.V. Cosofret, E. Lindner, R.P. Buck, R.P. Kusy and J.Q. Whitley, Electroanalysis, 5 (1993) 725.
[23] E. Bakker, M. Willer and E. Pretsch, in preparation.
[24] E. Bakker and W. Simon, Anal. Chem., 64 (1992) 1805.
[25] C. Behringer, B. Lehmann, J.-P. Haug, K. Seiler, W.E. Morf, K. Hartman and W. Simon, Anal. Chim. Acta, 233 (1990) 41.
[26] R.E. Dohner, D. Wegmann, W.E. Morf and W. Simon, Anal. Chem., 58 (1986) 2585.
[27] E. Pungor, Pure Appl. Chem., 64 (1992) 503.
[28] Rakhman'ko, V.V. Yegorov, A.L. Gulevich and Y.F. Lushchik, Sel. Electrode Rev., 13 (1991) 5.
[29] A.D.C. Chan and D.J. Harrison, Anal. Chem., 65 (1993) 32.
[30] R.D. Armstrong and G. Horvai, Electrochim. Acta, 35 (1990) 1.
[31] E.A. Guggenheim, J. Phys. Chem., 34 (1930) 1540.
[32] G.G. Guilbault, R.A. Durst, M.S. Frant, H. Freiser, E.H. Hansen, T.S. Light, E. Pungor, G. Rechnitz, N.M. Rice, T.J. Rohm, W. Simon and J.D.R. Thomas, Pure Appl. Chem., 48 (1976) 127.
[33] F.M. Karpfen and J.E.B. Randles, Trans. Faraday Soc., 49 (1953) 823.
[34] K. Sollner and G.M. Shean, J. Am. Chem. Soc., 86 (1964) 1901.
[35] W.E. Morf, in E. Pungor, W. Simon and J. Inczédy (Eds.), Studies in Analytical Chemistry, Vol. 2, Akadémiai Kiadó, Budapest, 1981, p. 223.
[36] A. Xu, Diss. ETH Zürich, No. 9516, 1991.

[37] P.C. Meier, W.E. Morf, M. Läubli and W. Simon, Anal. Chim. Acta, 156 (1984) 1.
[38] E. Lindner, E. Graf, Z. Niegreisz, K. Tóth, E. Pungor and R.P. Buck, Anal. Chem. 60 (1988) 295.
[39] A. van den Berg, P.D. van der Wal, M. Skowronska-Ptasinska, E.J.R. Sudhölter, D.N. Reinhoudt and P. Bergveld, Anal. Chem. 59 (1987) 2827.
[40] T. Rosatzin, E. Bakker, K. Suzuki and W. Simon, Anal. Chim. Acta, 280 (1993) 197.
[41] J.K. Sears and J.R. Darby, The Technology of Plasticizers, Wiley, New York, 1982.
[42] O. Dinten, Diss. ETH Zürich, No. 8591, 1988.

ELSEVIER

Analytica Chimica Acta 295 (1994) 263–272

ANALYTICA CHIMICA ACTA

Determination of some redox properties of humic acid by alkaline ferricyanide titration

Robin S. Helburn [1], Patrick MacCarthy *

Department of Chemistry and Geochemistry, Colorado School of Mines, Golden, CO 80401, USA

Received 3rd September 1993; revised manuscript received 18th April 1994

Abstract

A method for the direct potentiometric oxidation titration of aqueous phase humic substances with potassium ferricyanide ($K_3Fe(CN)_6$) has been developed. Oxidative titrations of humic acid were carried out at varying analyte concentrations, and at values of pH ranging from 5.0 to 11.0. Model synthetic mixtures of phenols and hydroquinones were examined in the same pH range. Ferricyanide titrations of humic acid at pH 9.0 yielded single discrete endpoints, and generally stable potential measurements in the pre-equivalence point region of the titration curve. Cyclic voltammetry of alkaline solutions of humic acid provides evidence for direct interaction between phenolic components in the humic acid and the electrode surface, and that for titrations conducted at pH 9.0 and above, humic acid can contribute to the poising of the potential measurements in the region of the half-titration point.

Keywords: Potentiometry; Titrimetry; Humic substances

1. Introduction

Humic substances play an important role in the fate and transport of toxic chemicals, and in nutrient cycling throughout the environment [1]. These materials result from the decomposition of plant and animal residues. They are that portion of natural organic matter which is heavily decomposed and refractory in nature [2]. Humic substances are comprised of a complex mixture of organic components, and do not fall into any of the known classes of discrete organic compounds [3].

It is well established that humic materials are redox active [4]. Despite the many studies of the redox interactions of humic acids and of natural organic matter in general, relatively few investigations have focused on the fundamental redox properties of these systems. Polarographic studies have generated conflicting views regarding the presence or absence of a reduction wave due to an unaltered humic or fulvic acid (as distinct from degradation products of humic substances) [5–8]. There have been some attempts to determine a value of $E°$ for humic substances from single-point potentiometric measurements [9,10]. In the one

* Corresponding author.

[1] Current address: Department of Chemistry, Northern Arizona University, P.O. Box 5698 Flagstaff, AZ 86011-5698, USA.

SSDI 0003-2670(94)00189-S

instance where a potentiometric titration of humic acid was mentioned, the titrimetric data were not provided [11]. The present paper describes a detailed investigation of the oxidative titration of a humic acid as a function of pH, and the modelling of the redox behavior of the humic acid using synthetic phenolic mixtures.

A major obstacle to the electrochemical characterization of humic acid lies in the fact that the redox active component of the material is an inseparable mixture of individual redox couples. The structures of these moieties, and the degree to which any one couple can produce a measurable potential are not known. Presumably, at the surface of a working electrode, humic substances *may*, at best, produce a "mixed potential".

1.1. Theory of mixed potentials

In a mixed potential measurement, several redox couples having different equilibrium (Nernstian) potentials may coexist at an electrode surface. Hence, the mixed potential is the potential of that electrode at which the sum of anodic and cathodic currents resulting from several components of these redox systems is equal to zero [12,13]. A mixed potential represents a steady state rather than an equilibrium potential, and it is not quantified by the Nernst equation. In the case of humic substances, a mixed potential may be due to many contributing potentials. The theory and limitations of mixed potential measurements have been previously addressed [12–15].

While a single potential measurement of humic substances yields little information, a series of measurements performed in the context of a titration may provide more useful information about the nature of the analyte provided that: (1) there is some direct interaction between the analyte and the monitoring electrode, and (2) the change in that interaction is proportional to the amount of added titrant.

1.2. Ferricyanide titration

The objectives of this research were to investigate the redox properties of humic substances through titration with potassium ferricyanide ($K_3Fe(CN)_6$) at various pH values. Cyclic voltammetry was used to confirm the ability of the analyte to affect the measured potentials (at pH 9.0) in the region of the half-titration point. Potassium ferricyanide ($E^\circ = +360$ mV vs. SHE) is a commonly used oxidizing agent which has been applied to the study of the redox properties of proteins [16,17], carbohydrates [18,19], lignins [20] and other natural phenolic materials [21,22]. The anionic ferri- and ferrocyanide complexes are stable over a wide range of pH values, and neither species binds to negatively charged polyelectrolyte materials.

2. Experimental

A humic acid isolated from a sample of peat collected at the Peatland Experimental Station, Glenamoy, Co. Mayo, Ireland was obtained in the salt form. The material had been characterized as to its elemental composition [23], by potentiometric and thermometric titration with base [23,24], and by infrared and solid-state ^{13}C NMR spectroscopy [25,26]. Research grade hydroquinone (1,4-dihydroxybenzene) and gallic acid (3,4,5-trihydroxybenzoic acid) were purchased from Sigma. Catechol (1,2-dihydroxybenzene), resorcinol (1,3-dihydroxybenzene), pyrogallol (1,2,3-trihydroxybenzene) and commercially prepared buffers were obtained from Fischer Scientific. Research grade potassium chloride (KCl) and potassium ferricyanide were obtained from EM Science. All reagents were used as received.

All titrations were monitored using a platinum loop electrode. In some early experiments, the humic acid was physically isolated from the indicator electrode by a dialysis membrane, while in some other experiments the indicator and reference electrodes were in direct contact with the humic acid solution. Under alkaline conditions, both types of experiments yielded comparable results, showing that for the condition of our experiments (pH 9.0), humic acid does *not* foul the electrode surface [27]. Accordingly, all potentiometric experiments described in this paper involved a platinum electrode in direct contact with the analyte solution.

Gold wire, 0.25 mm in diameter and of 99.9% purity, used for both working and auxilliary electrodes in the voltammetric measurements, was purchased from Aldrich. Gold was used instead of platinum for the voltammetry work because it provides fewer interferences due to oxidation of the working electrode, in the range of potentials scanned in this work [28–30]. Voltammograms were initiated at 0.0 V and scanned from −0.68 to +0.68 V vs. SCE. The scan rate was 500 mV/s. The reference electrode used in both potentiometric and voltammetric cells was a Fischer Scientific saturated calomel electrode (SCE).

Buffered solutions of the humic acid (pH 5.0, 6.0, 7.0, 8.0, 9.0 and 11.0) were prepared and filtered through a 0.45-μm pore size membrane at concentrations of 0.05, 0.10, 0.15 and 0.20 g/l. Commercially prepared buffers (pH-Hydrion) were employed. The buffers for pH 5.0, 6.0 and 7.0 were mixtures of sodium and potassium phosphate. Buffers for pH 8.0 and 9.0 were mixtures of sodium phosphate and sodium borate. The pH 11 buffer was a mixture of sodium carbonate and sodium bicarbonate. Potassium chloride (0.1 M) was used as the supporting electrolyte. Synthetic mixtures consisting of 4 and 5 phenolic components were also prepared. A 5-component solution that was 2.0×10^{-4} M in each of catechol, pyrogallol, resorcinol, hydroquinone and gallic acid was prepared at pH 9.0 and 11.0. A 4-component unbuffered solution that was 2.5×10^{-4} M in each of catechol, pyrogallol, resorcinol and hydroquinone was prepared at pH 6.0. The latter solution (discussed in the final section of this paper) was also used in a series of pH-monitored titrations. Buffered solutions, each consisting of an *individual* model phenol were also prepared. The results for titrations of the single component analyte solutions were compared to those of the synthetic mixtures.

All titrations were carried out in a Forma Scientific model 1025 anaerobic chamber, consisting of an atmosphere of 95% N_2 and 5% H_2. The 5% H_2 served to reduce traces of O_2 over a palladium catalyst. All solutions were purged with pure N_2, and allowed to equilibrate with the atmosphere of the chamber for at least 2–3 h (usually overnight) prior to use. Aliquots of ferricyanide solution were delivered using a glass syringe. In all titrations, the reaction mixture was stirred continuously and equilibrated for 12 h between successive additions of titrant (preliminary experiments conducted at pH 8.0 suggested that the reaction was not equilibrated after 4 h). All electrodes were stored inside the anaerobic chamber when not in use. The platinum electrodes were treated with aqua regia between titrations, and then soaked in de-ionized water. The electrodes were periodically checked in Light's solution [31]. All titrations were carried out at ambient temperature, which ranged from 22 to 27°C.

In addition to monitoring solution potential, we employed simultaneous pH and potential monitoring in the titration of some unbuffered solutions of both humic acid and the 4-component model phenolic mixture. In these experiments, an unbuffered synthetic mixture (pH 6.0) and humic acid solution (pH 5.72) were titrated with $Fe(CN)_6^{3-}$ and monitored using both platinum and pH electrodes. The pH measurements were made using an Orion combination pH electrode. A digital mV/pH Orion voltmeter was used for all pH and potential measurements. All mV measurements are reported relative to the SCE (246 mV).

Cyclic voltammograms (CVs) of the humic acid were obtained from a 3.0 g/l solution prepared at pH 9.0. CVs were measured using a Princeton Applied Research (PAR) Model 173 potentiostat and Model 179 digital coulometer, with a Model 175 Universal Programmer. The instrument was connected to a PAR Model RE0074 X–Y recorder. The sensitivity and proper functioning of the instrument were verified by reproducing published voltammograms of the ferri/ferrocyanide redox couple. CVs of several discrete hydroquinones and reducing sugars were measured in addition to those of the humic acid, for comparison. All voltammograms were collected at ambient temperatures (23–25°C). Recorded CVs were digitized and transferred to an IBM computer using Sigmascan@software. Solutions were purged with helium prior to the collection of a CV. All sample scans were preceded by a scan of the blank supporting electrolyte. For each experi-

ment, several successive scans were taken of both the sample and the supporting electrolyte solution. The amount of working electrode surface area exposed to the analyte solution was held constant between measurements of the background and sample solutions by using equal volumes of solution, and by not disturbing the position of the electrodes when changing samples. The gold electrodes were cleaned prior to each experiment by dipping the gold wires into aqua regia, and then sonicating them for about 5 min in deionized water.

3. Results and discussion

Fig. 1 illustrates ferricyanide titrations for a fixed concentration of humic acid at different values of pH. Curves for the titration of humic acid at a single pH (pH 9.0), but for varying analyte concentrations are illustrated in Fig. 2. The changing shape of the curves in Fig. 1, and the occurrence of a single discrete endpoint in ferricyanide titrations of humic acid conducted at pH 9.0 and 11.0 (Figs. 1 and 2), are of primary interest in the analysis of these data.

The reactions of phenols with one-electron-transfer oxidizing agents such as potassium ferricyanide are complex, consisting of numerous dimerization and oxidative coupling processes [32–34]. These reactions are especially facile following formation of the phenoxide ion under alkaline conditions [35,36]. While humic substances are known to contain several types of functional groups, there are a number of features of the titration curves in Figs. 1 and 2 which suggest that the ferricyanide titration of humic acid at pH 9.0 involves the oxidation of the phenolic component of that material.

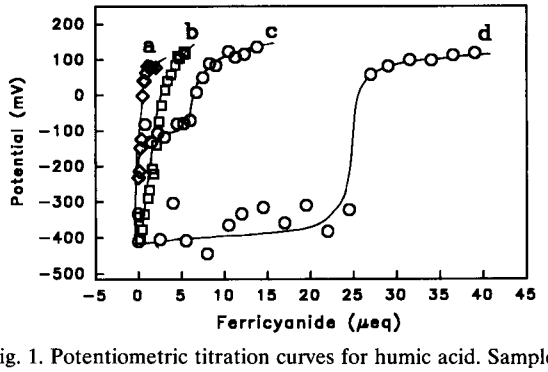

Fig. 1. Potentiometric titration curves for humic acid. Sample: 30 ml of 0.15 g/l humic acid in 0.1 M KCl buffered at: pH: (a) 5.0; (b) 7.0; (c) 9.0; (d) 11.0.

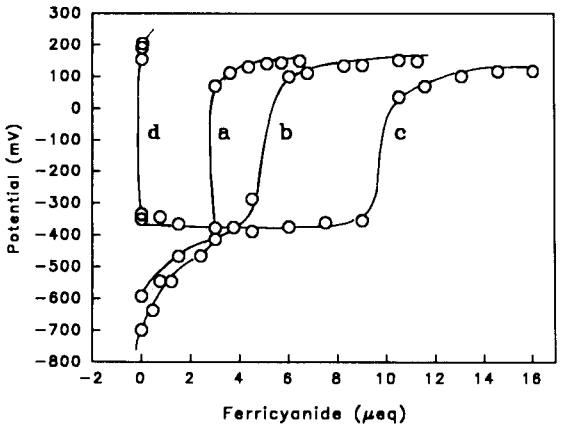

Fig. 2. Potentiometric titration curves for humic acid buffered at pH 9.0 in 0.1 M KCl. Sample: 30 ml of (a) 0.05 g/l; (b) 0.10 g/l; (c) 0.20 g/l; (d) blank buffer solution.

Early electron spin resonance (ESR) spectroscopic studies of humic acids from a variety of sources have attributed ESR signals to quinone and hydroquinone-like moieties [37,38]. More recent research has confirmed the existence of quinones in some soil-derived humic acids, by means of hydroxyl amine derivatization in conjunction with ^{13}C NMR spectroscopy [39]. In this work, we note that the titration curves for a synthetic mixture of phenols and hydroquinones display features in common with those obtained from titration of a peat humic acid. In fact, the synthetic phenolic mixture (Fig. 3) mimics the observed behavior of humic acid (Fig. 1) remarkably well.

3.1. Effect of pH on the ferricyanide titration of humic acid

Changes in pH produce several interesting effects in the ferricyanide titration of humic acid. Adjustment of pH to values of 9.0 and above leads to the production of a more well defined titration curve, i.e., a clearly defined "poised"

region followed by a discrete inflection. The recording of a single discrete endpoint (Figs. 1 and 2) in the titration of a mixture as complex as that of humic acid is unusual. The use of alkaline conditions, as will be discussed in the following sections, appears to be an important factor in producing this effect. There are three important observations relating to Figs. 1 and 2: (1) the negative shift in the potentials of the redox active components in humic acid with increase of pH (Fig. 1); (2) the ability of humic acid to stabilize the measured potentials in the pre-equivalence point region of the titration curve (Figs. 1 and 2); and (3) an increase in the *apparent* reducing capacity of the humic acid with increasing pH.

Negative shifting of potentials

The appearance of an inflection and a distinctly measurable apparent reducing capacity at pH 9.0, but not at lower pH values (Fig. 1), is consistent with the fact that for many discrete di- and polyphenols, ionization constants for the first hydroxyl (pK_1) are near 9.0, and that it is the ionized form of these phenolic species which is strongly reducing [40]. The formal potentials of several natural hydroxy quinones are known to decrease with increasing pH, where the nature and magnitude of that decrease is related to their pK_1 and pK_2 values [41]. Kinetic studies of the ferricyanide oxidation of phenols suggest that it is the phenoxide ion, rather than the undissociated phenol, that is electron releasing [40].

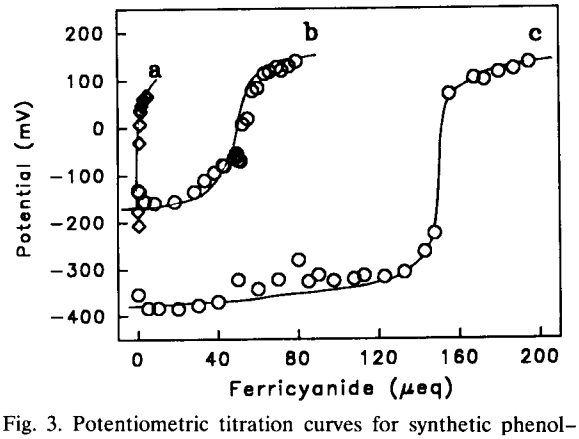

Fig. 3. Potentiometric titration curves for synthetic phenol–hydroquinone mixtures in 0.1 M KCl. Sample: 30 ml of (a) 4-component mixture at pH 6.0: (b) 5-component mixture buffered at pH 9.0; (c) 5-component mixture buffered at pH 11.0.

Table 1
Values of $E°$ (V), pK_1 and pK_2 for components in the synthetic mixtures from Martell and Smith (1974) [42], Clark (1960) [43], Ball and Chen (1933) [44], Fieser and Peters (1931) [45] and Fieser (1930) [46]

Compound	$E°$	pK_1	pK_2
Hydroquinone	+0.699	9.85	11.39
Gallic acid [a]	+0.799	8.70	11.45
Pyrogallol	+0.713	8.94	11.08
Catechol	+0.792	9.40	12.80
Resorcinol	+1.043	9.30	11.06

[a] pK_1 and pK_2 are for phenolic hydroxyl groups only.

Table 1 lists values of pK_1, pK_2 and $E°$ for a series of di- and triphenols used in the preparation of the two model synthetic mixtures. The $E°$ values of these phenols (measured under strong acid conditions) [43–45] are considerably higher than the $E°$ of the $Fe(CN)_6^{3-}/Fe(CN)_6^{4-}$ couple showing that the *individual* compounds will not be oxidized by $Fe(CN)_6^{3-}$ under acidic conditions. However, it is important to recognize that for a mixture of phenols, interactions among those species may result in the formation of new couples with different values of $E°$. This is especially true for mixtures prepared under neutral and alkaline conditions.

Curves produced from the titration of the synthetic mixtures at pH 6.0, 9.0 and 11.0 are shown in Fig. 3. The titration curves for the synthetic mixtures, and their variation with pH, are very similar to those of the humic acid (Figs. 1 and 2), suggesting that a mixture of phenolic compounds *can* be used to model the redox behavior of humic acid. The negative shifting of potentials in the pre-equivalence point region of the titration, for titrations of both the synthetic mixture (Fig. 3) and humic acid (Fig. 1) at pH 9.0 and 11.0, relative to that at lower pH values, is consistent with the above-described trend for the known behavior of several monomeric quinone and phenolic compounds.

It should be noted that, even though the synthetic mixture consisted of five components with $E°$ values differing by more than 300 mV (Table

1), the titration curves (curves b and c, Fig. 3) resemble that of a single component system. Several factors contribute to this behavior: (1) under alkaline conditions, the formal potentials of the individual components become increasingly negative compared to that for the $Fe(CN)_6^{3-}/Fe(CN)_6^{4-}$ couple so that differences among formal potentials for individual couples in the analyte mixture are small relative to that of the $Fe(CN)_6^{3-}/Fe(CN)_6^{4-}$ couple; (2) each component is present at a small stoichiometric concentration; and (3) under alkaline conditions (pH 11.0 and higher), the individual components interact chemically in a complex manner giving rise to various other products (discussed later in this paper). For these reasons, the pre-equivalence point region of the titration curve becomes smeared out, and contributions from individual components in the mixture are not discernable. These effects would also pertain to the considerably more complex mixture in humic acid, and could account for the discrete shape of the titration curve of humic acid under alkaline conditions.

"Poising" due to humic acid

The regularity of the potential measurements in the region of the half-titration point is an important consideration for titrations of humic acid conducted at pH 9 and 11 (Figs. 1 and 2). We suggest that quinonoid and phenolic constituents in the humic acid may be contributing to the stability of the measured potentials in this region of the titration curve. While we do not know the nature or structure of any individual redox couple(s) in humic acid, we suggest that under alkaline conditions, *especially* at pH 9.0, these components can produce a steady state mixed potential, and that the discrete shape of the titration curves obtained at pH 9.0 is due, in part, to this effect. It is known that the rate of heterogeneous electron transfer for the quinone/hydroquinone redox couple at platinum electrodes is highest for the monophenolate form of the species ($k = 160$ cm s^{-1} for the monophenolate and 0.0016 cm s^{-1} for the diphenolate) [47]. The rate is lowest for the fully protonated form. The high degree of stability for potential measurements in the pre-equivalence point region, for titrations of humic acid conducted at pH 9.0 (Figs. 1 and 2) is thus consistent with known heterogeneous kinetics of the quinone/hydroquinone redox couple [47].

The cyclic voltammogram produced from a solution of humic acid (Fig. 4), demonstrates that at pH 9.0, humic acid can produce a measurable exchange current. The scans, beginning and ending at 0 V vs. SCE, were reproducible in either direction. The potential range for the CV in Fig. 4 is limited, and there is no resolution of individual waves. However, the scan shows considerable anodic and cathodic current above that of the supporting electrolyte. The CV in Fig. 4 *cannot* be interpreted as being chemically reversible. The anodic oxidation of phenols under alkaline conditions is known to be a one-electron-transfer process, resulting in dimerization of those species at the working electrode surface [48]. A CV very similar to that of the humic acid was produced from the 5-component synthetic mixture at pH 9.0. The existence of phenols in the peat humic

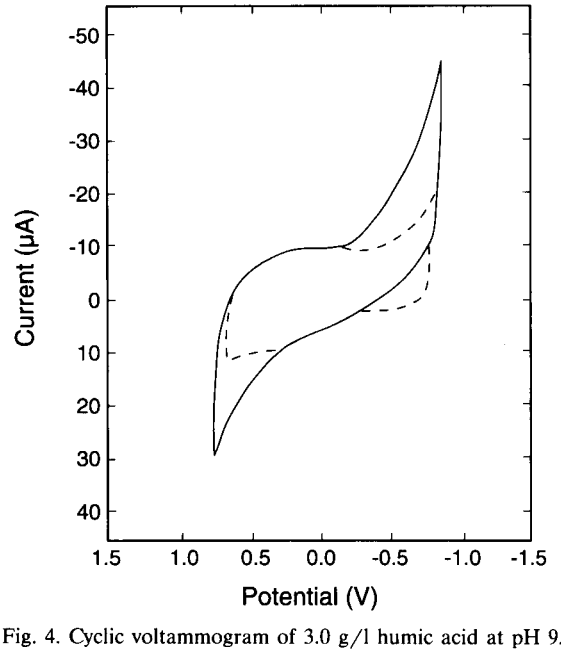

Fig. 4. Cyclic voltammogram of 3.0 g/l humic acid at pH 9.0 in 0.5 M KCl; Dotted line: background electrolyte. Solid line: humic acid.

acid used in this work has been confirmed by solid state ^{13}C NMR spectroscopy [26].

While we have some evidence that a solution of humic acid at pH 9.0 can affect the measured potential at an "inert" potentiometric monitoring electrode, we cannot explain the difference in the magnitude of the pre-equivalence point potentials for curve c in Fig. 2 (ca. −350 mV), and those for the pH 9.0 curve in Fig. 1 (ca. −100 mV). Preliminary studies have shown that the concentration of the humic acid plays an important role in our ability to successfully titrate the material. Where the concentration of *reversible* redox active moieties in humic acid is presumed to be low compared to other functionality, one must titrate a high enough concentration of the analyte *as a whole* in order to obtain sufficient poising due to those moieties, and due to the added $Fe(CN)_6^{3-}/Fe(CN)_6^{4-}$ couple [27]. We are currently examining the effect of humic acid concentration, as well as the relative contributions of both the humic acid and the $Fe(CN)_6^{3-}/Fe(CN)_6^{4-}$ redox couple to the pre-equivalence point potentials.

The measured potentials in the "post-equivalence point" region of the titration curve, for titrations of humic acid and the synthetic mixture at pH 9.0 and 11.0 are in close agreement to the $E°$ of the $Fe(CN)_6^{3-}/Fe(CN)_6^{4-}$ redox couple. These potentials ranged from 95 to 110 mV vs. SCE.

Reducing capacity of the humic acid

The ferricyanide titration of a synthetic mixture of phenolic compounds at pH 9.0 (Fig. 3, curve b) yielded a single endpoint and an apparent reducing capacity that was consistent with a two-electron-transfer oxidation of each of the individual phenolic compounds in the mixture (i.e., 60 μeq $Fe(CN)_6^{3-}$ added to 30 μmoles of the phenolic mixture at the inflection). The apparent reducing capacity of the synthetic mixture at pH 11.0 was in considerable excess of that of a 2-electron-transfer oxidation of components in the analyte mixture. The increased consumption of $Fe(CN)_6^{3-}$ at pH 11.0 may be explained in terms of a higher concentration of phenoxy radicals and increased oxidative coupling. The dimerization of phenoxy radicals is an irreversible process. Tautomerization of the coupled product results in regeneration of phenolic hydroxyl groups, which may undergo further oxidation (Fig. 5) [32,34–36]. The mechanism for the oxidative coupling of di- and polyphenols as induced by alkaline ferricyanide has been studied [35,36]. An example of these processes is given in Fig. 5, where it is shown that successive one-electron transfer oxidations of the mono-anion of catechol may give rise to the oxidation products B (with resonance forms B′ and B″) and C. The species B″ then dimerizes to give compound D and its tautomer E. Compound E is chemically similar to the original starting material A, and can undergo a series of one-electron oxidations, the first of which is shown, to produce the free radical F. Thus, the product is recycled, and the oxidative process continues beyond that of a stoichiometric two-electron transfer.

The apparent reducing capacity of the humic acid, as determined by ferricyanide titration is 1.73 meq/g at pH 9.0 (Fig. 2, curve d). Values determined from several experiments (at pH 9.0) ranged from 1.58 to 1.73 meq/g. A value of 5.50 meq/g was obtained for the titration at pH 11.0 (Fig. 1). Because humic acid contains aliphatic and carbohydrate-like structures which can be oxidized by potassium ferricyanide at pH 11.0 but not at pH 9.0 and because of the more complex

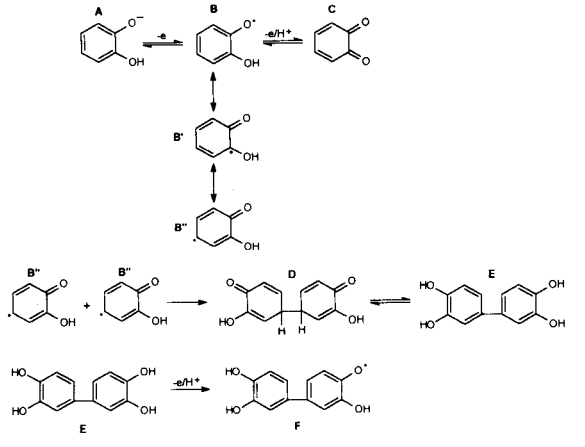

Fig. 5. Proposed mechanism for the oxidative coupling of phenols as induced by alkaline ferricyanide.

reactions of phenols at higher pH values, we suggest that the titration at pH 9.0 yields a more quantitative estimate of the reducing capacity as exerted by species such as hydroquinones and polyphenols [27]. The quantitative nature of the titration of the synthetic mixture at pH 9.0 is in support of this contention. The range of values for the apparent reducing capacity of the humic acid at pH 9.0 is within the range of estimates of the phenolic hydroxyl content of other humic acids, as determined by ^{13}C NMR spectroscopy [49].

3.2. Titration of unbuffered solutions

In the stoichiometric one-electron-transfer oxidation of a discrete hydroquinone by potassium ferricyanide at low pH, one can expect the number of equivalents of added $Fe(CN)_6^{3-}$ to equal that of the protons released upon oxidation as illustrated in the following equation:

$$QH_2 + 2Fe(CN)_6^{3-} \rightarrow Q + 2H^+ + 2Fe(CN)_6^{4-} \quad (1)$$

where QH_2 and Q represent hydroquinone and quinone species, respectively. We have used simultaneous pH and potential monitoring to demonstrate this effect in the titration of unbuffered solutions of a 4-component synthetic mixture of phenols and quinones, and solutions of humic acid under acidic conditions (Fig. 6).

Fig. 6A illustrates the simultaneous behavior of pH and potential for the ferricyanide titration of the unbuffered four-component synthetic mixture (gallic acid was excluded from the mixture so that pH measurements would not be affected by dissociated carboxylic acid functional groups). The analyte mixture was adjusted to pH 6.0 prior to the start of the titration. The steep rise in potential following the addition of the first two aliquots of ferricyanide might suggest that there was no reaction between titrant and analyte. However, the sharp drop in pH upon addition of $Fe(CN)_6^{3-}$ confirms that a fraction of the analyte mixture was oxidized. The pH and potential measurements level off following the addition of about 1 μeq of $Fe(CN)_6^{3-}$ (Fig. 6A). The number of equivalents of *observed* released protons, as determined from pH measurements (without correction for activity), and the number of equivalents of added ferricyanide after addition of the second aliquot of titrant (point A, Fig. 6A) are listed in Table 2. Considering the complexity of the system, these values are in reasonable agreement with the stoichiometry of reaction 1.

The application of this type of experiment to humic acid (Fig. 6B) is made more complex by the presence of carboxylic acid groups, a dominant functionality in humic acid which can be

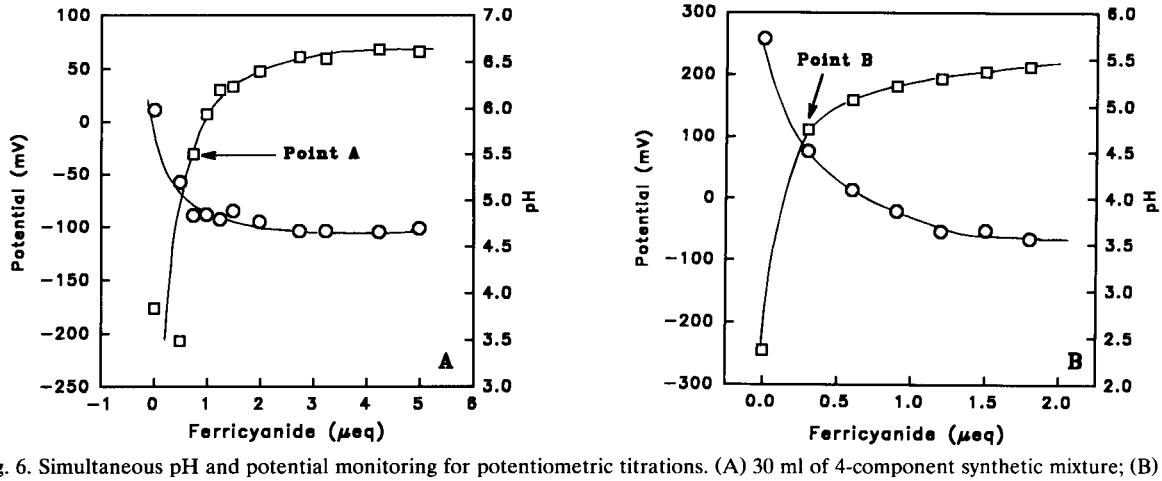

Fig. 6. Simultaneous pH and potential monitoring for potentiometric titrations. (A) 30 ml of 4-component synthetic mixture; (B) 30 ml of 0.15 g/l humic acid; (□) potential, (○) pH.

Table 2
Observed equivalents of H^+ released and $Fe(CN)_6^{3-}$ consumed at indicated points in the titration of humic acid and the four-component synthetic mixture

Sample	$Fe(CN)_6^{3-}$	Equiv. H^+	Fraction titrated [a]
Synthetic mixture (Fig. 6A)	7.3×10^{-7}	5.0×10^{-7}	0.012
Humic acid (Fig. 6B)	6.06×10^{-7}	8.6×10^{-7}	–

[a] Fraction of the synthetic mixture titrated; equivalents $Fe(CN)_6^{3-}$/total equivalents in the mixture.

expected to exert a buffering effect on pH measurements. The trends displayed by the humic acid (Fig. 6B) and the synthetic mixture (Fig. 6A) are very similar. These results further strengthen our hypothesis that a synthetic phenolic mixture can be used to model the redox behavior of humic acid. Values for the number of equivalents of protons released vs. $Fe(CN)_6^{3-}$ consumed following addition of the first aliquot of ferricyanide (point B, Fig. 6B) are listed in Table 2.

For the ferricyanide titration of humic acid and the synthetic mixture under acidic conditions (starting at pH 5.0–6.0), the measured *apparent* reducing capacity is very small when compared to that determined at pH 9.0. Table 2 shows the fraction of the synthetic mixture that was oxidized at Point A (relative to that for a stoichiometric two-electron transfer oxidation). The existence of *some* reducing capacity under acidic conditions may be of significance, i.e., the small capacity (at low pH) may be due to reversible species alone. At low pH, the formal potentials of reversible systems such as pyrogallol and hydroquinone, as determined from polarographic measurements, are much lower than those of species such as resorcinol and phenol whose heterogeneous electron transfer processes are irreversible [21]. Accordingly, we have found that individual species such as pyrogallol and catechol react readily with potassium ferricyanide at pH 6.0 and 7.0, whereas resorcinol reacts minimally under those conditions. While we have not fully evaluated the behavior of a *mixture* of these species, such differences in pH-dependent reactivity could lead to methods for quantifying the hydroquinone portion of the phenolic fraction of humic substances.

3.3. Redox behavior of synthetic mixtures

The ability to model the ferricyanide titration of humic acid with that of a synthetic phenolic mixture is important. However, we note that the composition of the mixture plays a role. That the 4- and 5-component mixtures contained *both* hydroquinones and non-quinonoid phenols is significant. Hydroquinones alone are highly reactive, and their titration at pH 9.0 does not yield a stoichiometric result. Conversely, individual non-quinonoid phenols, and mixtures of phenols and hydroquinones can be quantitatively titrated at pH 9.0. Careful study of model phenolic mixtures may lead to improved understanding of the mechanisms involved in the titration reaction and provide additional insight into the redox properties of humic substances themselves.

Acknowledgments

We thank Dr. Carl Koval of the University of Colorado at Boulder for helpful discussions. This work was supported, in part, by a Grant-in-Aid from Sigma Xi.

References

[1] F.H. Frimmel and R.F. Christman, in F.H. Frimmel and R.F. Christman (Eds.), Humic Substances and Their Role in the Environment, Wiley, Chichester, 1988, pp. 1–2.
[2] F.J. Stevenson and J.H.A. Butler, in G. Eglinton and M.T.J. Murphy (Eds.), Organic Geochemistry, Springer Verlag, New York, 1969, pp. 534–557.
[3] G.R. Aiken, D.M. McKnight, R.L. Wershaw and P. MacCarthy, in G.R. Aiken, D.M. McKnight, R.L. Wershaw and P. MacCarthy (Eds.), Humic Substances in Soil, Sediment and Water: Geochemistry, Isolation and Characterization, Wiley, Chichester, 1985, pp. 1–12.
[4] T.D. Waite, in P. MacCarthy, M.H.B. Hayes, R.L. Malcolm and R.S. Swift (Eds.), Humic Substances III: Interactions with Metals, Minerals and Organic Chemicals, Wiley, Chichester, 1995, in press.
[5] A. Comminoli, J. Buffle and W. Haerdi, J. Electroanal. Chem. 110 (1980) 259.
[6] M.R. Lindbeck and J.L. Young, Soil Sci., 101 (1966) 366.

[7] A.F. Cody, S.R. Milliken and C.R. Kinney, Anal. Chem., 27 (1955) 362.
[8] D.S. Orlov, Humus Acids of Soils, Moscow Univ. Publishers, Moscow, 1985, pp. 235–236.
[9] M. Szilagyi, Soil Sci., 115 (1973) 434.
[10] S.A. Wilson and J.H. Weber, Chem. Geol., 26 (1979) 345.
[11] S.A. Visser, Nature, 204 (1964) 581.
[12] M. Spiro, Chem. Soc. Rev., 15 (1986) 141.
[13] J.O'M. Bockris and A.K.N. Reddy, Modern Electrochemistry, Vol. 2, Plenum Press, New York, 4th edn., 1973, pp. 1104–1105.
[14] I.M. Kolthoff and C.S. Miller, J. Am. Chem. Soc., 62 (1940) 2171.
[15] G.P. Power and I.M. Ritchie, J. Chem. Educ., 60 (1983) 1022.
[16] F.M. Hawkridge and T. Kuwana, Anal. Chem., 45 (1973) 1021.
[17] E. Antonini, J. Wyman, M. Brunori and J.F. Taylor, J. Biol. Chem., 239 (1964) 907.
[18] T.E. Friedemann, C.W. Weber and N.F. Witt, Anal. Biochem., 4 (1962) 358.
[19] A. Srivastaya, A.K. Singh, B. Singh and B. Krishna, Proc. Indian Natl. Sci. Acad. Part A, 48 (1982) 236.
[20] N.G. Moskovtsev and E.I. Chupka, Khim. Drev., 4 (1977) 67.
[21] H. Musso, Angew. Chem. Int. Ed., 2 (1963) 723.
[22] T.A. Geissman and D.H.G. Crout, Organic Chemistry of Secondary Plant Metabolism, Freeman, Cooper and Co., San Francisco, CA, 1969, Chap. 14.
[23] P. MacCarthy, Ph.D. Thesis, University of Cinncinati, 1975.
[24] K.Y. Khalaf, P. MacCarthy and T.W. Gilbert, Geoderma, 14 (1975) 331.
[25] P. MacCarthy, H.B. Mark, Jr. and P.R. Griffiths, J. Agric. Food Chem., 23 (1975) 600.
[26] R.L. Malcolm and P. MacCarthy, Environ. Sci. Technol., 20 (1986) 904.
[27] R.S. Helburn, Ph.D. Thesis, Colorado School of Mines, Golden CO, 1991.
[28] I.M. Kolthoff and N. Tanaka, Anal. Chem., 26 (1954) 632.
[29] F. Bauman and I. Shain, Anal. Chem., 29 (1957) 303.
[30] R.N. Adams, Electrochemistry at Solid Electrodes, Marcel Dekker, New York, 1969, pp. 191–194.
[31] T.S. Light, Anal. Chem., 44 (1972) 1038.
[32] H. Musso, in W.I. Taylor and A.R. Battersby (Eds.), Oxidative Coupling of Phenols, Marcel Dekker, New York, 1967, pp. 1–94.
[33] P.D. McDonald and G.A. Hamilton, J. Am. Chem. Soc., 95 (1973) 7752.
[34] B.S. Thyagarajan, Chem. Rev., 58 (1958) 439.
[35] M. Bhattacharjee and M.K. Mahanti, Indian J. Chem., 22 (1983) 634.
[36] M. Battacharjee and M.K. Mahanti, Polish J. Chem., 58 (1984) 1099.
[37] R.W. Rex, Nature, 188 (1960) 1185.
[38] C. Steelink and G. Tollin, Biochim. Biophys. Acta, 59 (1962) 25.
[39] K.A. Thorn, J.B. Arterburn and M.A. Mikita, Environ. Sci. Technol., 26 (1992) 107
[40] R. Stewart, Oxidation Mechanisms, W.A. Benjamin Inc., New York, 1964, Chap. 6.
[41] S.A. Petrova, M.V. Kolodyazhny and O.S. Ksenzhek, J. Electroanal. Chem., 277 (1990) 189.
[42] A.E. Martell and R.M. Smith, Critical Stability Constants, Plenum Press, New York, 1974.
[43] W.M. Clark, Oxidation–Reduction Potentials of Organic Systems, The Williams and Wilkins Co., Baltimore, MD, 1960, Chap. 14.
[44] E.G. Ball and T.T. Chen, J. Biol. Chem., 102 (1933) 691.
[45] L.F. Fieser and M.A. Peters, J. Am. Chem. Soc., 53 (1931) 793.
[46] L.F. Fieser, J. Am. Chem. Soc., 52 (1930) 5204.
[47] J.Q. Chambers, in S. Patai and Z. Rappoport (Eds.), The Chemistry of Quinonoid Compounds, Vol. 2, Part 1, Wiley, Chichester, 1988, pp. 719–757.
[48] F.J. Vermillian, Jr. and I.A. Pearl, J. Electrochem. Soc., 111 (1964) 1392.
[49] D. Folan, Ph.D. Thesis, Colorado School of Mines, Golden, CO, 1990.

ELSEVIER

Analytica Chimica Acta 295 (1994) 273–282

ANALYTICA CHIMICA ACTA

Determination of organophosphorus and carbamic pesticides with an acetylcholinesterase amperometric biosensor using 4-aminophenyl acetate as substrate

C. La Rosa, F. Pariente, L. Hernández, E. Lorenzo *

Departamento de Química Analítica y Análisis Instrumental, Universidad Autonoma de Madrid, Cantoblanco, Madrid 28049, Spain

Received 3rd January 1994; revised manuscript received 15th April 1994

Abstract

Organophosphorus and carbamic pesticides have been determined with an amperometric acetylcholinesterase-based 4-aminophenyl acetate biosensor. The glassy carbon enzyme membrane covered electrode poised at +250 mV (vs. sodium chloride saturated calomel electrode) oxidizes the 4-aminophenol formed in the hydrolysis of 4-aminophenyl acetate by acetylcholinesterase in the glutaraldehyde cross-linked layer. The activity of acetylcholinesterase is inhibited in the presence of pesticides. The decrease in activity of the enzyme is monitored by the 4-aminophenyl acetate sensor and is correlated to the concentration of pesticide present in solution. The influence of the acetylcholinesterase loading and the acetylcholinesterase to neutral protein (bovine serum albumin) ratio on the biosensor response was studied and the measuring conditions including pH, substrate concentration, and others were optimized. Detection limits of 4.0 and 13.0 nmol l^{-1} for paraoxon and carbaryl, respectively, were achieved with a 3-min preincubation time.

Keywords: Amperometry; Biosensors; Enzymatic methods; Pesticides

1. Introduction

Organophosphorus and carbamates represent a large number of pesticides. Because of their low persistence and high effectiveness, they are widely employed in agriculture. Their mode of action has been ascribed to their ability to inhibit acetylcholinesterase [1]. These pesticides exhibit fairly high acute toxicity, thus, sensitive, rapid and reliable detection and determination of these toxic substances are very important for protection of the environment and human health. The determination of these molecules in residues can be performed by various chemical methods [2]. The techniques most widely used are gas chromatography, liquid chromatography and spectroscopy [3–6]. However, methods which identify simple compounds in complex matrices and reach detection limits compatible with those imposed by law for pesticide residues in the environment, generally require tedious extraction and clean-up procedures prior to instrumental analysis and, thus,

* Corresponding author.

SSDI 0003-2670(94)00192-0

are not very suitable for routine analysis. Enzymatic methods based on the inhibition of acetylcholinesterase activity have recently been the object of intense investigation due to their sensitivity and specificity. In addition, their use can be coupled to various analytical techniques by the use of different substrates. The inhibition of this enzyme has been determined by gas chromatography [7] and by electrochemical methods [8,9]. Biosensors, for the detection of the above mentioned compounds, based on acetylcholinesterase (AChE) or cholinesterase (ChE) activities as molecular recognition elements, can be combined with a variety of transducers. Thus, pH electrodes [10–14], and pH-sensitive ion-selective field effect transistors (ISFETs) [15], spectrophotometric [16,17] and fluorimetric [18], voltammetric [19] and piezoelectric [20] systems have been investigated. When ChE or AChE is used in conjunction with choline oxidase, the resulting enzyme system can be linked with O_2 or H_2O_2 probes, thus providing an amperometric sensor suitable for analysis for pesticides [21–23]. When acetyl- or butyrylthiocholine (BTCh) is chosen as substrate, the thiocholine produced in the enzymatic reaction can be anodically oxidized on platinum [24,25], mercury [19] or chemically modified carbon-paste electrodes [26]. In the same way, if a substance, which gives an electroactive compound as product of the enzymatic reaction, is chosen as substrate of AChE, the enzymatic activity can be followed by the oxidation or reduction of the enzymatic reaction product. Indeed many enzymatic activities have been measured in vitro by using non-natural substrates.

In previous work [27] we demonstrated that 4-aminophenyl acetate (PAPA) represents an improved substrate for the determination of esterase activities via oxidation of 4-aminophenol (PAP), the product of the enzymatic reaction. Furthermore, the response time, pH response, linear range, kinetic parameters and other features of an amperometric biosensor based on immobilized AChE using PAPA as substrate were described. In this work we describe the possibility of extending this approach to inhibition studies of esterase activities by xenobiotic agents and the application of this inhibition for the determination of several organophosphorus and carbamate pesticides.

2. Experimental

2.1. Reagents

Acetylcholinesterase (EC 3.1.1.7; type III) from electric eel was purchased from Sigma as a solution containing 5 mg of ammonium sulfate per mg of protein and 0.8 IU per μl of solution. This enzyme preparation was stored frozen at −20°C. The stability of the enzymatic activity was excellent when frozen. 4-Nitrophenyl acetate (PNPA) (M_r 181.15) was purchased from Aldrich and PAPA was synthesized by catalytic hydrogenation of the nitro group of PNPA as described below. PAP was purchased from Merck. Glutaraldehyde (grade I, 25% aqueous solution) was obtained from Sigma and stored below 0°C. Nylon filter meshes of 150 μm pore size were obtained from Nytal. 2-Pyridinealdoxime methiodide (2-PAM) was purchased from Aldrich, Steinheim. Deionized water from Milli-Q and Milli-RO systems (Millipore) was used to prepare all solutions. Pesticide preparations of carbofuran, carbaryl, benomyl and parathion were obtained from Aragonesas (Madrid), and Paroxon was obtained from Aldrich. All other chemicals were of analytical reagent grade and were used as received.

2.2. Preparation of 4-aminophenyl acetate

In a previous article [27] we described a method to synthesize PAPA based on the selective reduction of the nitro group of PNPA using $SnCl_2 \cdot 2H_2O$ as reductant. After reduction the product was obtained by extraction with ethyl acetate and several additional steps to clean this extract. Here we report on an improved synthesis of PAPA by catalytic hydrogenation of PNPA [28]. Two gram of PNPA were dissolved in 75 ml of distilled and dry ethyl acetate, 276 mg of Pd/C catalyst (Aldrich No. 20,569-9) were added to the solution in a thick-walled vessel. The vessel was attached to a hydrogen shaker for 90 min The catalyst was filtered from the solution and the solvent was

removed by rotary evaporation. The pale yellow solid was stored at 4°C. The yield was 80 mol%. The purity of PAPA prepared was checked by paper chromatography.

2.3. Samples

Determinations on ecologically important matrices were carried out on water from a spring near Madrid sampled by the authors. Spring water samples were stored at 4°C and analyzed without prior treatment.

2.4. Instrumentation and procedures

Cyclic voltammetric and chronoamperometric studies were carried out with a BAS 100 voltammetric analyzer. Glassy carbon, obtained from BAS, was used as the working electrode and a platinum wire served as the auxiliary electrode. All potentials are referenced to a sodium chloride satured calomel electrode (SSCE).

The 4-aminophenyl acetate biosensor was constructed by placing a 6.0 mm diameter enzyme membrane disc, prepared as previously described [27], over a base-activated glassy carbon electrode [29] and fixing it with an O-ring.

The activity of free AChE was determined in the absence of pesticides by cyclic voltammetry in 0.1 M phosphate buffer with 1.0 mM PAPA. When measuring the inhibition, the reaction was started by addition of 0.33 IU ml^{-1} of enzyme into the buffer solution containing the required concentrations of pesticide. The enzymatic constants, I_{max} and apparent K_m (K'_m), were obtained from Lineweaver–Burk reciprocal plots [27] or by fitting the experimental data to Michaelis–Menten kinetics using a non-linear regression fitting program. The enzyme–inhibitor and enzyme–substrate–inhibitor complex breakdown constants (K_i and K_I) were obtained from the secondary plots [30].

Two methods were employed in the determination of pesticides using AChE biosensors. The experiments were done in 5 ml of 80 mM sodium phosphate buffer (pH = 7.9) at 25°C. In the first, the sensor was placed in the buffer solution at an applied potential of 0.25 V and the background current was allowed to decay to a steady-state value. After the addition of 1.2 mM PAPA and stirring for 10 s the resulting current from the oxidation of PAP reached a steady state (I_{ss}) within 1 min. The addition of a sample containing pesticide followed and the resulting steady-state current decrease was measured. The second method was based on a preincubation step of the biosensor in the presence of inhibitor in a stirred solution at open circuit for 1–3 min Afterwards, the biosensor was removed from the preincubation solution, rinsed briefly, placed in the measurement cell countering 1.2 mM PAPA and the steady-state current was recorded. The percentage inhibition was calculated according to:

$$I(\%) = 100(I_{ss1} - I_{ss2})/I_{ss1}$$

where I_{ss1} is the initial steady-state current and I_{ss2} the steady-state current reached after the addition of a determined amount of inhibitor or after the preincubation of biosensor with inhibitor.

A method to reactivate the inhibited enzyme, described by Schwedt and Hauck [31], was modified. Immediately after use the enzyme membrane was immersed in a reactivation solution (24.8 mg of 2-pyridinealdoxime methiodide in 100 ml of phosphate buffer) for at least 4 h. After washing in buffer for at least 2 h the enzyme membrane was ready to be used again.

3. Results and discussion

3.1. Enzymatic hydrolysis of PAPA in the presence of pesticides

The catalytic activity of free AChE using PAPA as substrate in the presence or absence of pesticides can be followed in solution by cyclic voltammetry since the peack current is proportional to the bulk concentration of an electroactive species [32]. For the oxidation of PAP, the slope obtained from a plot of i_p vs. bulk concentration (33 μA μmol^{-1} cm^{-3}) is in excellent agreement with the value calculated from the Randles–Sevcik equation for an electrode with a geometric area of 0.071 cm^2, a diffusion coefficient of 7.9×10^{-6}

$cm^2\ s^{-1}$, with two electrons involved in the electrochemical reaction [33] and a scan rate of 0.05 $V\ s^{-1}$ [27]. Based on these results, the peak current obtained at different times can be related to the amount of PAP generated by the enzymatic hydrolysis of PAPA. Fig. 1 shows the time evolution of the enzymatic reaction obtained at several carbaryl concentrations. Similar results were obtained for organophosphorus pesticides such as paraoxon or parathion (data not shown). The experimental data can be fitted to a first-order kinetic equation. The pesticide acts, in a form dependent on concentration, by decreasing both the initial rate and the horizontal asymptotic values. These results are in agreement with a gradual diminution of active enzyme concentration due to the formation of a dead-end complex with the inhibitor. The exponential decrease in the initial rate is showed in Fig. 2 and the linear dependence of this rate on the logarithm of pesticide concentration is displayed in the inset. These results were particularly useful for construction of amperometric biosensors based on the inhibitory effect of these pesticides, since, for kinetically controlled biosensors, the steady-state current is proportional to the initial rate of the enzymatic process [34].

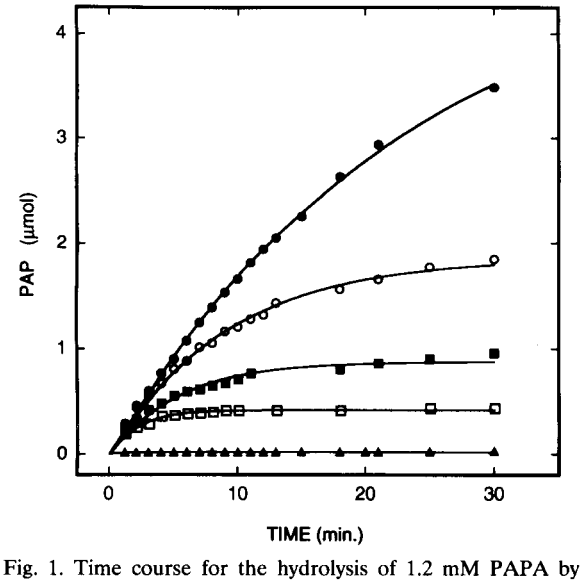

Fig. 1. Time course for the hydrolysis of 1.2 mM PAPA by free AChE in the absence of inhibitors (●) or in the presence of the following carbaryl concentrations: (○) 2.6, (■) 8.0, (□) 26.0 and (▲) 80.0 µM. All reactions were carried out in 0.1 M phospate buffer solution, pH 7.9, and started by addition of 1.0 IU of AChE.

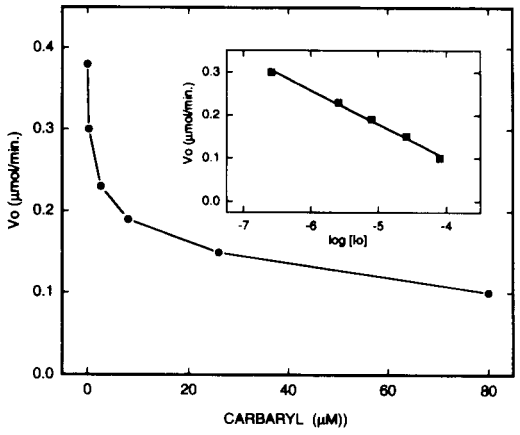

Fig. 2. Effect of carbaryl on the initial rate (V_0) of 1.2 mM PAPA hydrolysis by 1.0 IU of free AChE in 0.1 M phosphate buffer, pH 7.9. Insert: linear decrease of V_0 values with the logarithm of molar concentration of carbaryl [I_0].

3.2. Optimization of enzyme layer

For stationary enzyme electrodes, Mell and Malloy [34] have shown, through digital stimulation, that the steady-state current is determined by the proper balance of the catalysis rate of the enzyme on one hand and the diffusion rate of the substrate on the other. In enzymatic biosensors for analytical applications, diffusion control of the response is preferred, since it provides a wide linear working range. Diffusional limitations are usually achieved by using enzyme layers containing high loading of protein and enzymatic activity. In enzyme-inhibition based biosensors, kinetic control of the response is preferred since the signal will be proportional to the non-inhibited enzyme activity present. Generally, these conditions can be obtained using enzyme layers with low protein content and low enzyme activity [35]. Here, the enzyme layer has been prepared by immobilization of AChE activity in a nylon filter mesh using glutaraldehyde as cross-linker and bovine serum albumin (BSA) as inert protein supplier of amino groups to increase the stability

of the immobilized enzyme. The BSA content and the loading of enzyme activity were optimized during the immobilization process. The influence of the AChE/BSA ratio on the voltammetric response to PAP is shown in Fig. 3. There was an increase of up to 250 μg in protein content, followed by a sharp decrease, which was probably due to unfavorable thickness of the enzyme layer. The influence of AChE loading on the sensitivity to substrate is shown in Fig. 4. An increase in the biosensor response to substrate and I_{max} (Fig. 4, insert) were observed for enzyme layers containing high loading of activity. The apparent K_m value also increased with the enzyme activity immobilized in the mesh (see Fig. 4, insert). This result indicates that diffusional barriers are present in membranes with high enzyme content. However, kinetic control and high sensitivity, especially for low concentrations of inhibitor, were achieved for sensors containing low loading of activity. Thus, subsequent measurements were made with layers prepared from 200–250 μg of BSA and 0.6–1.2 IU of AChE. The resulting biosensor constructed with 0.6 IU of AChE has an I_{max} 3.6 ± 0.1 μA and an apparent K'_m of 1.4 ± 0.1 mM. This K'_m value is very similar to that obtained for the enzyme in solution [27] as would be expected for biosensors with kinetic control of the response and without diffusional impediments.

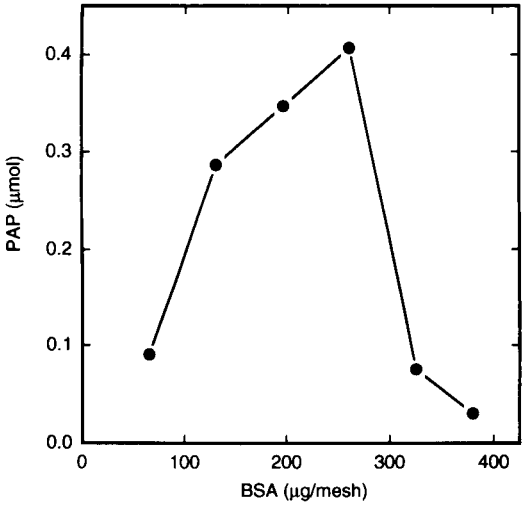

Fig. 3. Influence of the amount of BSA in the AChE membrane on the voltammetric response to PAP generated during enzymatic hydrolysis of PAPA. AChE, 1.0 IU. Voltammograms recorded 6 min after reaction started.

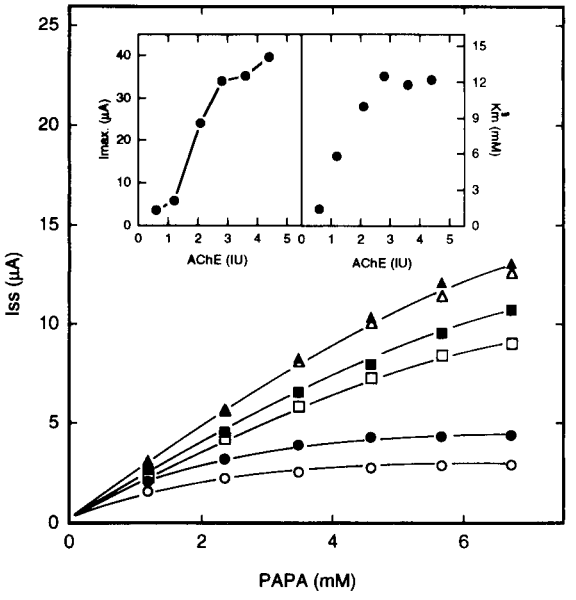

Fig. 4. Influence of AChE loadings on the steady-state current response to 1.0 mM of PAPA. AChE amounts: (○) 0.6; (●) 1.2; (□) 2.1; (■) 2.8; (△) 3.6 and (▲) 4.4 IU. 200 μg of BSA were added with the enzyme in all meshes. Inserts: dependence of I_{max} and K'_m values on the enzyme activity present in the sensor.

3.3. Optimization of enzyme electrode response

The effect of different experimental conditions was studied, in order to optimize the biosensor response in the presence or absence of pesticides. PAPA shows redox activity only above +0.4 V with an anodic peak potential around +0.6 V, whereas PAP shows redox activity below +0.2 V with an anodic peak around +0.05 V. The hydrodynamic voltammograms for PAPA and PAP using a glassy carbon electrode with and without an AChE containing membrane are shown in Fig. 5. It can be seen that whilst the oxidation of PAP is not affected by the substrate, a decrease of 20–30% in the electrochemical response is observed when the electrode is covered with the enzyme membrane. A potential of 0.25 V was selected for further amperometric measurements since it is

sufficiently low to minimize possible interferences.

The acetylcholinesterase activity can be greatly influenced by the pH and nature of the buffer system. Therefore, phosphate, Tris and borate buffers were tested. The best enzyme activity was found for phosphate buffer. There was an increase in the steady-state current with increasing buffer concentration up to 0.1 M and then leveled off. The pH range studied was 6.0 to 9.0. The optimum pH region for inhibition was found to be from 8.0 to 8.5. This pH range is similar to that which generates optimal response of the biosensor to substrate [27] and to that obtained with the enzyme in solution.

The stability of the response to substrate of immobilized AChE is presented in Fig. 6. For all enzyme loadings assayed, the sensor response decreases during the first or second use, which is probably due to loss of enzyme molecules weakly attached to the filter mesh. After these initial uses, the sensor response to substrate remains constant for at least 40 days.

When the biosensor was treated with pesticides, the resulting enzyme–inhibitor bond cannot be broken with water, but more nucleophilic reagents, such as 2-pyridinealdoxime methiodide, are able to reactivate the inhibited enzyme layer

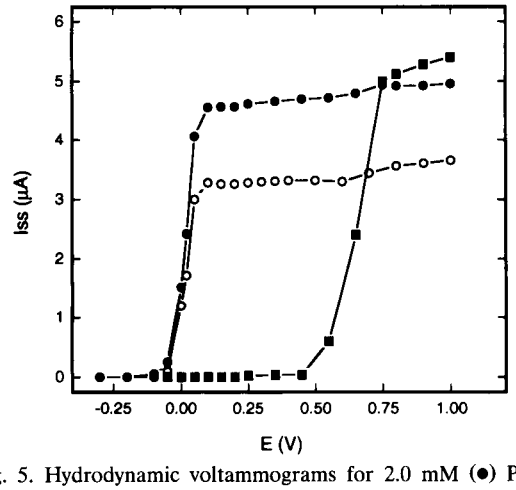

Fig. 5. Hydrodynamic voltammograms for 2.0 mM (●) PAP and (■) PAPA obtained at a bare glassy-carbon electrode and (○) PAP at an AChE (1.2 IU/300 μg^{-1} of BSA) biosensor in 0.1 M phosphate buffer, pH 7.9.

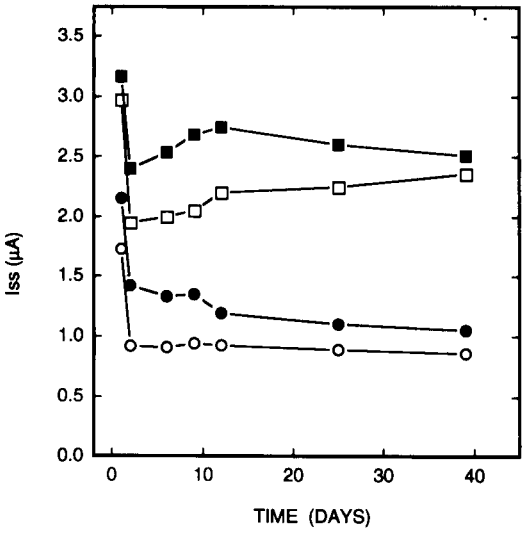

Fig. 6. Influence of AChE loadings on the stability of the biosensor response to 1.2 mM PAPA. Immobilized AChE activity: (○) 0.6; (●) 1.2; (□) 3.6; and (■) 4.4 IU containing 200 μg of BSA. After use the grits with the immobilized enzyme were stored at 4°C in phosphate buffer solution suplemented with 0.01% of sodium azide.

[36]. Thus, subsequent utilizations of enzyme membranes, after pesticide treatment, are possible if they are reactivated before use. However, after three times, the steady-state current response of the biosensor to substrate shows a 40% decrease. This is probably due to a progressive denaturation of AChE molecules induced by the reactivation procedure.

3.4. Determination of pesticides and mechanism of inhibition for organo-phosphorus and carbamates

The mechanism of chemical action of organophosphorus and carbamates on AChE is well established [37]. On one hand, the hydrolysis of organophosphorus by the enzyme blocks the active center in a substrate independent manner. On the other hand, carbamates compete with the substrate for the active center and their inhibitory effect can be prevented in the presence of high concentrations of substrate [38]. Based on these mechanisms, two approaches to the analysis of these pesticides with AChE sensors can be made based on inhibition in the presence of substrate

or on preincubation of the biosensor with the inhibitor. The study of the type of inhibition thatcarbaryl and paraoxon present in our system for each approach, is most important in the establishment of experimental conditions for pesticide determinations.

In the preincubation approach, the incubation time is an important parameter in order to obtain reproducible results. The relationship between inhibition and preincubation time was obtained by the Aldridge equation [39]:

$$\log(100/a) = K_2[\mathrm{I}]t$$

where a is the percentage of inhibition, K_2 is the bimolecular rate constant for inhibition [35], [I] is the concentration of inhibitor and t is the preincubation time. It is evident that the degree of inhibition is dependent on incubation time and this fact is often used to make detection more sensitive. Thus, analyses are performed for long incubation periods (10–60 min) [12,21]. In our system, at a fixed concentration of pesticide, the degree of inhibition increases with the incubation time. However, for incubation times over five minutes, the increase in inhibition becomes negligible. Here, 3–5 min incubations with samples were used.

Fig. 7A shows the steady-state current response for various concentrations of substrate in the presence of carbaryl. Lineweaver–Burk reciprocal plots were constructed for each concentration of inhibitor (Fig. 7B). Under these conditions, carbaryl shows a competitive inhibition with an apparent K_i of 0.44 ± 0.02 μM. When the AChE sensor was preincubated with carbaryl the steady-state current response to substrate and the reciprocal plots were quite different (Fig. 8). In this case, the inhibition becomes non-competitive with an apparent K_i of 0.47 ± 0.03 μM. The inhibitor produces a dead-end complex with the enzyme that minimizes the competitive effect of substrate. In both cases the apparent K_i is very similar and the reciprocal plots are linear. This fact is indicative of a kinetic control of the sensor response. For paraoxon, the steady-state current responses obtained for inhibition in the presence of substrate or with preincubation are very similar (see Fig. 9). In both cases a decrease in I_{max}

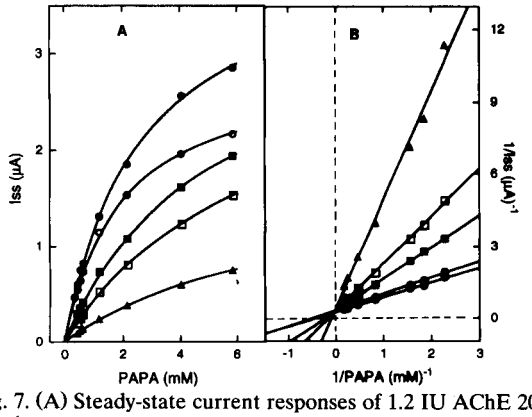

Fig. 7. (A) Steady-state current responses of 1.2 IU AChE 200 μg^{-1} BSA sensor to (●) 1.2 mM substrate and in the presence of several carbaryl concentrations: (○) 0.01; (■) 0.89; (□) 2.6 and (△) 16.0 μM. (B) Lineweaver–Burk reciprocal plots constructed with the data of Fig. 7A. All measurements were done in 0.08 M phosphate buffer solution, pH 7.9.

and K_m values in a manner dependent on inhibitor concentration was observed. This behaviour is typically observed in systems with mixed inhibition. The reciprocal plots have good linearity (indicative of kinetic control) and cross below the x-axis, which is indicative of an inhibition pattern intermediate between non-competitive and uncompetitive. The inhibitor binds to enzyme

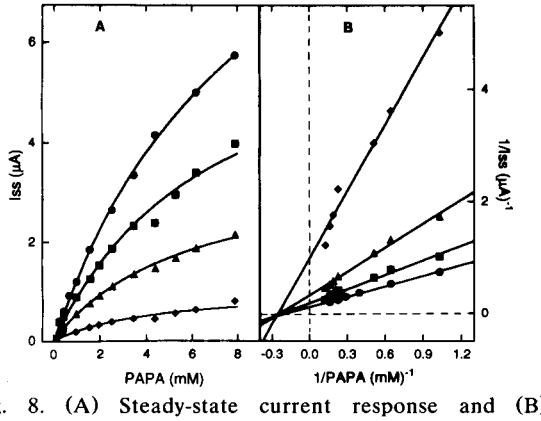

Fig. 8. (A) Steady-state current response and (B) Lineweaver–Burk reciprocal plots for a sensor similar to that described in Fig. 7 preincubated for 3 min in a solution containing the following carbaryl concentrations: (●) control without pesticide; (■) 0.026; (▲) 0.26 and (◆) 2.6 μM. The electrode reponse was obtained in a 1.2 mM substrate in 0.08 M phosphate buffer solution, pH 7.9.

molecules or to enzyme–substrate complexes. The apparent K_i for breakdown of the enzyme–inhibitor complex is 0.53 ± 0.05 μM and the apparent K_I for breakdown of the enzyme–substrate–inhibitor complex is 0.14 ± 0.08 μM.

For pesticide determinations with the AChE biosensor both approaches, inhibition in the presence of substrate and preincubation of the biosensor with inhibitor, were compared. Calibration graphs for paraoxon and carbaryl are shown in Fig. 10. As was expected the preincubation method exhibited the lowest detection limits (defined as the concentration of inhibitor required to obtain 5% of inhibition). An amount as low as 4.0 nmol l^{-1} of paraoxon can be measured with only three minutes of preincubation. This sensitivity is comparable to literature data [12,21,40] for this pesticide, but in all cases at least 10 min preincubation were necessary. Thus, enhanced sensitivity or throughput is achieved here.

For carbaryl the detection limit with the preincubation method was 13.0 nmol l^{-1}. However, for the method based on inhibition in the presence of substrate, the detection limit was dramatically decreased by about 60-fold when compared to the one above. The differences in the detection limits reached using one approach vs. the other were not so marked for paraoxon as for carbaryl,

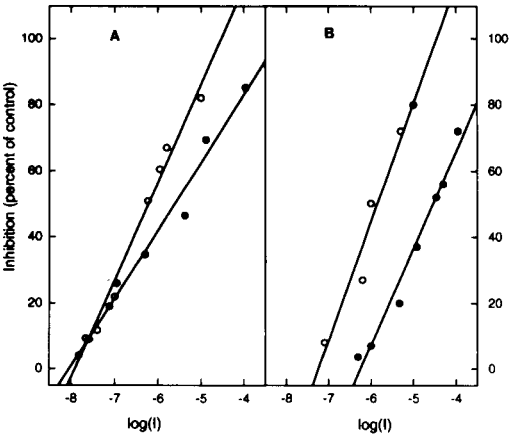

Fig. 10. Calibration plot of percentage inhibition, $I\%$, vs. decimal logarithm of molar concentration of pesticide, $\log(I_0)$, for (●) carbaryl and (○) paraoxon. Calibrations were done with a 1.2 IU AChE 200 μg^{-1} BSA sensor in phosphate buffer pH 7.9 under the following conditions: (A) preincubation (3 min) with pesticide and subsequent measurement in the presence of 1.2 mM PAPA, and (B) incubation in the presence of 1.2 mM of PAPA (30 s) prior to pesticide addition.

which is in accord with a mixed inhibition as determined earlier.

The accuracy of this sensor was tested for five consecutive assays of 1.0 μM l^{-1} of paraoxon using the same AChE membrane. The relative standard deviation calculated was less than 5%.

3.5. Applicability of the AChE sensor

The application of the proposed AChE biosensor was focused on the analysis of ecologically important matrices, like spring waters containing high degree of salinity and organic material. The samples were spiked with increasing concentrations of carbaryl or paraoxon for analysis. The method based on a preincubation of the biosensor for 3 min in 5 ml of samples containing the inhibitors was used. The response of non-inhibited AChE was evaluated in 1.2 mM PAPA in 0.1 M phosphate buffer. Under these conditions, the enzyme acts as a highly specific sensor to its inhibitors independent of the nature of the sample submitted to analysis. Binding of pesticide to protein is completed in a few minutes and persis-

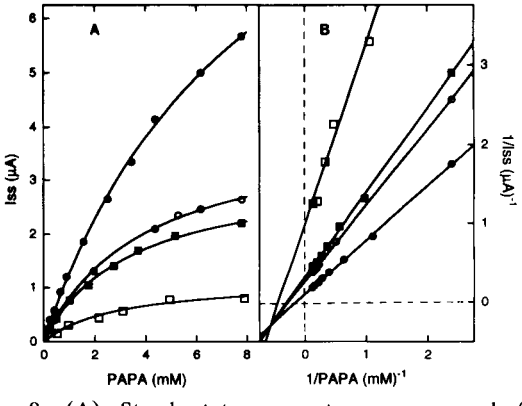

Fig. 9. (A) Steady-state current response and (B) Lineweaver–Burk reciprocal plots of 1.2 IU AChE 200 μg^{-1} of BSA sensor to 1.2 mM substrate (●) and in presence of paraoxon: (○) 0.026; (■) 0.5 and (□) 1.0 μM. All measurements were done in 0.08 M phosphate buffer solution, pH 7.9.

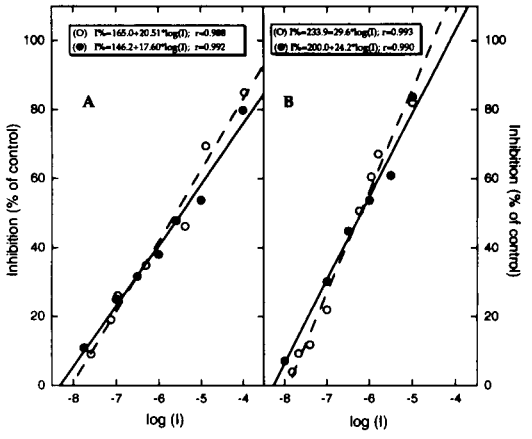

Fig. 11. Comparative response of AChE biosensor preincubated in (○) 0.1 M phosphate buffer or (●) in a real sample of spring water, both doped with (A) carbaryl or (B) paraoxon. Samples were preincubated for 3 min at room temperature. The electrode response was recorded in 1.2 mM PAPA in 0.1 M phosphate buffer (pH 8.0). An electrode response of 1.87 μA obtained from the controls without pesticide was used in the inhibition percentage calculations. The values presented in the figure were the average of three different experiments for each pesticide.

tent after the washing steps. The results of such experiments are displayed in Fig. 11. We have observed that the electrode response obtained for a control sample (preincubation in spring water without pesticides) and a blank sample (preincubation in phosphate buffer without pesticides) are very similar, indicating absence of AChE inhibitors in the original sample. When the pesticides were added to the sample, significant and remarkable percentages of inhibition were obtained with values very close to those presented in the calibration graphs of Fig. 10. Detection limits of the method in these experiments are similar to those previously mentioned and we can detect 9.5 and 8.8 nmol l^{-1} of carbaryl and paroxon in real samples, respectively. Electrochemical interferents present or added to these samples, such as ascorbate, did not exhibit remarkable variation in the biosensor response, due to specific binding of AChE with its inhibitors. For example, AChE biosensors preincubated in spring waters doped with 10 mM of ascorbate shows a response, in the presence of 1.2 mM PAPA, similar to the controls and no decrease in the percentage of inhibition, when pesticides are present, was observed. In the same way, the presence of organic material, such as proteins or nucleic acids, do affect neither the response of AChE immobilized on grits nor the percentage of inhibition obtained in the presence of pesticides. In the case of measurements where the preconcentration procedure could not be used, a detailed study of interferent compounds would be necessary. Nevertheless, biosensors based on the measurement of PAP generated as product of the enzymatic reaction, whose oxidation potential is reasonably lower than the more common interfering electroactive compounds in biological samples, as ascorbate or urate, have been previously described, and their excellent response in the presence of the mentioned interferents is broadly documented [41–43]. Furthermore, the possibility of having a molecule immobilized in nylon grits (0.1 mm thickness and 5 mm diameter), highly specific to organophosphorus and carbamic pesticides, makes this arrangement useful for preincubations in situ and after transfer of the samples to the laboratory for the analysis.

At the moment the AChE biosensors are being used in a flow-injection analysis arrangement for the construction of a continuously working monitoring system for pesticides.

Acknowledgements

This work was supported by the Comunidad Autónoma de Madrid, through the grant No. 199/92. The authors acknowledge Dr. H.D. Abruña for his contributions in critically reading this manuscript, Dr. P. Prados for her kind help in the PAPA synthesis and the NATO Scientist Program.

References

[1] I.R. Corbett, The Biochemical Mode of Action of Pesticides, Academic Press, New York, 1974, p. 540.
[2] K.A. Mc Cully, J. Assoc. Off. Anal. Chem., 64 (1981) 401.
[3] J.S. Scherma, Manual of Analytical Quality Control for Pesticides and Related Compounds in Human and Environmental Samples, EPA-600/2-81-059.

[4] G.R. Pieper, Bull. Environ. Contam. Toxicol., 22 (1979) 167.
[5] A. Ambrus, J. Lantos, B. Visi, I. Cslatos and L. Sarvari, J. Assoc. Off. Anal. Chem., 68 (1985) 1095.
[6] J.J. Blama and P.J. Jacksdn, J. Assoc. Off. Anal. Chem., 64 (1981) 733.
[7] J. Kovac, V. Markova and P. Králik, J. Chromatogr., 100 (1974) 171.
[8] G. Baum and F. Ward, Pesticides and Chemistry, Proc. of the International Congress on Pesticides and Chemistry, Vol. 4, Gordon and Breach, New York, 2nd end., 1971, pp. 215–225.
[9] M. Granmer and A. Peolpes, Anal. Biochem., 55 (1973) 255.
[10] P. Durand, J. Mallevialle and J.M. Nicand, J. Anal. Toxicol., 8 (1984) 112.
[11] C. Tran-Minh, Ion-Sel. Electrodes Rev., 7 (1985) 41.
[12] C. Tran-Minh, P.C. Pandey and S. Kumaran, Biosensors Bioelectron., 5 (1990) 461.
[13] S. Kumaran, H. Meir, A.M. Danna and C. Tran-Minh, Anal. Chem., 63 (1991) 1914.
[14] S. Kumaran and C. Tran-Minh, Anal. Biochem., 200 (1992) 187.
[15] K.R. Rogers, M. Foley, S. Alter, P. Koga and M. Eldefrawi, Anal. Lett., 24 (1991) 191.
[16] R. Kindervater, W. Kunnecke and R.D. Schmid, Anal. Chim. Acta, 234 (1990) 113.
[17] M.F. Leon-Gonzalves and A. Townshend, Anal. Chim. Acta, 236 (1991) 267.
[18] K.R. Rogers, C.J. Cao, J.J. Valdes, A.T. Eldefrawi and M. Eldefrawi, Fundam. Appl. Toxicol., 16 (1991) 810.
[19] E.P. Medyantseva, G.K. Budnikov and S.S. Babkina, Zh. Anal. Khim., 45 (1990) 1386.
[20] G.G. Guilbault and J. Ngeh-Ngwainbi, in G.G. Guilbault and M. Mascini (Eds.), NATO ASI Ser. C. Mathematical and Physical Sciences, Vol. 226, Reidel, Dordrecht, 1989, p. 187.
[21] M. Bernabei, C. Cremisini, M. Mascini and G. Palleschi, Anal. Lett., 24 (1991) 1317.
[22] L. Campanella, M. Achilli, M.P. Sammartino and M. Tomassetti, Bioelectrochem. Bioenerg., 26 (1991) 237.
[23] U. Wollenberger, K. Setz, F. Sheller, U. Loffer and W. Gopel, Sensors Actuators B, 4 (1991) 257.
[24] L.H. Goodson and W.B. Jacobs, Methods Enzymol., 44 (1976) 647.
[25] R. Gruss, F. Sheller, M.J. Shao and C.C. Liu, Anal. Lett., 22 (1989) 1159.
[26] P. Skládal, Anal. Chim. Acta, 269 (1992) 281.
[27] F. Pariente, L. Hernández and E. Lorenzo, Anal. Chim. Acta, 273 (1993) 399.
[28] L.H. DeRiemer and C.F. Meares, Biochemistry, 20 (1981) 1606.
[29] D.M. Anjo, M. Kahr, M.M. Khodabakhsh, S. Nowinski and M. Wagner, Anal. Chem., 61 (1989) 2603.
[30] T. Palmer, in Understanding Enzymes, Ellis Horwood, New York, 1981, pp. 144–164.
[31] G. Schwedt and M. Hauck, Fresenius' Z. Anal. Chem., 331 (1988) 316.
[32] A.J. Bard and L.R. Faulkner, Electrochemical Methods: Fundamentals and Applications, Wiley, New York, 1976, p. 218.
[33] R.N. Adams, Electrochemistry at Solid Electrodes, Marcel Dekker, New York, 1969, p. 220.
[34] L.D. Mell and J.T. Malloy, Anal. Chem., 33 (1975) 299.
[35] P. Skladal and M. Mascini, Biosensors Bioelectron., 7 (1992) 335.
[36] I.B. Wilson and S. Ginsburg, Biochim. Biophys. Acta, 18 (1955) 168.
[37] M. Eto, Organophosphorus Pesticides: Organic and Biological Chemistry, CRC Press, Boca Raton, FL, 1974, pp. 131–133.
[38] R.D. O'Brien, B.D. Hilton and L. Gilmour, Mol. Pharmacol., 2 (1966) 593.
[39] W.N. Aldridge, Biochem. J., 46 (1950) 451.
[40] J.L. Marty, R. Rouillon, K. Sode and I. Karube, Biosensors '90, 2–4 May, 1990, Singapore, pp. 85–86.
[41] F. Pariente, L. Hernandez and E. Lorenzo, Bioelectrochem. Bioenerg., 27 (1992) 73.
[42] H.T. Tawg, C.E. Lunte, H.B. Halsall and W.R. Heineman, Anal. Chim. Acta, 214 (1988) 187.
[43] V.S. Razumas, J.J. Kulys and A.A. Malinauskas, Anal. Chim. Acta, 117 (1980) 387.

ELSEVIER

Analytica Chimica Acta 295 (1994) 283–286

ANALYTICA CHIMICA ACTA

Ag^+-sensitive ISFET with a chemically modified silica surface

A. Bouazizi [a,*], H. Maaref [a], N. Jaffrezic-Renault [b]

[a] *Laboratoire de Physique des Semiconducteurs, Département de Physique, Faculté des Sciences de Monastir, 5000 Monastir, Tunisia*
[b] *Laboratoire de Physico-chimie des Interfaces, U.R.A CNRS 404, Ecole Centrale de Lyon, BP163, 69131 Ecully Cedex France*

Received 17 December 1993; revised manuscript received 29 March 1994

Abstract

An Ag^+-sensitive ion-selective field effect transistor (ISFET) is prepared by deposition of the copolymer cyanopropyl methyl (10–12%)–dimethylsiloxane (88–90%) on the silica gate insulator. The corresponding REFET (reference field effect transistor) is prepared by deposition of polymethyl hexyl siloxane onto the silica gate insulator. The response of the differential system is 51 mV pAg^{-1} in the pAg range of 1 to 3 and 4.3 mV pH^{-1} in the pH range of 3 to 8. The response time is lower than 1 s and the life time more is than one month.

Keywords: Sensors; Ion-selective field effect transistors (ISFET); Silver-sensitive ISFET

1. Introduction

Good selectivity for silver detection was obtained with chemically modified field-effect transistors with plasticized PVC membranes on macrocyclic thioethers [1].

Previous work has shown that it is possible to obtain Ag^+-sensitive ion-selective field effect transistors (ISFETs) by grafting cyanopropyl groups directly on the silica gate insulator surface [2]. ISFETs developed according to this process have long life times. A sub-Nernstian response was also obtained, however. Interpretation in terms of low grafting density of surface sites was performed via the modified site-binding model.

The aim of this work is to present a simple and fast procedure to realize a ChemFET to detect silver ions by adsorption of a cyanopropylsiloxane copolymer on the silica gate insulator of an ISFET. This polymer contains cyanopropyl groups which will avoid leaching of the ion-sensitive group from the polymeric membrane. The high density of cyanopropyl ensures that a Nernstian response is obtained for the silver ion.

The Ag^+-sensitive ISFET was realized together with a REFET (reference field effect transistor) and the performances of the differential system were determined [3].

2. Experimental

2.1. The ISFET

The ISFETs were produced at CIME (Grenoble, France). The N-MOS planar type technology was used to manufacture the ISFETs [4].

* Corresponding author.

SSDI 0003-2670(94)00214-7

2.2. Individual measurements

Each ISFET was connected to a specially developed amplifier system allowing the source voltage (V_s) to be measured while the drain current (I_d) and the drain voltage (V_d) remained constant. Source and substrate were also connected. V_d was equal to 0.5 V and I_d to 100 mA. V_s was directly plotted on a Linear recorder. The voltage was measured against a calomel reference electrode.

2.3. Differential measurements

The experimental arrangement for differential measurements is presented in a previous paper [2]. Two ISFETs were connected to two identical amplifiers: an ISFET with an ion-sensitive polymeric membrane and a REFET with a polymeric membrane insensitive to the detected ion (Ag^+ in our case). Output signals V_s and V_s' were measured against a common platinum pseudo- reference electrode. This type of pseudo-reference electrode is used for the differential measurements because it avoids problems in silver titration which can be caused by casual anion diffusion (Cl^-). A differential amplifier also measures the difference of these two signals ($\Delta V = V_s - V_s'$).

2.4. Polymer deposition

Two commercial polymers from ABCR (Karlsruhe, Germany) were used: the copolymer cyanopropyl methyl (10–12%)–dimethylsiloxane (88–90%), and polymethyl hexyl siloxane.

The surface of the gate insulator was cleaned by dipping in a sulphochromic mixture for 3 min and then rinsed with pure water. This step allows the number of silanol groups on the Si/SiO_2 surface to be increased [2].

Samples were mounted on a horizontal rotator and the polymeric substance diluted in methylene chloride (2 wt.% of polymer in solvent) was deposited at a rotation speed of 300 rpm. The copolymer was deposited onto the ISFET and the polymethyl hexyl siloxane onto the REFET.

The homogeneity of the deposit was checked with optical microscopy. The thickness determined by weighing was about 4 mm.

2.5. Experimental conditions

pH measurements were carried out in a 2 wt.-% tris(hydroxylmethyl)aminomethane (Tris), 0.5 M KCl being added to keep a constant ionic strength. The pH was adjusted by additions of suitable quantities of HCl or KOH. pH measurements were performed in the electrochemical cell with a combined glass electrode (Solea-Tacussel) connected to a digital pH meter.

The determination of Ag^+ ion sensitivity was done in a buffer solution (0.01 M acetate–0.1 M $NaNO_3$, pH 4.3).

All measurements were performed at constant temperature (20°C) in a thermostatted electrochemical cell. The Ag^+ variations (pAg range, 1–4) were carried out by the addition of $AgNO_3$ solution in an acetate buffer. Only differential measurements using a platinum pseudo-reference electrode were performed.

3. Results and discussion

3.1. pH sensitivity

Individual measurements (cf. Fig. 1)

For the ISFET with polymethyl hexyl siloxane (REFET), the pH response is 22 mV pH^{-1} from pH 3 to 8. For the ISFET with the copolymer (cyanopropyl methyl–dimethylsiloxane), the pH response is 24.5 mV pH^{-1}. The decrease in pH

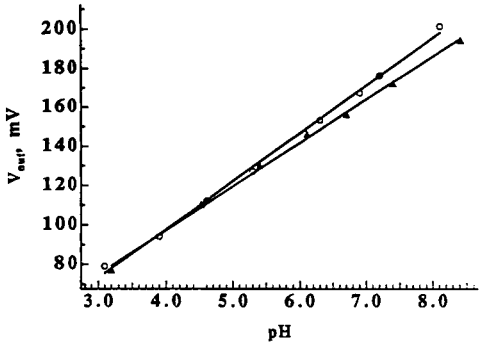

Fig. 1. Output voltage of the ISFET amplifiers (V_{out}) versus pH using the individual measurement mode. (○) ISFET with polymethyl hexyl siloxane (REFET), (▲) ISFET with copolymer (cyanopropyl methyl–dimethylsiloxane).

sensitivity compared to a classical SiO_2 ISFET is due to the disappearance of some hydroxyl groups at the SiO_2 surface, masked by the deposited polymeric substances. This change in the sensitivity is in agreement with the site binding model [5,6].

Differential measurements

The measurements were made in the differential mode. Both the FETs and reference electrode (calomel) were connected to the amplifier.

The ΔV–pH experimental results are represented in Fig. 2. The differential system shows a linear response from pH 3 to 8 with a slope equal to 4.3 mV pH^{-1}.

3.2. Ag^+ sensitivity using differential measurements

The measurements were made in the differential mode [3] and both the FETs and the pseudo-reference electrode (platinum) were connected to the amplifier.

The ΔV–pAg experimental results are represented in Fig. 3. The differential system shows a linear response from 0.001 to 0.1 M with a sensitivity of ca. 51 mV pAg^{-1}. The response time is lower than 1 s and the life time is higher than 1 month. The deterioration process of the ChemFET membrane is certainly due to the poor adhesion of this membrane on the silica gate insulator.

In Ref. [3] the response of the cyanopropyl grafted ISFET is reported to be 20 mV pAg^{-1}. This sub-Nernstian response is attributed to the low surface density of the complexing sites. In our case, the chemical modification by the cyanopropyl polymeric membrane provides a higher density of complexing sites and thus a higher response is observed..

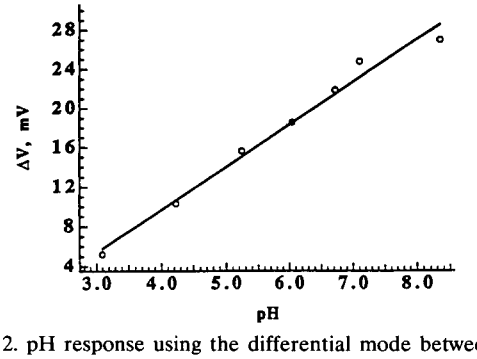

Fig. 2. pH response using the differential mode between the ISFET and the REFET.

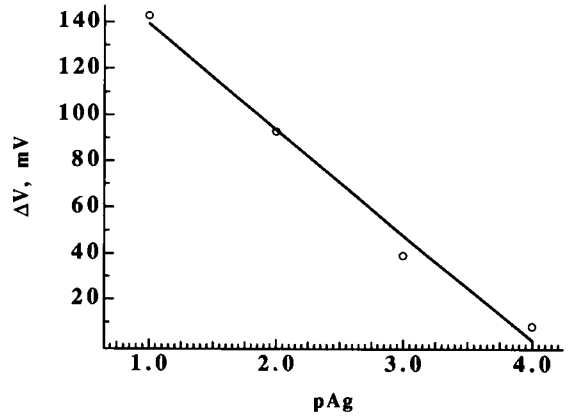

Fig. 3. Response for silver ions in the differential mode between the ISFET and the REFET.

4. Conclusion

The Ag^+-sensitive ISFET, obtained by physical adsorption of the copolymer cyanopropyl methyl (10–12%)–dimethyl siloxane (88–90%) on the silica gate insulator, shows an interesting performance when working in a differential measurement mode with a REFET. The response of the differential system is 51 mV pAg^{-1} and 4.3 mV pH^{-1}.

It is possible to apply this physical adsorption method to polymers with other ion-specific groups.

Acknowledgments

The authors thank the Region Rhone-Alpes for the financial support of the Franco-Tunisian collaboration.

References

[1] Z. Brzoaka, P.L.H.M. Cobben, D.N. Reinhoudt, J.J.M. Edema, J. Buter and R.M. Kellog, Anal. Chim. Acta, 273 (1993) 139.

[2] P. Clechet, N. Jaffrezic-renault and C. Martelet, in S. Yamauchi (Ed.), Chemical Sensor Technology, Vol. 4, Kodansha, Tokyo and Elsevier, Amsterdam, 1992, p. 205.
[3] H. Perrot, N. Jaffrezic-Renault, N.F. de Rooij and H.H. van den Vlekkert, Sensors Actuators, 20 (1989) 293.
[4] N. Jaffrezic-Renault, V. Rocher, J.M. Chovelon, P. Gentil, J. M. Terrot and J. J Fombon, Procédé de fabrication avec encapsulation, d'un capteur de type ISFET et capteur en faisant application, French Patent, 1992.
[5] D.N. Reinhoudt and E.J.R. Sudholter, Adv. Mat., 2 (1990) 23.
[6] A. van den Berg, P. Bergveld, D.N. Reinhoudt and E.J.R. Sudholter, Sensors Actuators, 8 (1985) 129.

ELSEVIER

Analytica Chimica Acta 295 (1994) 287–296

ANALYTICA CHIMICA ACTA

Reactivation of an immobilized enzyme reactor for the determination of acetylcholinesterase inhibitors Flow injection determination of paraoxon

Cándido García de María [a], Teresa Manzano Muñoz [a], Alan Townshend [b,*]

[a] *Dpto. Química Analítica, Nutrición y Bromatología, Universidad de Salamanca, Plaza de la Merced s / n 37008, Salamanca, Spain*
[b] *School of Chemistry, University of Hull, HU6 7RX, Hull, UK*

Received 23rd December 1993; revised manuscript received 12th April 1994

Abstract

A stopped-flow/flow-injection procedure is proposed for the spectrophotometric determination of paraoxon based on the inhibition of immobilized acetylcholinesterase. The irreversibly inhibited enzyme is reactivated with 1,1'-trimethylene-bis(4-formylpyridinium bromide) dioxime. The proposed procedure has a detection limit of 4×10^{-9} M, a linear calibration range of 9×10^{-9}–5×10^{-7} M, a R.S.D. of 1.6% ($n = 10$) at 5.0×10^{-8} M and a sample throughput frequency of 10 h^{-1}. The enzyme reactor can be used for more than one thousand inhibition-reactivation cycles.

Keywords: Flow injection; Spectrophotometry; Enzyme reactor; Inhibition; Reactivation; Acetylcholinesterase; Pesticides; Paraoxon

1. Introduction

The high toxicity of pesticides and their widespread use and commercial diversity have led to a large number of procedures for their detection and quantification [1]. In this sense, gas chromatography coupled with different types of detection is the technique most commonly used. In particular, organophosphorus pesticides can be analyzed by selective enzymatic procedures based on their ability to inhibit irreversibly the catalytic activity of certain enzymes such as lipase [2,3], acid and alkaline phosphatases [4], acylase [2], chymotrypsin [2] and, most frequently, cholinesterases [5–14].

From the point of view of economy and ease of handling, conventional enzymatic procedures can be dramatically improved by using immobilized enzymes [15,16] and flow methods [17]. However, procedures based on the inhibition of an immobilized enzyme have a serious drawback when the inhibition is irreversible; the immobilized enzyme gradually loses its activity and becomes useless after a few analyses. This is the case of procedures for the determination of organophosphorus pesticides by inhibition of immobilized acetylcholinesterase, and similar problems arise with

* Corresponding author.

SSDI 0003-2670(94)00183-M

sensors for pesticides based on such inhibition processes. This problem has partly been overcome by means of an exchangeable immobilized enzyme reactor where acetylcholinesterase is linked to magnetic particles which are easily replaced as the enzyme loses its activity [9]. Other authors have proposed the reactivation of the inhibited immobilized enzyme by nucleophilic agents such as pyridine-2-aldoxime methiodide (2-PAM iodide) or obidoxime [6,7,13,14,18]. The use of 2-PAM chloride for reactivation of immobilized acetylcholinesterase in a flow-injection system, after inhibition by paraoxon or carbamoylcholine was described recently [19].

The present paper describes a wider study of the reactivation of acetylcholinesterase immobilized on controlled porosity glass (CPG) after inhibition with organophosphorus pesticides such as paraoxon, parathion, parathion-methyl, guthion, fenthion and fenitrothion. Among the nucleophilic agents investigated, TMB-4 [1,1'-trimethylene-bis(4-formylpyridinium bromide) dioxime] was observed to be the most efficient reactivator. Since paraoxon showed a maximum inhibition capacity, it was chosen to illustrate the reactivation process by setting up a stopped-flow/flow-injection procedure for the spectrophotometric determination of this pesticide.

2. Experimental

2.1. Reagents

The following reagents were supplied by Sigma: controlled porosity glass, PG 240-120 (pore size 240 Å; mesh size 80–120); 3-aminopropyltriethoxysilane; glutaraldehyde, 50% w/v aqueous solution; 1-naphthyl acetate, crystalline; 1-naphthol; *p*-nitrobenzenediazonium tetrafluoroborate (Fast Red GG Salt), > 90%; 1,1'-trimethylene-bis(4-formylpyridinium bromide) dioxime (TMB-4); pyridine-2-aldoxime methiodide (2-PAM iodide); diethyl *p*-nitrophenyl phosphate (paraoxon), 95%, specific gravity 1.274; acetylcholinesterase (E.C. 3.1.1.7), type VI-S, from electric eel, 200–400 U mg^{-1}. The pesticides parathion, parathion-methyl, fenthion, fenitrothion and guthion (azinphos-methyl) were supplied by Riedel-de Haën. Other chemicals were of analytical-reagent grade. Stock solutions of each pesticide (4.40×10^{-3} M) were prepared in acetone and working solutions were prepared by dilution of the stock with water or buffer solution just before the experiments. Stock solutions of 1-naphthyl acetate (2.0×10^{-3} M in 10% aqueous acetone), Fast Red GG (1.2×10^{-3} M, aqueous) and TMB-4 (1.0×10^{-3} M, aqueous) were prepared daily. Buffer solutions were prepared from potassium dihydrogenorthophosphate and 2 M sodium hydroxide as necessary to adjust the pH to the working conditions. All stock solutions were kept refrigerated. Distilled–deionized water was used throughout.

2.2. Apparatus

The following apparatus was used: a SPD 6AV UV–visible spectrophotometric flow detector with a Chromatopac C-R5A data processor (Shimadzu), two minipuls 2-HP4 peristaltic pumps (Gilson), an L-100-1 rotary injection valve (Tecator) and a six-position selector valve (Rheodyne). A laboratory-made timer interconnected the injector and the main peristaltic pump. Standard joints (Rheodyne) and PTFE tubing of 0.5 mm i.d. were also used. A circulation thermostat and laboratory-made glass columns with outer water-circulation jackets were used to keep the enzyme reactor and the coils at constant temperature during the experiments.

2.3. Enzyme reactors

Acetylcholinesterase (AChE) was immobilized on controlled porosity glass (CPG) previously alkylaminated with 3-aminopropyltriethoxysilane and cross-linked with glutaraldehyde, as described earlier [10]. 2000 U of AChE were used per 0.5 g of CPG. Immobilized enzyme stock was kept wet in phosphate buffer (0.1 M, pH 6.0) under a toluene atmosphere at 4°C. Under these conditions, the immobilized enzyme is highly stable, maintaining almost 100% of its activity after one year of storage. Enzyme reactors were built by packing the CPG-immobilized AChE into

PTFE columns (0.8 mm i.d. and different lengths). A more homogeneous packing was achieved by submerging the columns in an ultrasonic bath for 1–2 min; this minimized the void volume and prevented the troublesome generation of bubbles in the working flow systems. When not used in the experiments, the enzyme reactors were stored wet and refrigerated.

2.4. Measurement of enzymatic activity

Enzymatic activity was measured through the catalytic effect of AChE on the hydrolysis of 1-naphthyl acetate (NA) used as substrate. As the indicator reaction, the 1-naphthol produced by the hydrolysis was made to react with *p*-nitrobenzenediazonium ions, giving rise to an addition compound which was detected spectrophotometrically. The resultant product depends on pH: at pH < 10, the compound A is produced with maximum absorbance at 440 nm ($\varepsilon = 2.8 \times 10^4$ l mol^{-1} cm^{-1}, pH ≤ 7). This reaction is faster in acidic media and is not observed at pH > 10.

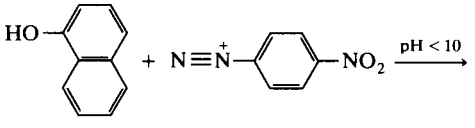

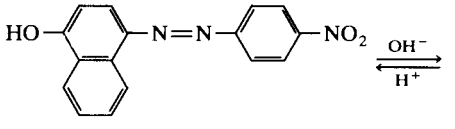

A

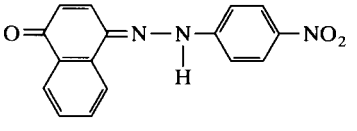

B

In a basic medium, A is slowly and reversibly transformed into compound B, which shows maximum absorbance at 560 nm ($\varepsilon = 4.0 \times 10^4$ l mol^{-1} cm^{-1} at pH ≥ 11). Compound B is stable for at least two weeks, both in aqueous solution and phosphate buffer solution. By contrast, solutions of A are not stable and within 5–10 min form a precipitate; this is soluble in sodium hydroxide solution or acetone, giving rise to solutions similar to those of B. Although B is more stable and would provide higher sensitivity than A, the detection of the latter at 440 nm and pH 7 was chosen in order to have a faster indicator reaction.

2.5. Flow system

All experiments were performed in the flow system depicted in Fig. 1. By means of a selection valve (V) coupled with the injection system (I), solutions of substrate, inhibitors and reactivators can be alternately inserted into a carrier stream (C_1) and made to pass through an enzyme reactor (IMER) packed with AChE immobilized on CPG. The flow leaving the enzyme reactor is mixed with a stream of *p*-nitrobenzenediazonium solution which is prepared in situ by confluence of an aqueous solution of Fast Red GG (C_2) and a phosphate buffer solution at pH 7.0 (C_3); this layout must be used because solutions of Fast Red GG in phosphate buffer are not stable and slowly decompose to give a brown-reddish precipitate. A timer (T) controls the stop and run periods of the main peristaltic pump (P_1) so that the injected solutions can be retained in the enzyme reactor for fixed periods of time.

Enzyme reactors with the smallest practicable size (5 × 0.8 mm i.d.) were used in all the experiments. This choice was made because in preliminary qualitative experiments, small enzyme reactors were observed to be more sensitive to low concentrations of inhibitors than reactors containing a large amount of active immobilized enzyme.

An injection volume of 100 μl was used except for those experiments where other values are specified. The flow rates of streams C_1, C_2 and C_3 were fixed at 1.00, 0.30 and 0.30 ml min^{-1}, respectively. The compositions of streams C_2 and C_3, concerning only the indicator reaction and the detection, were also fixed: a 1.2×10^{-4} M aqueous solution of Fast Red GG salt and a 0.5 M phosphate buffer solution at pH 7.0 were respectively used in all the experiments.

In the flow system described, different sets of experiments were performed. First, the variables affecting the enzymatic hydrolysis of NA were

studied. Then, the abilities of certain organophosphorus pesticides to inhibit the catalytic activity of immobilized AChE were compared. Finally, the effects of pH, temperature and some nucleophilic species were investigated as potential reactivators of inhibited immobilized AChE.

2.6. Conditions for determination of paraoxon

In the flow system described in Fig. 1, the following working conditions were used for the determination of paraoxon: enzyme reactor (IMER), 5×0.8 mm i.d.; injection volume, 100 μl; mixing coils, M_1 and M_2, 40 cm $\times$ 0.5 mm i.d.; indicator-reaction coil, R, 50 cm $\times$ 0.5 mm i.d.; stream C_1, 0.025 M phosphate buffer solution, pH 8.0, 1.0 ml min^{-1}; stream C_2, 1.2×10^{-4} M aqueous solution of Fast Red GG salt, 0.30 ml min^{-1}; stream C_3, 0.50 M phosphate solution, pH 7.0, 0.30 ml min^{-1}; substrate solution, 2.0×10^{-4} M NA in 0.025 M phosphate buffer, 1% acetone, pH 8.0; reactivating solution, 5.0×10^{-5} M TMB-4 in 0.025 M phosphate solution, pH 8.0; temperature, 25°C; detection wavelength, 440 nm.

3. Results and discussion

3.1. Enzymatic hydrolysis

The effect of pH on the catalytic hydrolysis of NA was investigated by varying the pH of stream C_1 (0.025 M phosphate solution) from 6 to 9. For each pH value, the extent of hydrolysis was evaluated by comparing the height of the peaks obtained in the continuous-flow mode when solutions (2.0×10^{-6} and 1.0×10^{-5} M) of NA and 1-naphthol were injected. For a given concentration of NA injected, the peak height was taken as a measure of the enzymatic activity. Immobilized AChE showed a maximum catalytic activity at pH 8.0.

Similar experiments performed at pH 8.0 and different temperatures indicated maximum enzymatic activity at 37–38°C. Above 40°C an irreversible fall in activity due to the denaturation of the immobilized enzyme was observed.

3.2. Enzyme inhibition

The inhibition of immobilized AChE by six organophosphorus pesticides was investigated. It had previously been established [10] that inhibition of immobilized AChE in a flow system could be monitored if inhibitor and substrate were present together in the sample, thus competing for enzyme sites. This procedure was also used in this study. The activity of the immobilized enzyme before and after the injection of a sample containing pesticide was monitored by injecting 2.0×10^{-4} M NA solution in the continuous-flow mode. The decrease in peak height was taken as a measure of enzyme inhibition.

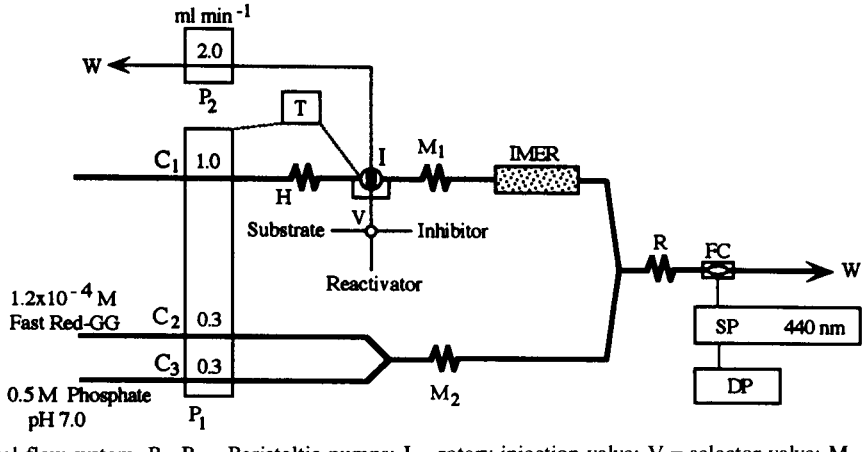

Fig. 1. Experimental flow system. P_1, P_2 = Peristaltic pumps; I = rotary injection valve; V = selector valve; M_1, M_2 = mixing coils; R = indicator-reaction coil; H = thermostatic coil; IMER = immobilized enzyme reactor; FC = flow cell (8 μl); SP = spectrophotometer; DP = data processor; T = timer; W = waste.

In preliminary experiments performed at pH 8.0 and 25°C, samples containing substrate (NA, 2.0×10^{-4} M) mixed with each pesticide (2.3×10^{-5} M) were injected and their response registered in the continuous-flow mode. Both transitory (competitive) and permanent inhibitions were observed to occur, the former being greater than the latter in all cases. The response peaks when paraoxon was used as an inhibitor are shown in Fig. 2A: when samples containing both NA and paraoxon were injected, a decrease (28%) in peak height was observed (peak b), mainly due to the competitive effect of paraoxon and substrate; however, permanent inhibition of the enzyme reactor was also produced to some extent (3%) since the initial peak height was not completely restored when samples containing only NA were next injected (peaks a').

Considering that reactivation is only necessary to remove 'permanent' inhibition, another series of experiments was performed with samples containing pesticide without NA. Using the stopped-flow mode, the samples were retained in the enzyme reactor for a fixed period of time. In these experiments, only permanent inhibition is measured. The responses obtained are illustrated in Fig. 2B for paraoxon: after the injection of the pesticide solution, enzyme activity decreases drastically, then taking a constant value for at least 150 min. Quantitative results for the pesticides investigated are summarized in Table 1.

Since paraoxon showed much the strongest inhibition, it was chosen for a study of the reactivation process. Inhibition by paraoxon was observed to be maximum at pH 8.0 and at temperatures close to 30°C (Fig. 3A and B).

The extent of inhibition increases linearly with time for at least 10 min when the paraoxon sample injected is retained in the enzyme reactor using the stopped-flow mode (Fig. 3C). A larger absolute decrease in peak height is obtained when the concentration of substrate injected is increased, although the relative decrease is almost constant for concentrations of NA $> 2 \times 10^{-5}$ M (Fig. 3D).

3.3. Enzyme reactivation

Temperature, pH and some nucleophilic reagents were investigated as potential reactivators of immobilized AChE after inhibition with paraoxon, extending the range studied previously [19]. In each experiment, performed at a fixed temperature, an immobilized enzyme reactor was first partly inhibited at pH 8.0 by injecting a 1.0×10^{-6} M solution of paraoxon which was stopped in the enzyme reactor for 1 min. The inhibited enzyme reactors thus obtained were subjected to different potentially reactivating treatments. The regeneration of enzymatic activity after the inhibition or after each treatment

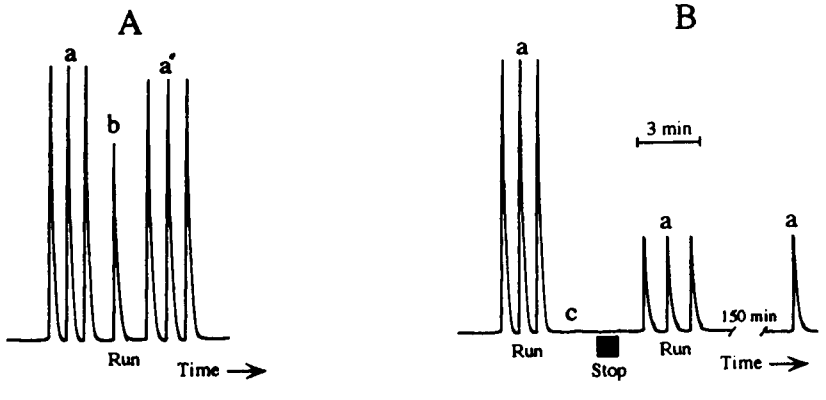

Fig. 2. Simultaneous competitive and permanent inhibition (A) and permanent inhibition alone (B) of immobilized AChE by paraoxon. Small letters indicate the injection of solutions containing (a, a') only 2.0×10^{-4} M NA; (b) 2.0×10^{-4} M NA and 2.3×10^{-5} M paraoxon; (c) only 2.3×10^{-5} M paraoxon.

was evaluated by periodically injecting 2.0×10^{-4} M NA in the continuous-flow mode.

When a set of such inhibited enzyme reactors was rinsed with a phosphate buffer solution of pH 8.0 at temperatures ranging from 15 to 40°C, no reactivation was observed in the experiments performed below 30°C; at higher temperatures, a slow recovery of enzymatic activity occurred. At 38°C, for example, about 18% of the inhibited activity was recovered after 20 min of rinsing; after 40 min, the activity reached a constant value (22% of the inhibited activity was then restored) and after 1 h it slowly decreased again, probably due to denaturation of the enzyme.

When a set of inhibited enzyme reactors was rinsed at 25°C with phosphate buffer solutions of pH ranging from 6 to 9, reactivation was not observed in any case within the first 30 min.

The reactivating effect of reagents such as fluoride, molybdate, hydroxylamine, 2-PAM iodide and TMB-4 [20] was investigated at pH 8.0 and 25°C. In the experiments, an inhibited enzyme reactor was first rinsed with phosphate buffer for 1 min. Then a 1.0×10^{-5} M or 1.0×10^{-3} M solution of the potential reactivator was

Table 1
Degree of permanent inhibition for a set of enzyme reactors after the injection of a 2.3×10^{-5} M solution of pesticide

Pesticide	%Inhibition	
	2 min [a]	10 min [a]
Paraoxon	91	98
Parathion	4	7
Guthion	3	6
Fenitrothion	1	3
Parathion-methyl	1	3
Fenthion	<1	1

[a] Stop period in the enzyme reactor.

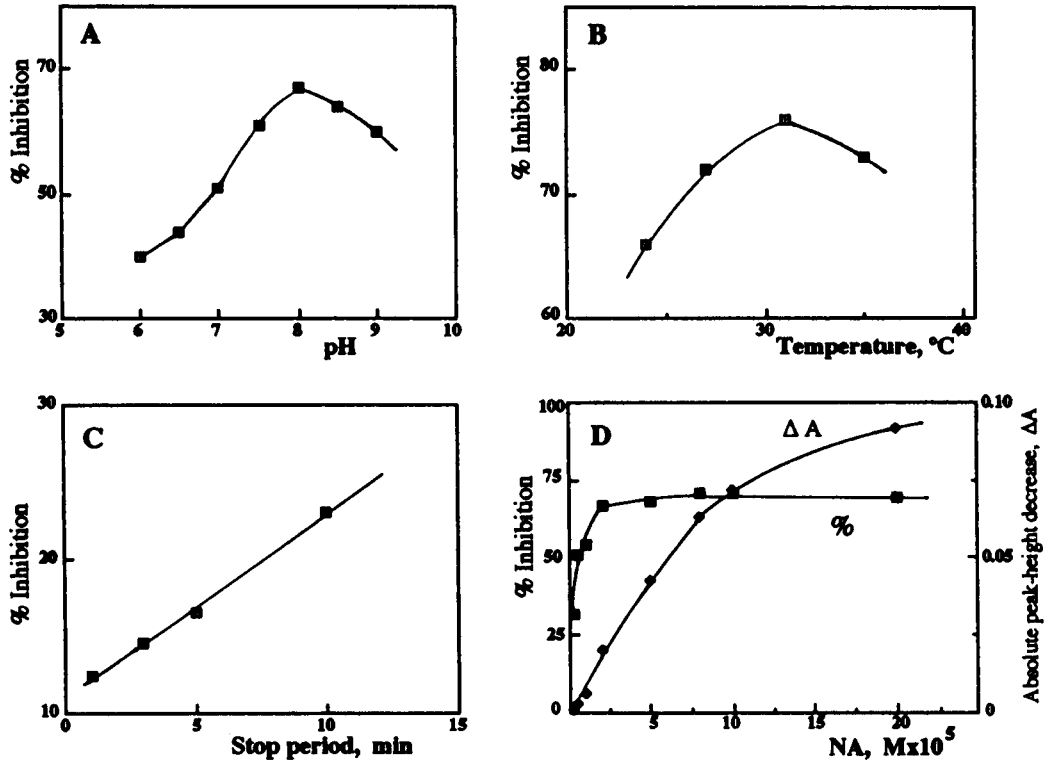

Fig. 3. Inhibition of immobilized AChE by paraoxon. (A) Effect of pH (samples of 2.3×10^{-5} M paraoxon; stop period, 1 min; 25°C). (B) Effect of temperature (pH 8.0; 2.3×10^{-5} M paraoxon; stop period, 1 min) (C) Effect of the stop period in the enzyme reactor (pH 8.0; 4.6×10^{-7} M paraoxon; 25°C). (D) Effect of the concentration of substrate (pH 8.0; 2.3×10^{-5} M paraoxon; stop period, 1 min; 25°C).

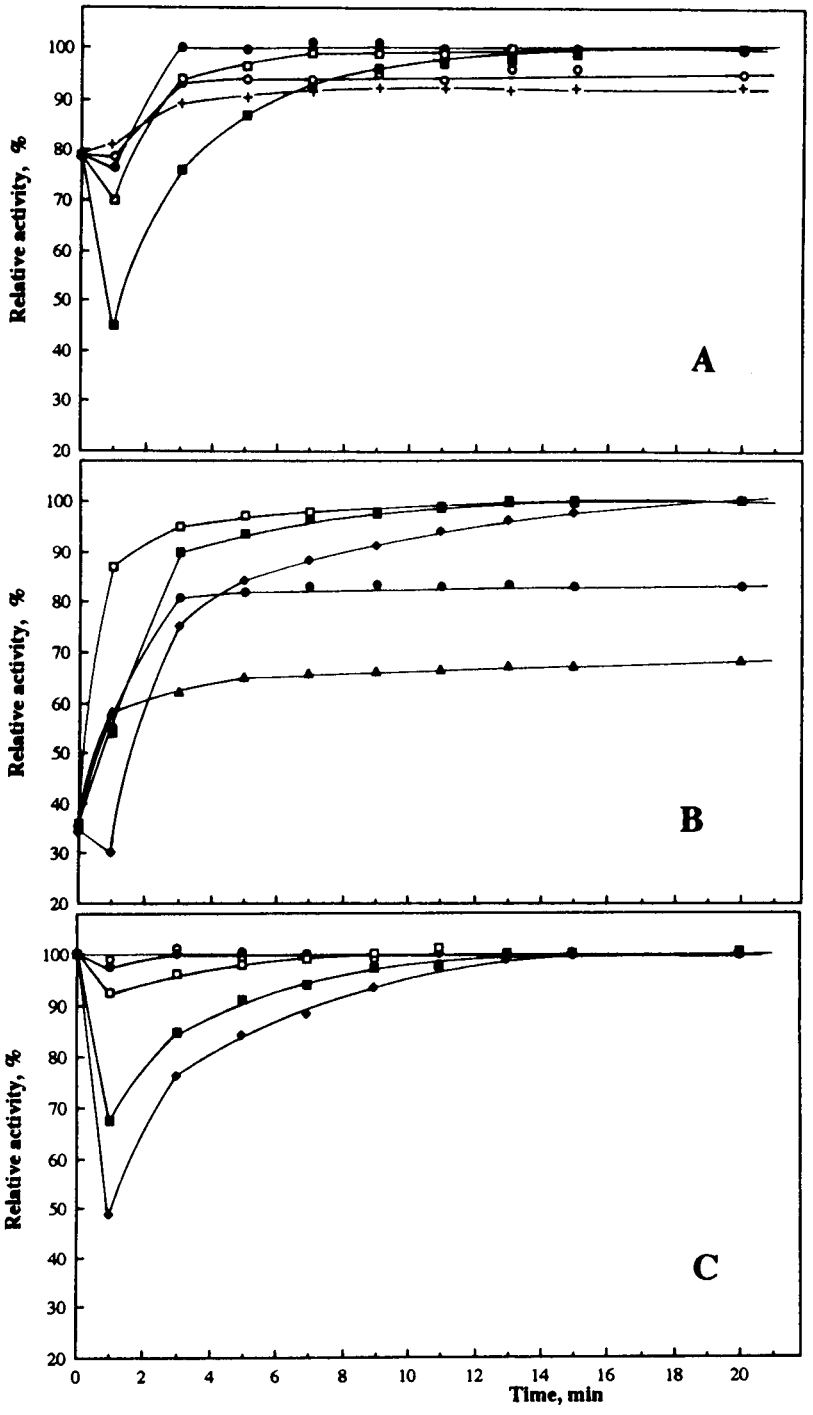

Fig. 4. Relative activity–time profiles after the injection of different solutions of TMB-4 for: (A) enzyme reactors inhibited with 1.0×10^{-6} M paraoxon and stop period of 1 min; (B) enzyme reactors inhibited with 2.3×10^{-5} M paraoxon and stop period of 1 min; (C) enzyme reactors not inhibited. Molar concentration of TMB-4 injected: (+) 1×10^{-6}; (▲) 5×10^{-6}; (○) 1×10^{-5}; (●) 5×10^{-5}; (□) 1×10^{-4}; (■) 5×10^{-4}; (◆) 1×10^{-3}.

injected and made to pass through the enzyme reactor or stopped in it for periods ranging from 30 s to 5 min. Finally, the enzyme reactor was rinsed again with phosphate buffer solution. Within the first 30 min after the injection of the nucleophilic reagent, only TMB-4 showed reactivating properties under these conditions, although 2-PAM, fluoride and magnesium ions have been found to restore activity under other conditions [19]. Subsequent experiments were therefore limited to this compound.

The concentration of TMB-4 used affects both the resulting reactivation yield and the reactivation rate. Fig. 4A shows the change in activity with time for a set of inhibited enzyme reactors after the injection of solutions of TMB-4 of different concentrations in the continuous-flow mode. Within the first 20 min, the extent of reactivation increases with the concentration of TMB-4 injected and is complete for concentrations $\geq 5 \times 10^{-5}$ M. Below this value, the reactivation ceases after ca. 3 min. Concentrations higher than 1×10^{-5} M first cause a further drop in enzyme activity before reactivation occurs. This effect is more pronounced as the concentration of TMB-4 is increased and leads to longer reactivation periods. For a given concentration of TMB-4, the reactivation process depends on the extent of the inhibition by paraoxon: the higher the concentration of paraoxon injected or the longer the stop period in the enzyme reactor, the smaller the reactivation efficiency; Fig. 4B shows the reactivation profiles for a set of enzyme reactors inhibited with 2.3×10^{-5} M paraoxon instead of 1.0×10^{-6} M.

The above-described behaviour could be explained if TMB-4 itself inhibited the immobilized AChE. Indeed, when TMB-4 was injected and made to pass through an enzyme reactor not inhibited by paraoxon, the enzymatic activity was observed to decrease. Fig. 4C shows the activity–time profiles for a set of enzyme reactors, not inhibited with paraoxon, after the injection of different solutions of TMB-4 in the continuous-flow mode. Unlike the inhibition of immobilized AChE by paraoxon, the inhibition by TMB-4 is transitory, and enzymatic activity is completely recovered after a few minutes. The higher the concentration of TMB-4 injected, the higher the inhibition and the longer the reactivation period.

With or without previous inhibition by paraoxon, the reactivation of immobilized AChE after contact with TMB-4 only occurs if NA is present. This effect is illustrated in Fig. 5A and B for an inhibited enzyme reactor continuously rinsed with phosphate buffer solution: reactivation only begins when the first sample of NA is injected; it is then completed after further injec-

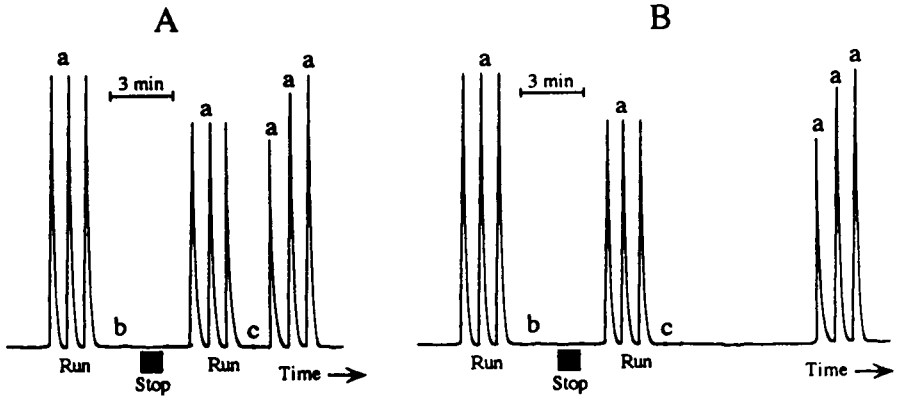

Fig. 5. Reactivation of immobilized AChE with TMB-4/NA after inhibition by paraoxon. (A) When substrate is injected immediately after the reactivator solution; (B) When the injection of substrate is delayed 6 min. Small letters indicate the injection of solutions containing (a) only 2.0×10^{-4} M NA; (b) only 1.0×10^{-6} M paraoxon; (c) only 5×10^{-5} M TMB-4.

tions over the next few minutes. Experiments were made varying the volume (43–200 μl) of the solution of NA injected and the duration of its stay in the enzyme reactor (continuous-flow and stopped-flow periods of 5–30 s) but no relationship between these variables and the reactivation rate or the reactivation yield was observed.

3.4. Determination of paraoxon

Based on the previous experiments, a procedure involving inhibition and subsequent reactivation of immobilized AChE is proposed for the determination of paraoxon. Under the conditions proposed in the Experimental section, the solution of substrate is first injected to set the reference peak height corresponding to the fully active enzyme reactor. A sample solution containing paraoxon is next injected and 6 s later the flow is stopped for 60 s. After 20 s of rinsing with the carrier buffer solution, the substrate solution is again injected and the peak height is recorded. The enzyme reactor is then reactivated by a single injection of TMB-4 solution followed by consecutive injections of substrate solution until the reference peak height is reached again. After this, the next sample of paraoxon is injected, and so on. The absolute decrease in peak height is proportional to the concentration of paraoxon injected and it is taken as the analytical signal.

Concentrations of paraoxon $\geq 4 \times 10^{-9}$ M can be detected (the detection limit is considered as the minimum concentration of paraoxon injected that affords a decrease in peak height of 3σ, σ being the standard deviation ($n = 10$) of the reference peak height). This limit could be lowered by increasing the stop period of the samples in the enzyme reactor. Even so, it is four orders of magnitude lower than that obtained previously [19]. The proposed procedure has a R.S.D of 1.6% (calculated for ten samples of 5.0×10^{-8} M) and a linear calibration range between 9×10^{-9} and 5×10^{-7} M ($\Delta A = 8.18 \times 10^{-4} + 2.66 \times 10^{4} M$; $r = 0.998$, $n = 7$; where ΔA = absolute decrease in peak height absorbance, M = molar concentration of paraoxon). These concentrations of paraoxon are so low that they do not affect the reactivation period, this being determined by the concentration of TMB-4 used and, in all the cases, reactivation is complete ca. 3 min after the injection of the reactivating solution. A sampling frequency of 10 h^{-1} is achieved.

The enzyme reactor can be reused for a large number of assays: after more than one thousand inhibition–reactivation cycles, it retains about 90% of its enzymatic activity.

Acknowledgments

C. García de María thanks the Scientific Committee of NATO for partial financial support. The results of the present paper were presented at the Fourth International Symposium on Kinetics in Analytical Chemistry (Erlangen-Germany, 1992) through a travel grant from the University of Salamanca.

References

[1] J. Sherma, Anal. Chem., 63 (1991) 118R.
[2] G.G. Guilbault and D.N. Kramer, Anal. Chem., 36 (1964) 409.
[3] G.G. Guilbault and M.H. Sadar, Anal. Chem., 41 (1969) 366.
[4] G.G. Guilbault, M.H. Sadar and M. Zimmer, Anal. Chim. Acta, 44 (1969) 361.
[5] P.A. Giang and S.A. Hall, Anal. Chem., 23 (1951) 1830.
[6] S. Bhattacharya, C. Alsen, H. Kruse and P. Valentin, Environ. Sci. Technol., 15 (1981) 1352.
[7] G. Schwedt and M. Hauck, Fresenius' Z. Anal. Chem., 331 (1988) 316.
[8] F. Galgani and G. Bocquene, Environ. Technol. Lett., 10 (1989) 311.
[9] R. Kindervater, W. Künnecke and R.D. Schmid, Anal. Chim. Acta, 234 (1990) 113.
[10] M.E. León González and A. Townshend, Anal. Chim. Acta, 236 (1990) 267.
[11] P. Herzsprung, L. Weil, K.E. Quentin and I. Zombola, Vom Wasser, 74 (1990) 339.
[12] P. Skladal, Anal. Chim. Acta, 252 (1991) 11.
[13] C. Dumschat, H. Müller, K. Stein and G. Schwedt, Anal. Chim. Acta, 252 (1991) 7.
[14] J.L. Marty, K. Sode and I. Karube, Electroanalysis, 4 (1992) 249.
[15] P.W. Carr and L.D. Bowers, Immobilized Enzymes in Analytical and Clinical Chemistry, Wiley, New York, 1980.

[16] G.G. Guilbault, Analytical Uses of Immobilized Enzymes, Dekker, New York, 1984.
[17] R.D. Schmid (Ed.), Flow Injection Analysis (FIA) based on Enzymes or Antibodies, GBF Monographs, Vol. 14, VCH, Cambridge, 1991.
[18] A.M. Trammel, J.E. Simmons and R.T. Borchardt, Pharm. Res., (1984) 115.
[19] I.A. Takruni, A.M. Almuaibed and A. Townshend, Anal. Chim. Acta, 282 (1993) 307.
[20] W.N. Aldridge and E. Reiner, Enzyme Inhibitors as Substrates. Interactions of Esterases with Esters of Organophosphorus and Carbamic Acids, North-Holland, Amsterdam, 1972.

ELSEVIER

Analytica Chimica Acta 295 (1994) 297–305

ANALYTICA CHIMICA ACTA

Extraction and analysis of various benzothiazoles from industrial wastewater

Oliver Fiehn, Thorsten Reemtsma *, Martin Jekel

Department of Water Quality Control, Technical University of Berlin, Sekr. KF 4, Strasse des 17. Juni 135, D-10623 Berlin, FRG

Received 26th October 1993; revised manuscript received 15th March 1994

Abstract

A method was developed for the analysis of benzothiazole, 2-mercaptobenzothiazole, 2-(methylthio)benzothiazole and 2-(thiocyanomethylthio)benzothiazole from industrial wastewater. It includes liquid–liquid extraction with ethyl acetate and toluene at pH 8.5, followed by liquid chromatographic (LC) analysis using a RP-18 column and an acetonitrile–water gradient with UV detection at variable wavelengths. LC analysis is compared with the potential of gas chromatography and its advantages are discussed. Solid-phase extraction appeared not to be suitable for all compounds. The method allows the determination of benzothiazole derivatives without further clean-up down to contents of about 5 $\mu g\ l^{-1}$, with recovery rates exceeding 90% for all compounds. Dissolved organic carbon contents of up to 900 $mg\ l^{-1}$ did neither interfere with extraction nor with chromatographic separation.

Keywords: Liquid chromatography; Extraction; Benzothiazoles; Wastewater; Waters

1. Introduction

Benzothiazole based substances have gained widespread application in industrial processes. 2-Mercaptobenzothiazole (MBT) and 2,2′-(dithiobis)benzothiazole (MBTS) are well-known vulcanization accelerators in the rubber industry [1]. MBT is also contained in metal finishing liquors [2]. 2-(Thiocyanomethylthio)benzothiazole (TCMTB) is widely used as fungicide for wood protection [3–5] and in the leather industry as substitute for chlorinated phenols, namely pentachlorophenol (PCP) [6–8]. Benzothiazole (BT) is also mentioned as fungicide [9]. Correspondingly, benzothiazole and its derivatives are widely distributed and have been detected by screening analyses in industrial and municipal wastewater [10–12] as well as in various environmental compartments such as in groundwater and river water [9,13,14], tap water [14] as well as in landfill leachates [15], in atmospheric deposition [16], coastal sediments [1] and fish [17].

However, reports on the specific extraction and analysis of BT derivatives from aqueous media are rarely found. Warner et al. [10] employed liquid–liquid extraction (LLE) with dichloromethane for TCMTB and MBTS from spiked distilled water, but recovery from wastewater was poor. An on-line trace enrichment methodology for various pesticides including BT on PLRP-S

* Corresponding author.

SSDI 0003-2670(94)00179-P

polymer is reported by Liska et al. [9] for surface water monitoring. Analysis of BT derivatives by reversed-phase liquid chromatography (LC) [3,6,18] and of TCMTB and MBTS by normal-phase LC [10] is reported.

In order to determine these compounds in effluents of industrial processes involving BT derivatives as fungicides, and to study their behaviour in biological wastewater treatment, a method was required for the parallel extraction and analysis of several BT compounds from wastewater. We here report on the development of a suitable method for these purposes. LLE is compared with solid-phase extraction (SPE) and the potentials of LC and gas chromatography (GC) for the detection of BT derivatives are investigated. The use of the finally selected method is illustrated by its application on various wastewater samples. According to the obtained detection limit, the method appears not to be limited to industrial wastewater analyses.

2. Experimental

2.1. Chemicals and materials

TCMTB was received from the Dr. Eberle Co. (Tübingen). BT was obtained from Aldrich (Steinheim) and MBTS and MTBT from Ferak (Berlin). MBT and all solvents were purchased from Merck (Darmstadt).

Solid-phase extraction tubes of the following companies were investigated: 500 mg RP-18 (ww18) from Worldwide Monitoring (Horsham, USA); 400 mg Adsorbex RP-18 (mer18) from Merck; Supelclean LC-18 (Su18), Envi-18 (SuEn), LC-CN (SuCN), EnviCarb (SuCa), LC-8 (Su8) all as 500 mg cartridges from Supelco (Bellefonte, CA).

Trimethylanilinium hydroxide (TMAH, 0.2 M in methanol) for methylation was purchased by Regis (Norton Grove, USA) and *N,O*-bis(trimethylsilyl)trifluoroacetamide (BSTFA) for silylation by Fluka (Buchs, Switzerland). Glassfibre-filters were obtained from Schleicher and Schuell (Dassel, Germany) and 0.45-μm cellulose acetate filters from Sartorius (Göttingen).

Solvents were redistilled in an all-glass apparatus prior to use. Doubly distilled water was used for standard solutions.

2.2. Analytical apparatus and procedure

LC

LC analyses were carried out on a 30 cm x 4.6 mm i.d. Eurosphere 80 C_{18} column, 5 μm (Knauer, Berlin) with an L-6200A gradient pump, an AS-2000 A autosampler and a T-6300 column thermostat (all from Merck-Hitachi, Darmstadt). 20 μl samples were injected. UV detection was performed with a SPD-10A UV–visible detector (Shimadzu, Kyoto) and data storage and processing with ChromStar V 3.11 software (Bruker, Bremen).

LC separation was performed with an acetonitrile–water gradient. Distilled water, containing 4 mmol l^{-1} NaH_2PO_4 and adjusted to pH 4.5 with H_3PO_4 was employed as solvent A. Solvent B was an acetonitrile–solvent A mixture (90:10), acidified to pH 4.5 with H_3PO_4. Elution started with 70% B at a flow rate of 0.5 ml min^{-1} and was linearly shifted to 90% B (flow rate, 0.5 ml min^{-1}) at 11 min. After 3 min of isocratic elution the gradient was shifted to 100% B and 1.0 ml min^{-1} at 14.5 min. Separation was completed within 10 min of isocratic elution followed by 6 min of equilibration. Column temperature was held at 40°C.

UV detection was performed by time-programmed wavelength changes according to the absorption maxima of the individual compounds in the higher wavelength range: MBT was detected at 325 nm after 6 min, BT at a wavelength of 250 nm around 8 min, TCMTB and MTBT at 280 nm between 10 and 13 min, and MBTS at 280 nm after 19 min. These UV maxima are less affected by coeluting contaminants compared to the maxima in the low-UV range. No fluorescence activity of benzothiazole derivatives could be determined. The pH of the eluents has a significant influence on the retention times of the analytes. Moreover, quantification of MBT is strongly affected by the pH of the eluents. By raising the pH above 6.5, its absorbance maximum is shifted from 325 nm to 309 nm and the

absorbance at 325 nm is, hence, reduced to 10%. Therefore, LC eluents and sample solutions have to be buffered as given above.

Identification

Peak identification was based on the retention times of the corresponding standards and on the analysis of spiked samples. Comparison of the UV spectra gained by a diode array detector (DAD) supports peak assignment in critical cases. If no DAD is available, dual wavelength detection at the first and second maxima can be employed to ensure peak identity and purity. The absorbance ratio for MBT at 228 to 325 nm is 2.05, for BT it is 0.33 between 284 and 250 nm, for TCMTB it is 1.73 between 224 and 280 nm and for MTBT a ratio of 1.56 is recorded between the absorbance at 224 and 278 nm.

LC–mass spectrometry (LC–MS) was recently shown to be a powerful method for the identification of benzothiazoles [19], but it was not available to us. Collecting the LC peaks of interest and subsequent analysis by GC–MS offers an alternative route for some of the benzothiazole derivatives (see below).

GC

Gas chromatography was performed with a PE 8420 gas chromatograph (Perkin-Elmer, Überlingen) with a flame ionization detector (FID) on a 30 m × 0.25 mm i.d. SPB 5-column (Supelco) and Helium as carrier gas (112 kPa). Injector and detector temperatures were 250 and 300°C, respectively. Oven temperature was held at 100°C for 2 min, followed by a ramp rate of 6°C min^{-1} to a final temperature of 280°C, which was kept constant for 10 min.

GC–MS was done on a HP 5989 A quadrupole mass spectrometer coupled with a HP 5890 II gas chromatograph (Hewlett-Packard, Böblingen, Germany) in the electron impact mode (EI) at 70 eV on a 30 m x 0.25 mm i.d. SPB5 column. Injector temperature was 250°C, GC–MS interface temperature was 280°C, and source temperature was kept at 200°C.

UV absorbance and DOC

UV absorption spectra of the benzothiazoles were measured on a Lambda-2 spectrophotometer (Perkin-Elmer). An RF-551 LC fluorescence detector (Shimadzu) was employed for determining fluorescence activity. Dissolved organic carbon (DOC) of wastewater samples was determined with an Astro LiquiTOC 2001-MB analyzer (Foss-Heraeus, Hanau, Germany).

2.3. Extraction

Aqueous standard solution of 100 $\mu g\ l^{-1}$ MBT, 90 $\mu g\ l^{-1}$ MTBT, 117 $\mu g\ l^{-1}$ TCMTB and 175 $\mu g\ l^{-1}$ BT were prepared by adding appropriate amounts of a stock solution of the analytes in acetone to a dry flask. The acetone was allowed to evaporate and the dry residue redissolved in water by ultrasonification. 4 g l^{-1} NaCl were added and the pH values adjusted (NaOH–H_3PO_4). 25 ml aliquots were employed for extraction.

MBTS was originally intended to be included in the analytical procedure. However, it was found to be poorly soluble in water and to decompose quickly. Mixtures of MBTS with distilled water at levels between 200 $\mu g\ l^{-1}$ and 4 mg l^{-1} remained turbid after 30 min in an ultrasonic bath or stirring overnight. After filtration over a 0.45-μm cellulose acetate filter, the filtrates were extracted with dichloromethane at pH 6.5 and no MBTS was detectable. However, varying amounts of MBT and MTBT were detectable as well as several unidentified peaks. MBTS is, thus, suggested to be of minor importance in the context of industrial wastewater analysis. Astonishingly, Warner et al. [10] reported the recovery of MBTS up to 940 $\mu g\ l^{-1}$ from distilled water.

Wastewater samples from the different steps of a tannery wastewater treatment pilot plant [20] were stored frozen until analyzed, while effluents of a municipal wastewater treatment plant were instantly worked up. All samples were filtered over 0.45-μm cellulose acetate filters prior to extraction.

Due to possible photolytic reactions of TCMTB and MBT [18] all samples, standards and extracts were stored in the dark during work-up and, generally, exposed to daylight as shortly as possible (less than 60 min). Furthermore, hydrolysis of TCMTB to MBT was observed [18], with $t_{1/2}$ of

83 h at pH 9 and $t_{1/2}$ between 760 and 18800 h at pH 8. Therefore, the pH of aqueous samples must not be raised above 8.5.

Solid-phase extraction

Standard solutions containing 4 g l^{-1} NaCl and adjusted to pH 8.5 were extracted on the cartridges mentioned above at a flow rate of 2 drops s^{-1}. After a 2 ml wash with distilled water (4 g l^{-1} NaCl, pH 8.5) ambient air was sucked through the columns for 1 min. The analytes were then sequentially eluted with one of the following solvent systems: (i) 2 ml methanol, 2 ml methanol–dichloromethane (20:80, v/v), 2 ml dichloromethane, 2 ml toluene or (ii) 2 ml acetonitrile, 2 ml acetone, 2 ml toluene. Work-up of solid phase extracts followed the procedure for LLE given below.

Liquid–liquid extraction

LLE was performed at different pH values with three 5 ml portions of various solvents. The centrifuged organic phases were combined and reduced to approximately 0.5 ml with a rotary evaporator (50°C). The extracts were then evaporated to near dryness in 2 ml glass vials under a gentle stream of nitrogen at 50°C and redissolved in 1 ml of an acetonitrile–water mixture (60:40; v/v) buffered at pH 4.5 (H_3PO_4–NaH_2PO_4). Pure acetonitrile is also suitable as solvent. Owing to the volatility of BT, evaporation of the extracts to total dryness must be carefully avoided.

3. Results and discussion

3.1. Analysis

LC

Reversed-phase LC on C_{18} phases has been previously employed for the analysis of TCMTB [3,6,21,22] and other BT derivatives [18]. The structures of the benzothiazole derivatives under investigation are given in Fig. 1. They are well separated within 21 min under the selected chromatographic conditions (Fig. 2). Owing to the poor solubility and stability of MTBS in water

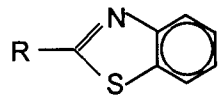

	R
MBT	-SH
BT	-H
TCMTB	-S-CH_2-SCN
MTBT	-SCH_3
MBTS	-S-MBT

Fig. 1. Structure of the employed benzothiazole derivatives.

(see above), only MBT, BT, TCMTB and MTBT were included in further work.

UV calibration curves following LC separation are linear for MBT, TCMTB and MTBT from 4 to 1000 ng injected onto the column, whereas linearity for BT was observed above 30 ng. The detection limit ($S/N > 3$) and the more rigid method detection limits, derived from the relative standard deviation of the regression lines [23] are given in Table 1. While the first are in the range of 0.2 to 1 ng, the latter vary between 4 ng and 13 ng, with relative standard deviations of 3–5%. Assuming, that 25 ml aliquots of samples are extracted and redissolved in 500 μl of solvent

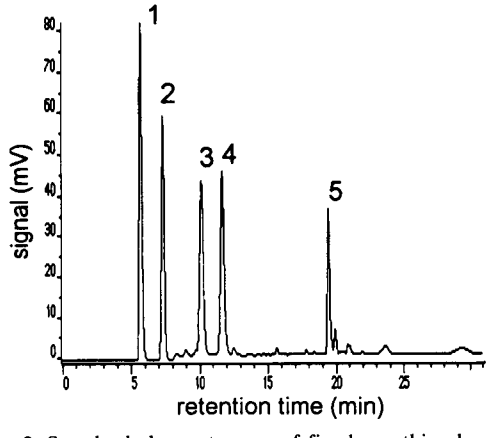

Fig. 2. Standard chromatogram of five benzothiazole components: 1 = MBT (44 ng), 2 = BT (180 ng), 3 = TCMTB (215 ng), 4 = MTBT (94 ng), 5 = MBTS (223 ng). Minor peaks are due to technical byproducts.

Table 1
Characteristics of UV detection of BT derivatives following LC separation (DL: detection limit; MDL: method detection limit; RF: response factor; R.S.D.: relative standard deviation, r: correlation coefficient of the linear regression)

	wavelength (nm)	DL (ng)	MDL (ng)	RF×10^{-4} (ng AU^{-1})	R.S.D. (%)	r
MBT	325	0.2	4	1.13	3.3	0.9960
BT	250	1	13	4.84	4.7	0.9975
TCMTB	280	0.5	5	6.09	3.5	0.9996
MTBT	280	0.5	4	2.68	2.6	0.9987

prior to analysis, this results in a detection limit of 5 $\mu g\ l^{-1}$.

GC

BT, MBT and MTBT are well detectable by GC-FID without derivatization. The detection limits ($S/N > 10$) under the above mentioned conditions are between 1 ng for MBT and 2 ng for BT and MTBT injected onto the column. However, peak tailing easily occurs, namely for MBT. These substances do not react with BSTFA. MBT is methylated with TMAH at the thiol S and at the ring N at a ratio of about 95:5. However, methylated MBT would interfere with the determination of originally occurring MTBT.

TCMTB was reported to be thermally labile and, therefore, not detectable by GC [3]. Correspondingly, only traces of the amount of TCMTB injected onto the column were detectable by GC–MS, provided that no derivatization reaction was performed prior to analysis. MBTS was not detectable by both, GC-FID and GC–MS.

Detection limits for BT, MBT and MTBT in GC-FID analysis appeared to be slightly lower than those of LC-UV. Nevertheless, LC analysis is favourable in wastewater analysis, since TCMTB and MBTS are not detectable by means of GC. Furthermore, wastewater extracts analyzed by GC-FID are usually too complex for reliable peak assignment. UV detection employed in LC (see above) appears to be more specific. Gas chromatography will be advantageous in the combination with MS detection for the structural elucidation of unknown BT derivatives and for environmental screening. Correspondingly, most reports on the appearance of BT derivatives were based on GC–MS screening analyses [9,11–16].

For the trace analysis of BT compounds by MS under single ion monitoring the fragment ions 108, (122) and 135 are suitable, whereas 108, 135 and 167 are characteristic for MBT derivatives.

3.2. Extraction

In recent years SPE is often favoured over LLE due to its ease of handling and low solvent consumption. SPE by on-line trace enrichment for the purpose of surface water pesticide residue analysis was reported [9]. The authors employed PLRP-S polymer, but of the four BT derivatives investigated here, only BT was included. The breakthrough volume was reported to exceed 30 ml. BT and MTBT have also been determined by SPE on C_{18} phases within toxicity fractionation procedures applied to surface waters [24,25]. The completeness of extraction was, however, not investigated. The use of LLE, on the other hand, was investigated by Warner et al. [10] but limited to TCMTB and MBTS and recovery from wastewater was reported to be low.

We, therefore, investigated the use of SPE and LLE for the parallel extraction of BT and its

Table 2
Recovery (%) of benzothiazole derivatives (around 100 $\mu g\ l^{-1}$) from distilled water by liquid–liquid extraction with various solvents

Solvent	MBT			BT			TCMTB			MTBT		
	pH 2	pH 5	pH8.5	pH2	pH5	pH 8.5	pH2	pH5	pH8.5	pH2	pH5	pH 8.5
Toluene	2	3	95	19	98	98	96	96	83	99	85	61
tert.-Butylmethyl ether	18	8	13	6	20	10	95	78	85	58	108	63
Dichloromethane	40	68	72	15	61	70	103	105	89	48	54	103
Ethyl acetate	68	74	105	85	51	60	102	99	90	92	92	89

three derivatives MTB, TCMTB and MTBT from wastewater.

Liquid–liquid extraction

LLE of the four compounds from distilled water was performed with four solvents at three pH values after the addition of 4 g l^{-1} NaCl (Table 2). MBT is well extractable under weakly alkaline conditions with ethyl acetate or toluene; the latter should be employed for the extraction of BT. TCMTB and MTBT appear to be best extracted from acidic or neutral milieu by either solvent, but extraction at pH 8.5 with ethyl acetate still provided acceptable results (89 and 90%). Table 2 further indicates, that the relationship between the polarity of a solvent and the polarity of the analyte is complex. Toluene, although being one of the less polar solvents investigated, exhibits comparatively high recoveries namely with the most polar compounds. This might be due to the aromatic nature of toluene and the BT derivatives.

Corresponding to earlier reports [10], TCMTB is readily extracted by dichloromethane. However, it becomes evident that dichloromethane is a poor solvent for the extraction of the more polar compounds MBT and BT. This finding might explain some inconsistent results reported by Brownlee et al. [18].

Considering these results, seven replicate extractions were carried out at three different pH values subsequently employing 5 ml portions of ethyl acetate (twice) and toluene (once) after the addition of salt (4 g l^{-1} NaCl).

While the recovery of BT, TCMTB and MTBT is between 94 and 97% at pH 6.5, MBT recovery requires a pH of 8.5 (Table 3). Recoveries of the first three components are still acceptable with 87 to 98% at this pH. Standard deviations for the whole procedure are below 9%. Recoveries at pH 8.5 without NaCl are poor for all components (Table 3).

Table 3
Recovery (%) and relative standard deviation (%) of benzothiazole derivatives (around 100 μg l^{-1}) from distilled water ($n = 7$)

	NaCl			No salt
	pH 2	pH 6.5	pH 8.5	pH 9
BT	89.4 (4.3)	95.9 (7.2)	88.1 (8.7)	52
TCMTB	98.5 (1.2)	96.9 (2.7)	87.4 (5.5)	70
MTBT	97.8 (8.1)	94.4 (5.9)	97.8 (3.7)	83
MBT	51.9 (6.0)	20.3 (3.8)	104.3 (5.4)	64

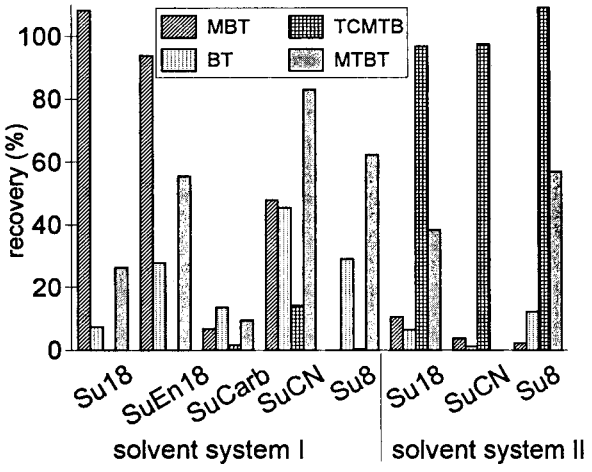

Fig. 3. Recovery of benzothiazole derivatives by solid-phase extraction. Solvent system I: MeOH–CH_2Cl_2–toluene; solvent system II: MeCN–acetone–toluene.

Brownlee et al. [18] observed enhanced hydrolysis of TCMTB to MBT above pH 9. In separate extractions of TCMTB-spiked wastewater at pH 8.5, however, MBT was not detectable, indicating that TCMTB is stable at pH 8.5 during work-up.

Solid-phase extraction

Solid phases of different polarity were employed for solid-phase extraction (SPE), and the samples adjusted to optimal conditions of LLE (pH 8.5, 4 g l^{-1} NaCl). The obtained results are quite heterogenous (Fig. 3). MBT is well recovered on C_{18} phases (Su18, SuEn) with the methanolic solvent system (I), while TCMTB is equally extractable by C_8 (Su8), Cyano (SuCN) and C_{18} phases (Su18) with the acetonitrile containing solvent system (II). MTBT was most efficiently extracted (around 85%) on the cyano phase employing the methanolic solvent system, whereas the recovery of BT was poor in all cases. The deactivated carbon (SuCarb) is not advantageous. Extraction by an endcapped C_{18} phase (ww18)

was comparable to the C_{18} phase shown in Fig. 3. (Su18).

Correspondingly, MBT and TCMTB might be well extractable on C_{18} reversed phases employing a methanol–acetonitrile solvent system. Under these conditions, however, the recoveries of MTBT and, moreover, BT will be insufficient.

The low recovery rates, however, appeared not to be due to incomplete adsorption of the analytes onto the solid phases. Filtrates of C_{18}, Cyano and C_8 SPE were reextracted by LLE at pH 8.5. A maximum of 6% of TCMTB and 8% of BT was recovered. On the other hand, additional elution of the cartridges with 2 ml portions of less polar solvents (cyclohexane, hexane) provided no additional amounts of benzothiazoles. The extremely poor recovery rates of BT, the most volatile BT derivative, might be due to the drying procedure applied before LC analysis. To some extent, this might also be true for MTBT, the second volatile compound. This problem would be avoided by on-line trace enrichment [9].

Considering these results SPE appears to be of limited value for the parallel extraction of MBT, BT, MTBT and TCMTB. Nevertheless, a method for the simultaneous quantitative extraction of MBT, BT and MTBT by solid phases would be of value for the monitoring of surface waters.

3.3. Application on wastewaters

LC analysis and extraction

LLE at pH 8.5 with ethyl acetate and toluene, followed by LC analysis of the BT derivatives was then applied on four different types of wastewater (industrial effluent, anaerobically treated, aerobically treated and effluent of a municipal wastewater treatment plant) spiked with the four BT derivatives between 90 and 175 $\mu g\ l^{-1}$.

Fig. 4 displays the liquid chromatogram of an extract from a spiked wastewater sample. All components are clearly detected and no interference with other coextracted contaminants was observed. The detection of the first peak (MBT) at 325 nm is advantageous within this respect, since potential polar contaminants are not detected at this wavelength. Furthermore, extraction under weakly alkaline conditions minimizes

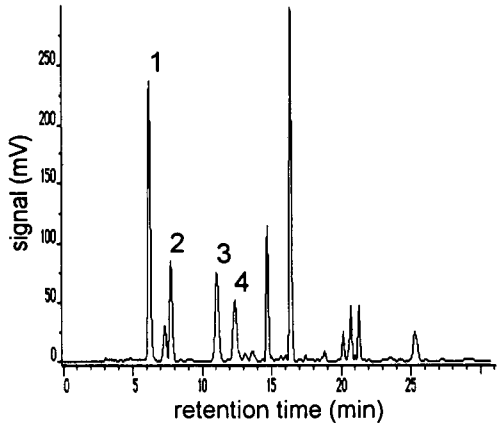

Fig. 4. Liquid chromatogram of an extract of spiked wastewater (for peak numbers and amounts see Fig. 2).

the coextraction of anionic compounds, which form a substantial portion of dissolved organic compounds in biologically treated wastewaters.

The recoveries of BT derivatives from the four types of wastewaters varied between 93% for MBT, 87% for BT, 95% for MTBT and 92% for TCMTB with relative standard deviations of 5 to 9%. These results correspond with those obtained for distilled water. The recovery of BT derivatives was, thus, neither affected by inorganic constituents of the wastewater, nor by its DOC content, which varied between 18 mg l^{-1} in the effluent of the municipal wastewater treatment plant and 900 mg l^{-1} in the untreated tannery wastewater.

Reproducibility

Real, not spiked, samples of tannery wastewater and the effluents of the tannery wastewater treatment pilot plant were analysed in duplicate within two months to examine the reproducibility of the whole analytical procedure (Table 4). Although originally applied within the tanning process, no TCMTB was detectable. This corresponds with the reported hydrolysis of TCMTB under alkaline conditions [18], such as in tannery effluent. Instead of TCMTB, the BT derivatives MBT, BT and MTBT were detected. Contents varied between 650–690 $\mu g\ l^{-1}$ of MBT in the untreated and anaerobically treated wastewater

Table 4
Content of BT derivatives in tannery wastewater samples ($\mu g\ l^{-1}$) and difference between duplicates (%) (TCMTB: below detection limit)

	Untreated		Anaerobic		Aerobic	
	Content ($\mu g\ l^{-1}$)	Diff. (%)	Content ($\mu g\ l^{-1}$)	Diff. (%)	Content ($\mu g\ l^{-1}$)	Diff. (%)
MBT	655	4.9	687	2.0	36	13.9
BT	10.5	4.8	99	6.1	5.5	9.1
MTBT	39	7.7	115.5	8.2	24.5	6.1

and 5.5 $\mu g\ l^{-1}$ of BT after the aerobic treatment. The deviation from the mean between duplicates is in the range of 2 to 14%, with an average of 7%. The method, thus, proves to be reliable over a concentration range of two orders of magnitude, even in extremely complex matrices such as untreated tannery wastewater.

4. Conclusions

A new method is developed for the analysis of benzothiazole, 2-mercaptobenzothiazole, 2-(methylthio)benzothiazole and 2-(thiocyanomethylthio)benzothiazole from industrial wastewater. 2.2′-(Dithiobis)benzothiazole, originally included in these investigations, was shown to be of comparatively limited relevance in aquatic environment, due to its low solubility and fast decomposition in water.

Highest recovery for all BT derivatives in LLE was obtained after the addition of 4 $g\ l^{-1}$ NaCl at pH 8.5 with ethyl acetate, followed by toluene. Recovery from different wastewaters was shown to exceed 90%. It was not affected by DOC contents of up to 900 $mg\ l^{-1}$ in a tannery effluent. LLE with dichloromethane, formerly employed in other reports, proved to be insufficient for the more polar substances MBT and BT. Furthermore, SPE appeared not to be suitable for the parallel extraction of all components.

Analysis of BT derivatives is best performed by LC with UV detection and time-programmed wavelength switching. Dual-wavelength detection supports peak assignment and monitors peak purity. The resolution and detection of BT derivatives is not deteriorated by coextracted dissolved organic compounds, even from highly loaded wastewater. Although GC-FID is more sensitive than LC-UV, it is limited to MBT, BT and MTBT. Chromatograms are, however, more complex and peak assignment is less reliable unless coupled to mass spectrometry.

The final procedure, consisting of liquid–liquid extraction and analysis by LC with UV detection provides detection limits around 5 $\mu g\ l^{-1}$. Reproducibility was around $\pm 7\%$ in wastewater analyses yielding between 5 and 700 $\mu g\ l^{-1}$ of BT derivatives. Due to the obtained detection limits, this method is suggested not to be limited to the analysis of industrial wastewater.

Acknowledgments

The financial support by the German Research Council (DFG, Bonn) through SFB 193: Biological Treatment of Industrial Wastewater, Project A3, is gratefully acknowledged. We thank the Dr. Eberle Chemical Company (Tübingen, Germany) for kindly providing reference materials.

References

[1] R.B. Spies, B.D. Andresen and D.W. Rice Jr., Nature, 327 (1987) 697.
[2] J.K. Reichert, J. Lochtman, R.J. Müller and I. Könen, Jahrestagung der FG Wasserchemie in der GdCh, Badenweiler, 1993.
[3] C.R. Daniels and E.P. Swan, J. Chromatogr. Sci., 25 (1987) 43.
[4] J.C. Dacre, NTIS, AD-A144526 (1984).
[5] M.J. Kennedy, Analyst, 111 (1986) 701.
[6] W.M. Fowler, A.E. Russell, I.H. Kruger and S.C. Pinchuck, J. Soc. Leather Technol. Chem., 71 (1987) 100.
[7] E. Heidemann, Das Leder, 39 (1988) 9.
[8] H. Gattner, W. Lindner and H.-U. Neuber, Das Leder, 39 (1988) 66.
[9] I. Liska, E.R. Brouwer, A.G.L. Ostheimer, H. Lingeman, U.A.T. Brinkman, R.B. Geerdink and W.H. Mulder, Int. J. Environ. Anal. Chem., 47 (1992) 267.
[10] J.S. Warner, T.M. Engel and P.J. Mondron, NTIS, PB 85-189025 (1985).
[11] L. Braunstein, K. Hochmüller and K. Spengler, Vom Wasser, 73 (1989) 167.

[12] W. Elsäßer, E. Gilbert and S.H. Eberle, Acta Hydrochim. Hydrobiol., 29 (1992) 82.
[13] A.M. Dietrich, D.S. Millington and Y.-H. Seo, J. Chromatogr., 436 (1988) 229.
[14] J. Rivera, F. Ventura, J. Caixach, M. de Torres and A. Figueras, Int. J. Environ. Anal. Chem., 29 (1987) 15.
[15] J.F. Barker, J.E. Barbash and M. Labonte, J. Contam. Hydrol., 3 (1988) 1.
[16] D.I. Welch and C.D. Watts, Int. J. Environ. Anal. Chem., 38 (1990) 185.
[17] G. Runge and H. Steinhart, Agribiol. Res., 43 (1990) 155.
[18] B.G. Brownlee, J.H. Carey, G.A. MacInnis and I.T. Pellizzari, Environ. Toxicol. Chem., 11 (1992) 1153.
[19] W.M.A. Niessen, C.C. McCarney, P.E.G. Moult, U.R. Tjaden and J. van der Greef, J. Chromatogr., 647 (1993) 107.
[20] E. Genschow and W. Hegemann, GWF, Wasser-Abwasser, 134 (1993) 262.
[21] A. Bugby, C. Parbery, R.L. Sykes and C.D. Taylor, J. Soc. Leather Technol. Chem., 74 (1990) 134.
[22] C. Parbery and C.D. Taylor, Analyst, 114 (1989) 361.
[23] W. Funk, V. Damman and G. Donnevert, in Qualitätssicherung in der Analytischen Chemie, VCH, Weinheim, 1992.
[24] L.P. Burkhard, E.J. Durhan and M.T. Lukasewycz, Anal. Chem., 63 (1991) 277.
[25] J.R. Amato, D.I. Mount, E.J. Durhan and M.T. Lukasewycz, Environ. Toxicol. Chem., 11 (1992) 209.

ELSEVIER

Analytica Chimica Acta 295 (1994) 307–313

ANALYTICA CHIMICA ACTA

Determination of acridine derived compounds in charcoal-grilled meat and creosote oils by liquid chromatographic and gas chromatographic analysis

M.T. Galceran *, M.J. Curto, L. Puignou, E. Moyano

Department de Química Analítica, Universitat de Barcelona, Av. Diagonal 647, 08028 Barcelona, Spain

Received 5th October 1993; revised manuscript received 8th April 1994

Abstract

A method is described for the determination of basic nitrogen-containing polycyclic aromatic compounds (PANHs, azaarenes) in charcoal-grilled meat and creosote samples. The enrichment procedure includes liquid–liquid partition (cyclohexane), extraction of PANHs with acid and re-extraction with cyclohexane after neutralization. Further purification is performed by column chromatography on alumina. Basic fractions were analyzed by liquid chromatography (LC) with UV detection and capillary gas chromatography (GC) with flame ionization detection (FID) and mass spectrometry (MS). The lowest detection limits ranged from 0.01 to 0.14 ng with GC–MS-SIM, allowing the determination of these compounds at the pg g^{-1} level in meat samples.

Keywords: Gas chromatography–mass spectrometry; Liquid chromatography; Acridine; Creosote oils; Meat samples; Polycyclic aromatic compounds

1. Introduction

Polycyclic aromatic hydrocarbons (PAH) are formed in combustion processes and are ubiquitous in environmental samples [1,2]. Less information is available on their nitrogen analogues, the basic azaarenes, but they have been shown to be present in association with PAHs in different samples. Although azaarenes may enter the environment from a variety of sources, such as cigarette smoke [3], automobile exhaust [4], industrial stack effluents, and urban suspended matter [5], coal tar and creosote (a distillate of coal tar) are two major sources of azaarenes [6,7] because of the large percentage of nitrogen and aromatic compounds in coal. The wood preservation industry generates significant quantities of creosote wastes and may be the major source of azaarene contamination in water and sediments [8].

Moreover, there is continuing worldwide concern about the contamination of foods by polynuclear aromatic hydrocarbons (PAH) with carcinogenic and mutagenic properties [9]. Four sources of PAHs in foods have been identified: natural causes, polluted environment, food additives and packaging, and curing smokes and other thermal

* Corresponding author.

SSDI 0003-2670(94)00180-T

processes [10]. Furthermore, nitrogen compounds (PANH) can be formed as products of pyrolysis or incomplete combustion of coal or organic matter that contains nitrogen. Some of these compounds, predominantly derivatives of benzo(*a*)- and benzo(*c*)acridine, are well-known carcinogens [11]. At present, there are only a few published articles dealing with analytical methodology for the determination of PANHs in foods [12,13]; these papers describe the isolation of PANHs from smoked foods but no measurable amounts of azaarenes were detected in such samples. Furthermore, since 1980, a series of potent heterocyclic amines (HAs) which are mutagenic and carcinogenic have been discovered in processed foods [14,15].

The determination of PANHs in environmental samples has been carried out by different chromatographic techniques, including liquid chromatography (LC) with fluorescence [5] or UV detection [12] and gas chromatography (GC) with flame ionization detection [13], with nitrogen selective detection [6,16], or with mass spectrometry (MS) as a specific ion detection method [17,18].

This paper describes the isolation and identification of PANHs in the basic fraction of grilled and charcoal-broiled beef and also in a creosote sample. The PANHs were isolated by liquid–liquid extraction, a clean-up on alumina was performed, and acridine derivatives were quantified by LC with UV detection and capillary GC–MS. Recoveries, detection limits and applicability of the method have been studied.

2. Experimental

2.1. Reagents

Benzo(*c*)acridine, dibenzo(*a*,*j*)acridine, dibenzo(*a*,*c*)acridine, dibenzo(*c*,*h*)acridine and dibenzo(*a*,*i*)acridine were obtained from the Commission of the European Communities, Bureau of Reference (BCR) (Brussels, Belgium) 99.0% purity; standard stock solutions of 100 μg ml^{-1} in acetonitrile or toluene were prepared and used for further dilutions. A list of compounds is given in Table 1.

Table 1
Identification, abbreviations, and structures of PANHs used in this study

Compound Name	Abbreviation	Structure
1. Benzo(*c*)-acridine	B(c)Ac	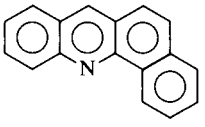
2. Dibenzo(*a*,*j*)-acridine	DB(aj)Ac	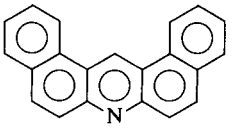
3. Dibenzo(*a*,*c*)-acridine	DB(ac)Ac	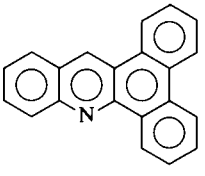
4. Dibenzo(*c*,*h*)-acridine	DB(ch)Ac	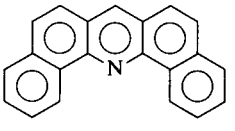
5. Dibenzo(*a*,*i*)-acridine	DB(ai)Ac	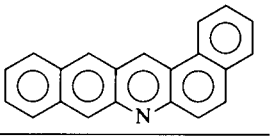

Neutral aluminium oxide (60–200 mesh) was provided by Merck (Darmstadt) and was activated at 150°C for 12 h and deactivated with 5% water. All solvents and chemicals were HPLC or analytical grade, and water was purified using a Culligan system (Barcelona). All the solutions were passed through a 0.45-μm filter before injection into the LC system.

2.2. Apparatus

A Knauer Model 64 high-pressure liquid chromatograph equipped with an Applied Biosystems Model 757 spectrophotometer with a wavelength of 280 nm was used for the LC analysis. Liquid chromatographic separations were performed on a Nucleosil (5 μm) C_{18} column (125 mm × 4 mm i.d.). The mobile phase was acetonitrile–water (90:10) at a flow-rate of 1.0 ml min^{-1}.

A Dani Model 3800 gas chromatograph with flame ionization detection was used for the gas chromatographic analysis. Compounds were separated on a DB-17 fused capillary column (25 m × 0.25 mm i.d., 0.25 μm film) (J Scientific, Folsom) with helium (30 cm s^{-1}) as carrier gas. Splitless injection (1 min) was used. The column was held at 140°C for 1 min, programmed to 270°C at 4°C min^{-1} and held isothermically for 15 min. The injection volume was 1 μl of standards in toluene. Chromatographic data were recorded with a Chrom-Card data system.

GC–MS analyses were performed by electron-impact (EI) (70 eV) in a Hewlett-Packard 5988A quadrupole mass spectrometer coupled to a 5890 gas chromatograph with a 9825A data system. Transfer line, ion source and analyzer temperatures were held at 280, 250 and 250°C, respectively. Samples were injected in the splitless injection mode. Scans were obtained from 40 to 400 amu every second in the multiple ion detection mode (MID) or alternatively, at 100 ms as dwell time for the window in the selected ion monitoring (SIM) detection mode (*m/z* 229, *m/z* 279). The GC separation was carried out on the same capillary column. Calibration of the mass spectrometer was checked daily, using perfluorobutylamine (PFBA).

2.3. Procedure

Beef samples were purchased from a local market and were broiled well done over a grill and a charcoal fire. A bed of charcoal was prepared and ignited. When all flames had subsided, the bed was levelled by raking. Patties of beef (100–200 g, 1 cm thick) were then cooked on a wire mesh placed 5 cm above the charcoal at a temperature of 200–250°C for 15 min. After broiling, 85% of the mass was removed. Each sample was thoroughly mixed in a mechanical blender. A 50-g minced meat sample was saponified with NaOH in ethanol for 2 h under reflux. The mixture was cooled and filtered through an ethanol-rinsed glass wool pad into a 500-ml separatory funnel and extracted three times with cyclohexane. Cyclohexane extracts were combined and washed with warm 0.1 M NaOH to decrease the emulsion formation at the liquid–liquid interface. The cyclohexane phase was evaporated under reduced pressure to 5–10 ml, transferred to a 100-ml separatory funnel, and partitioned with 6 M sulphuric acid. The acidic layer was diluted with water, neutralized with 10 M NaOH and extracted with three portions of cyclohexane. Cyclohexane layers were combined and further

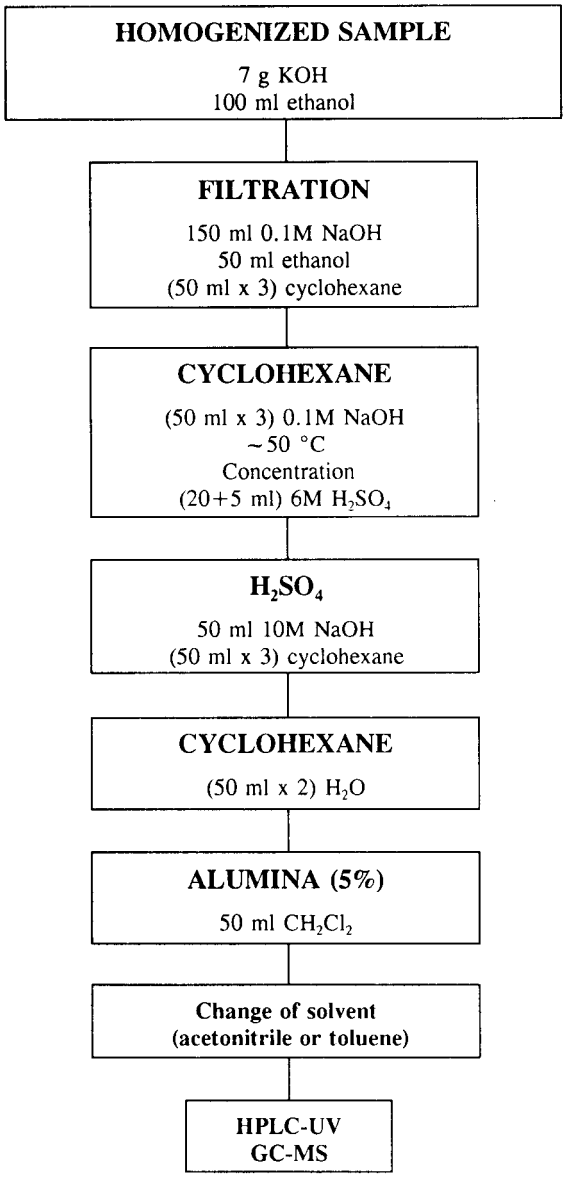

Fig. 1. Enrichment procedure of azaarenes from meat.

washed with 100 ml of water and concentrated to a small volume (1 ml) on a rotary evaporator at 30°C.

The concentrated extract was applied to the top of 10 g 5% aqueous (by weight) deactivated alumina in a column and eluted with 50 ml methylene chloride. The eluate was concentrated to near dryness on a rotary evaporator and then to dryness in a stream of nitrogen. The residue was dissolved in 0.5 ml acetonitrile (for LC analysis) or toluene (for GC analysis). The method is schematically presented in Fig. 1.

A 0.5–5 g of creosote oil sample (SANA, Spain) was dissolved in cyclohexane (25 ml) and extracted with 6 M H_2SO_4, then the above mentioned clean-up procedure was performed (Fig. 1).

3. Results and discussion

3.1. LC analysis

A C_{18} stationary phase was used to separate the azaarene compounds. Four acetonitrile–water mobile phases ranging from 70 to 100% acetonitrile were evaluated. The optimum separation between the compounds was obtained at 90% acetonitrile, although at these conditions no separation between Db(aj)Ac and Db(ai)Ac was obtained. This compounds could not be separated using other mobile phases. Fig. 2 illustrates a typical separation of a standard mixture, where enough resolution was obtained (1.45 for dibenzo(*a*,*j*)acridine and dibenzo(*a*,*c*)acridine) in a relatively short analysis time (8 min).

Calibration plots for the PANHs were found to be linear ($r > 0.999$) in the range of working concentrations (0.8–80 ng injected). The detection limits for the PANHs are shown in Table 2. These values based on a signal-to-noise ratio of 2:1 were in the range of 0.1 to 0.4 ng. Ten replicate determinations ($\sim 0.5\ \mu g\ ml^{-1}$ solution) of each acridine compound in acetonitrile were carried out under the optimum conditions to determine the precision of the method. Relative standard deviations (R.S.D., %) in the range 3.6–5.5% based on concentrations were obtained (Table 3). Higher R.S.D. values in the range 4.7–7.5% were obtained when the experiment was performed on three different days (Table 3).

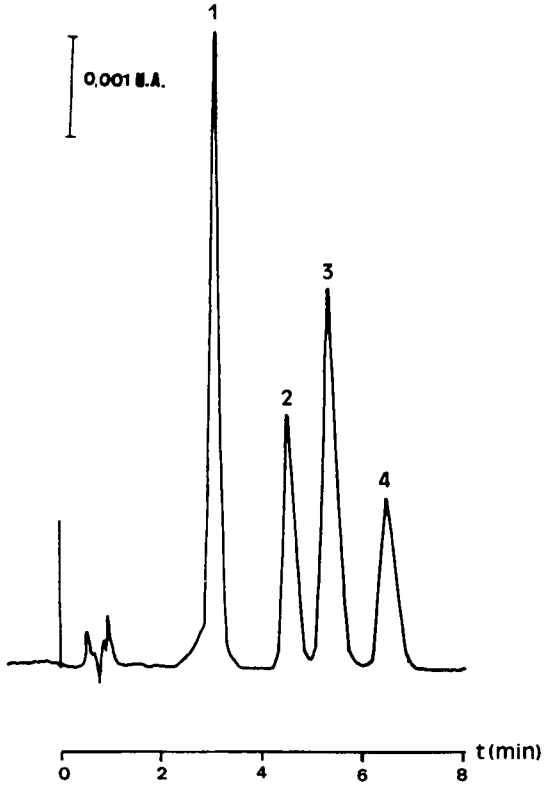

Fig. 2. Chromatogram of PANHs (0.4 $\mu g\ ml^{-1}$) by LC with UV detection. (1) B(c)Ac; (2) DB(aj)Ac; (3) DB(ac)Ac; (4) DB(ch)Ac.

3.2. GC analysis

Fused silica DB-17 was used for the separation of the PANHs, with FID and MS in MID and

Table 2
Detection limits of PANHs

PANH	Detection limits (ng injected)			
	LC-UV [a]	GC-FID [b]	GC–MS [b]	GC–MS/SIM [b]
B(c)Ac	0.11	0.55	0.05	0.01
Db(aj)Ac	0.30	1.23	0.29	0.04
Db(ac)Ac	0.15	1.50	0.26	0.04
Db(ch)Ac	0.40	0.75	0.21	0.04
Db(ai)Ac	–	3.20	0.76	0.14

[a] 10 μl injected.
[b] 1 μl injected.

Table 3
Reproducibility run-to-run ($n = 8$) and day-to-day ($n = 3$)

Acridines	Run-to-run		Day-to-day	
	Mean $\mu g\ ml^{-1}$	R.S.D. (%)	Mean $\mu g\ ml^{-1}$	R.S.D. (%)
B(c)Ac	0.39	3.66	0.38	4.72
DB(aj)Ac	0.47	5.45	0.45	7.50
DB(ac)Ac	0.60	4.57	0.60	6.15
DB(ch)Ac	0.53	4.12	0.53	7.00

SIM mode as detectors. The high resolving capability of GC together with the MS molecular structure information allows identification of PANHs in complex mixtures. EI mass spectrometry at 70 eV is frequently used for the identification of PAHs and their derivatives; typically, by comparison of sample mass spectra with published standard compound spectra found in the literature or in mass spectral libraries [19,20]. EI mass spectra of isomeric PANHs are very similar; the molecular ion is usually the base peak and normally little fragmentation is observed. The EI mass spectral data of the PANHs studied are given in Table 4.

Sensitivity and selectivity of GC–MS in both MID and SIM modes were also evaluated for compound identification. Ions for the SIM program were chosen according to maximum abundance, maximum specificity, and the lowest interference from other ions. Detection limits expressed as ng injected are based on a 2:1 signal-to-noise ratio (Table 2). The detection limits obtained with the MID mode are similar to those obtained using the LC-UV technique but the selectivity is higher in mass spectrometry. If the SIM mode is used the sensitivity is significantly enhanced in comparison to the MID trace and

Table 4
Electron impact mass spectrum data

PANH	MW	Electron impact mass spectrum, m/z (relative intensity)			
BcAc	229	229 (100)	228 (36)	230 (21)	114 (14)
DB(ch)Ac	279	279 (100)	139 (25)	280 (23)	278 (21)
DB(ac)Ac	279	279 (100)	139 (44)	278 (32)	280 (23)
DB(aj)Ac	279	279 (100)	280 (23)	140 (21)	277 (19)
DB(ai)Ac	279	279 (100)	280 (57)	139 (57)	154 (31)

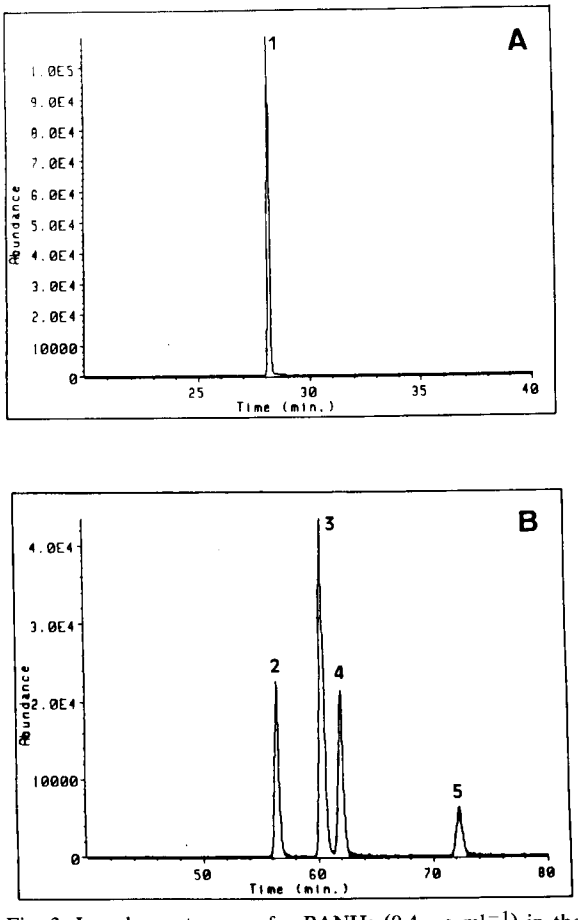

Fig. 3. Ion chromatograms for PANHs (0.4 $\mu g\ ml^{-1}$) in the SIM mode. (A) m/z 229; (B) m/z 279. (1) B(c)Ac; (2) DB(ch)Ac; (3) DB(ac)Ac; (4) DB(aj)Ac; (5) DB(ai)Ac.

the detection limits were in the range of 0.01 to 0.1 ng. These values are similar to those indicated in the literature for LC with fluorimetric detection [5,6] and lower than the values reported using GC with a thermionic detector [6]. The ion chromatograms for a standard mixture of PANHs in the SIM mode are given in Fig. 3.

3.3. Recovery and application

The enrichment procedure results in a fraction that contains the nitrogen compounds. Recoveries of the PANHs from beef samples using the proposed procedure were determined by spiking raw beef samples between 3 to 15 ng g^{-1} PANHs.

Table 5
Recoveries pf PANH standards ($n = 3$)

Compound	3 M H_2SO_4 meat	6 M H_2SO_4 meat	6 M H_2SO_4 creosote
Benzo(*c*)acridine	95.4±5.6	89.5±6.4	98.0±6.1
Dibenzo(*a*,*j*)acridine	61.5±3.9	71.0±1.8	77.0±3.0
Dibenzo(*a*,*c*)acridine	91.4±5.3	92.1±2.6	98.7±5.8
Dibenzo(*c*,*h*)acridine	9.8±1.8	97.7±3.8	99.2±3.3

Samples were analysed by LC using the aforementioned conditions. The percentage of recovery for each compound is given in Table 5. Dibenzo(*c*,*h*)acridine was extracted in low yield (~10%) using 3 M H_2SO_4, although for the other PANHs recoveries were much higher (60–95%). Steric factors account for differences in basicity and also in the extraction behaviour. Boparai [21] suggested the use of methanol or an increase in the concentration of the acid (6 M HCl) to improve the recoveries. Using 6 M H_2SO_4 the recovery of the dibenzo(*c*,*h*)acridine was significantly enhanced (98%) as can be seen in Table 5. Similar results (between 77 and 99%) were obtained for the creosote spiked samples using 6 M H_2SO_4. In Table 5 it can be seen that the recoveries for Db(aj)Ac are always somewhat lower (71%) than those obtained for the other compounds; this fact was also observed by Joe et al. [12] who obtained 65% recovery for this compound in smoked food samples. The behaviour of the dibenzo(*a*,*j*)acridine can be attributed to its higher basicity due to the absence of steric hindrance, which allows higher interactions with the polar phases used in the clean-up procedure.

The method was applied to the determination of PANHs in real samples: charcoal-grilled beef and creosote, which were analyzed by LC-UV

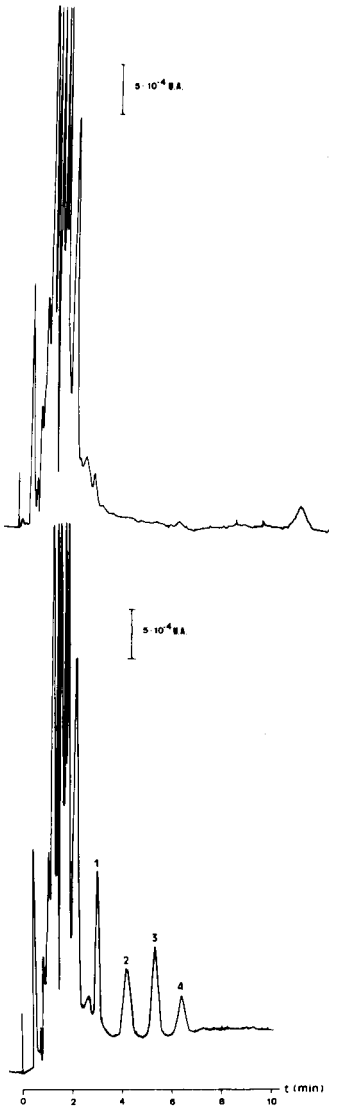

Fig. 4. Chromatogram of a processed meat sample and a spiked sample at ppb levels (5–7 ng g^{-1}). (1) B(c)Ac; (2) DB(aj)Ac; (3) DB(ac)Ac; (4) DB(ch)Ac.

Table 6
Analysis of charcoal-grilled meat and creosote (acridine derivative concentration, ng g^{-1})

sample	BcA		DBajA		DBacA		DBchA	
	Spiked	Found	Spiked	Found	Spiked	Found	Spiked	Found
Meat A	–	< 0.1	–	< 0.3	–	< 0.1	–	< 0.4
Meat B	4.9	4.7	5.6	5.8	7.3	6.8	5.8	5.8
Meat C	9.1	8.5	10.4	10.3	13.6	13.3	12.8	12.7
Creosote	–	547 [a]	–	< 3.0	–	< 1.5	–	< 4.0

[a] $\mu g\ g^{-1}$.

and GC–MS-SIM. The compounds were quantified by the standard addition method. No measurable amounts of azaarenes were detected (less than 400 pg g^{-1} of processed meat) in the beef samples (A). The results obtained for two different spiked samples at ppb levels (B,C) are given in Table 6 where good agreement between the spiked and found amounts is observed; a liquid chromatogram of a meat sample and a spiked sample are shown in Fig. 4. GC–MS has been shown to be highly sensitive and it is a useful mean of confirming the results obtained by LC. Although no PANHs were isolated from the grilled meat analyzed, the recovery data and the results of Table 6 indicate that the method is reliable. A sample of creosote was also analyzed and the results are given in Table 6. Mass spectrometry was used to confirm the occurrence of the benzo(*c*)acridine in this sample at the ppm level.

References

[1] D.W. Later, in A. Bjørseth and T. Ramdahl (Eds.), Handbook of Polycyclic Aromatic Hydrocarbons, Vol. 2, Marcel Dekker, New York, 1985, p. 265.
[2] M.L. Lee, M.V. Novotny and K.D. Bartle, in Analytical Chemistry of Polycyclic Aromatic Compounds, Academic Press, New York, 1981, p. 17.
[3] G. Grimmer, K.W. Naujack and G. Dettbarn, Toxicol. Lett., 35 (1987) 117.
[4] T. Handa, T. Yamauchi, K. Sawai, T. Yamamura, Y. Koseki and T. Ishii, Environ. Sci. Technol., 18 (1984) 895.
[5] T. Yamauchi and T. Handa, Environ. Sci. Technol., 21 (1987) 1177.
[6] N. Motohashi, K. Kamata and R. Meyer, Environ. Sci. Technol., 25 (1991) 342.
[7] M. Novotny, J.W. Strand, S.L. Smith, D. Weisler and E.J. Schwende, Fuel, 60 (1981) 213.
[8] M.G. Ondrus and T.R. Steinheimer, J. Chromatogr. Sci., 28 (1990) 324.
[9] C.A. Menzie, B.B. Potocki and J. Sandonato, Environ. Sci. Technol., 26 (1992) 1278.
[10] A.J. Miller, Food Technol., 2 (1985) 75.
[11] International Agency for Research on Cancer (IARC), Monographs, 3, Lyon, 1973.
[12] F.L. Joe, J. Salemme and T. Fazio, J. Assoc. Off. Anal. Chem., 69 (1986) 218.
[13] G. Grimmer and K.W. Naujack, J. Assoc. Off. Anal. Chem., 69 (1986) 537.
[14] T. Sugimura and M. Nagao, CRC Crit. Rev. Toxicol., 6 (1981) 189.
[15] M.T. Galceran, P. Pais and L. Puignou, J. Chromatogr. A, 655 (1993) 101.
[16] T. Nielsen, P. Clausen and F.P. Jensen, Anal. Chim. Acta, 187 (1986) 223.
[17] C.A. Krone, D.G. Burrows, W.B. Brown, P.A. Robisch, A.J. Friedman and D.C. Malins, Environ. Sci. Technol., 20 (1986) 1144.
[18] W.C. Brumley, C.M. Brownrigg and G.M. Brilis, J. Chromatogr., 558 (1991) 223.
[19] Eight Peak Index of Mass Spectra, Mass Spectrometry Date Centre, Awre, UK, 1974.
[20] S.R. Heller and G.W.A. Milne, EPA/NIH Mass Spectral Data Base, U.S. Department of Commerce, NSRDS-NBS/63, U.S. Government Printing Office, Washington, DC, 1978.
[21] A.S. Boparai, D.A. Haugen, K.M. Suhrbier and J.F. Schneider, in C.W. Wright, W.C. Weimer and W.D. Felix (Eds.), Advanced Techniques in Synthetic Fuels Analysis, National Technical Information Service, U.S. Department of Commerce, Springfield, VA, 1983, p. 3.

ELSEVIER

Analytica Chimica Acta 295 (1994) 315–324

ANALYTICA CHIMICA ACTA

Analytical performance of the microwave plasma torch in the determination of rare-earth elements with optical emission spectrometry

Yixiang Duan, Yimo Li, Xiaodan Tian, Hanqi Zhang, Qinhan Jin *

Department of Chemistry, Jilin University, Changchun 130023, China

Received 24th January 1994; revised manuscript received 15th April 1994

Abstract

A recently developed microwave discharge device called the microwave plasma torch (MPT) is used in this work to evaluate its analytical performance in the determination of rare earth elements with optical emission spectrometry. Optimization of the instrument was performed by using individual elements with emphasis on the plasma observation zone, carrier and support gas flow rates. The detection limits for 15 rare earth elements obtained by MPT atomic emission spectrometry at 70 W are in the order of ng/ml. The precision (R.S.D.%) calculated with eleven continuous measurements at a concentration of about two orders of magnitude higher than the detection limits is in the range of 2.0 (Y) to 4.9 (Tb). Some comparisons were made between inductively coupled plasma and MPT methods, and the results show that in some cases, most of the sensitivity lines observed in these two sources for rare-earth elements are not identical. Compared with the ICP emission spectrum, the MPT source gives relatively simple spectra and much lower background emission. A preliminary examination of matrix effects with varying matrix concentrations shows that some easily ionized elements give significant enhancement on analyte signal and that aluminum suppresses the signals considerably. For some other elements (Co, Ni and Zn) no remarkable matrix effects are observed at a concentration level of 10 μg/ml.

Keywords: Atomic emission spectrometry; Microwave plasma torch; Rare-earth elements; Matrix effects

1. Introduction

The rare-earth elements are becoming increasingly important in many aspects of science and industry. These elements play an important role in semi- or super-conductor research, metal alloy characteristics and materiel properties. Therefore, the determination of rare-earth elements in trace levels is an additional challenge in analytical atomic spectrometry since the rare-earth elements have very similar specific properties.

Atomic spectrometry is a relatively powerful technique for the determination of rare-earth elements. Although atomic absorption spectrometry (AAS) could give precise and accurate results for rare-earth element determination, as was reported in the literature [1], the applicability of this technique is limited to some extent by the

* Corresponding author. Department of Chemistry, Jilin University, Changchun 130023, China.

SSDI 0003-2670(94)00190-W

monoelement detection character. Actually, inductively coupled plasma atomic emission spectrometry (ICP-AES) has proved to be a useful method for routine determination of rare-earth elements with capability of simultaneous multi-element analysis. Several workers reported that rare-earth elements show good sensitivity in ICP-AES [2–4]. However, a large number of spectral lines from rare-earth elements and strong background emission from ICP somewhat restrict the applicability of this technique to mixed rare-earth element determination. The complexity of the analyte emission lines and the potential spectral line overlap interferences from co-existing rare-earth elements and other major elements, have led to the use of different separation methods to remove the bulk of major elements and at the same time to concentrate the rare-earth elements [5–7]. In most cases, an ion-exchange method was used for separation purposes, but this procedure is time consuming.

Plasma source mass spectrometry (PS-MS) is a powerful technique for rare-earth elements determination. This technique provides many advantages, such as high sensitivity, good selectivity and simultaneous multi-element analysis. It has been widely used in various real sample analyses [8–10]. However, the instrumentation of PS-MS is relatively expensive.

As an alternative source, microwave plasma techniques have received wide attention in spectrochemical analysis in the past decade [11,12]. Compared to ICP, the microwave plasma is usually far from local thermodynamic equilibrium. The thermal temperature in microwave plasma is substantially lower than that in the ICP and the electron temperature is much higher. The high electron temperature used in microwave plasma techniques provides MIP as an excellent source for atomic emission spectrometry, especially for high potential elements (e.g., non-metal elements). However, traditional microwave plasmas usually suffer some problems such as poor tolerance for solvent loading and instability when operated at low power. A recently reported microwave plasma device, called the microwave plasma torch (MPT) shows potential utilities in spectrochemical analysis [13]. Its excellent working stability [14], relatively higher tolerance to foreign materials [15] and fairly good detection sensitivity demonstrate that MPT may be a promising source for atomic spectrometry.

In this article, the MPT source was first applied to studies on the determination of rare-earth elements by optical emission spectroscopy. Factors that affect the analytical performance are investigated in detail using several typical rare-earth elements. The detection limits, linear dynamic range and precision for fifteen rare-earth elements were examined. A preliminary investigation was made on matrix interference for the determination of rare-earth elements. The typical spectra for rare-earth elements obtained by MPT in the wavelength range from 250 to 550 nm shows relatively simple spectral lines and usually give much lighter background emission.

2. Experimental

2.1. Instrumentation

The experimental set-up used in this study is similar to that described elsewhere [15]. It mainly consists of a microwave power supply (WB-WC, 2450 MHz, Wenzhou Instrument Co.), a monochromator (WDG 500-II, Beijing second optical Instruments Co.), a humidifier based ultrasonic nebulizer (CSW-1, Shento Optic-Electronic Instruments) and a locally fabricated microwave plasma torch (MPT). The MPT device was mounted on the translation stage which allows both horizontal and vertical adjustment for lens focusing and selection of plasma observation zone. Sample solution contained in a Pyrex glass cell was nebulized by an ultrasonic nebulizer and the aerosol produced was introduced into the plasma through a desolvation-desiccator system, which was developed and examined recently [16,17]. The desolvation efficiency for this system is as high as 99%. Therefore, the aerosol was almost completely dried before reaching plasma. A radial (side-on) viewing mode was used for signal measurements. In this arrangement, a lens assembly was used to focus the emission from the plasma onto the entrance slit of the monochromator, and

the produced signals were amplified by PMT and recorded by a chart-feed recorder (LM 14Y, Dahua, Shanghai). The experimental procedures are similar to those described in our previous work [16].

2.2. Reagents

All the reagents used in this work are of analytical grade. Distilled–deionized water was used for preparation of solutions. Stock solutions of rare-earth elements were prepared from rare-earth element oxides (99.99%). The concentration of stock solution is usually 1 mg/ml for rare-earth elements. The working standards were prepared from the stock solution by serial dilution with 0.1 M hydrochloric acid. Other solutions, which are used for matrix studies, were prepared according to the recommended standard procedures. The purity of argon used as working gas is 99.99%.

3. Results and discussion

3.1. Selection of optimal slit and plasma observation zone

Both the slit width and height have important influence on the signal-to-background (S/B) ratio. The selection of slit width was based on the following considerations: (1) high S/B ratio; (2) good precision. In the experiment, the inlet and outlet slits of the monochromator are 30 mm for La, Ce, Pr, Nd, Sm and 10–25 mm for Eu, Gd, Tb, Dy, Ho, Er, Tm, Yb, Lu and Y, respectively. A vertical examination of the signal-to-background intensity ratio shows that the best observation zone is located at the crossing point [18] of the MPT plasma. To minimize the background emission from the plasma, a 2 mm slit height was chosen, which corresponds to the best observation zone by changing the translation stage properly.

3.2. Optimization of plasma parameters

Optimization of plasma parameters was mainly performed on the microwave power, carrier and support gas flow rates. Usually, microwave power is one of the most important parameters which influence the plasma performance, such as plasma shape, stability and capability of atomization and excitation of analytes. The MPT plasma volume is usually enlarged with the increase of microwave power. For the determination of rare-earth elements, S/B usually tends to level off after the microwave power approaching 70 W. Although a small, but not significant increase on S/B was observed for some rare-earth elements, such as La, Ce, Nd, Y, Yb, Tm and Eu when 100 W power was used, usually the precision became a little bit worse at relatively high power (100 W) than at the low power (70 W). As a result of comprehensive consideration on the above influences, a compromised power (70 W) was selected as an acceptable value for all the subsequent experiments.

As we expected, both carrier and support gas flow rates have significant influence on S/B (Fig. 1 and Fig. 2). Usually, optimal S/B values were obtained in the flow rate range from 500 to 600 ml/min for both carrier and support flow rates when microwave power was fixed at 70 W. However, carrier gas plays an important role on sampling amount, dilution factor and even solvent loading, while the support gas considerably contributes to maintaining the plasma stability and plasma shape, as well as sample dilution in the

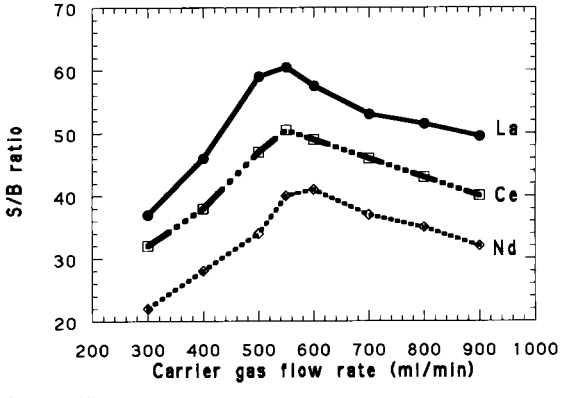

Fig. 1. Effect of carrier gas flow rate on signal to background ratio. Working solution: La, 2 μg/ml; Ce, 10 μg/ml; Nd, 3 μg/ml in 0.1 M HCl. Other experimental conditions are as shown in Table 1.

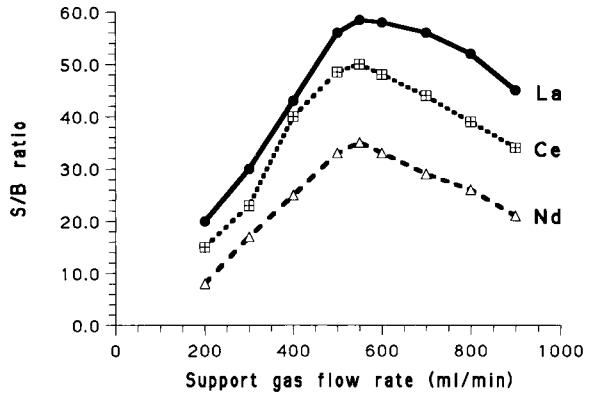

Fig. 2. Effect of support gas flow rate on signal to background ratio. Experimental conditions as in Fig. 1.

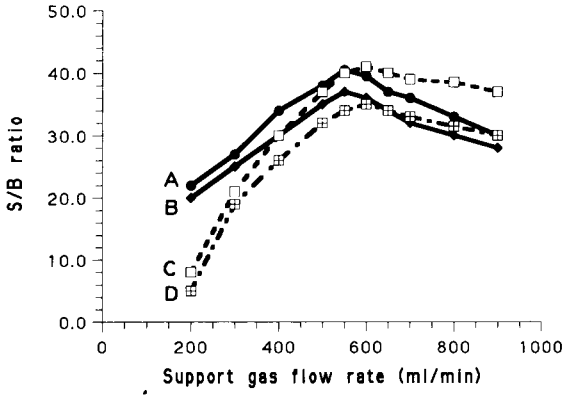

Fig. 4. Effect of support gas flow rate at varied microwave power. (A) Eu, 90 W; (B) Eu, 70 W; (C) Yb, 90 W; (D) Yb, 70 W. Other experimental conditions as in Table 1.

plasma. Examinations of carrier gas flow rate influence under different power conditions showed that the optimal values of carrier gas flow rate were shifted when the power varies (Fig. 3). Generally, a higher microwave power is needed to match a higher carrier gas flow rate. In the influence of support gas flow rate, however, such a shift is not observed at different power levels, though S/B also slightly increased with a relatively higher microwave power (Fig. 4). Again, as the precision becomes worse with the increased power, no improvement of the analytical figures was obtained.

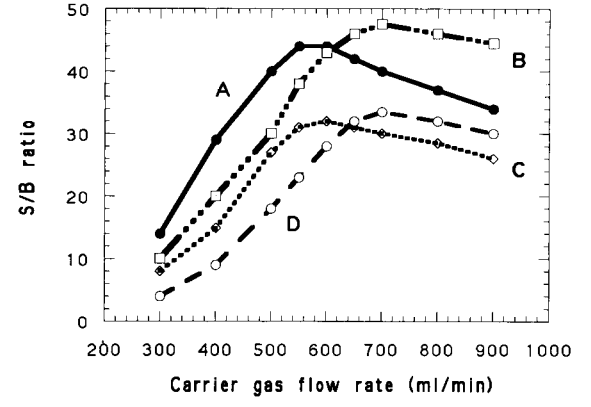

Fig. 3. Effect of carrier gas flow rate at varied microwave power. (A) Y, 70 W; (B) Y, 90 W; (C) Yb, 70 W; (D) Yb, 90 W. Other experimental conditions as in Table 1.

3.3. Analytical figures of merit

Under the compromised operating conditions, the detection limits, relatively standard deviation (R.S.D.) and linear dynamic range are evaluated for the MPT-AES system in the determination of rare-earth elements. The detection limits, as defined by IUPAC guidelines, were calculated based on the data obtained from pure individual analyte solutions. The standard deviation is estimated from 11 consecutive signals during the continuous nebulization of sample solutions which have concentrations of about two orders of magnitude higher than the detection limits. The R.S.D. obtained for MPT-AES is in a range from 2.0% (Y) to 4.9% (Tb). Standard solutions containing individual analytes with a series of concentrations one order of magnitude higher than the detection limits to an upper level of about 100 μg/ml were prepared and examined for different rare-earth elements. Calibration graphs (Fig. 5) show that the linear dynamic range is generally more than three orders of magnitude. The slopes for log–log plots determined by linear regression range from 0.94 to 1.01 for the three elements examined. The r^2 values are from 0.987 to 1.02. In most cases, the graphs curved towards the concentration axes when the concentration is over 100 μg/ml.

The analytical wavelengths for the calculation of detection limits for rare-earth elements were selected from available lists of prominent lines

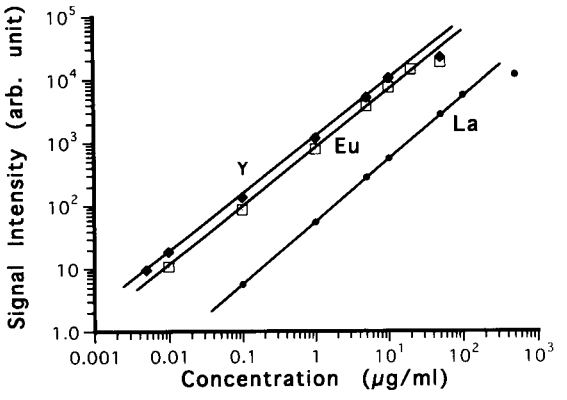

Fig. 5. Calibration graphs of rare-earth elements for MPT-AES.

reported in ICP-AES [19,20]. Since ionic lines of rare-earth elements are usually more intense than the atomic lines, only ionic lines were selected for analysis. The detection limits listed in Table 2 are defined as the concentration of the sample that produces a signal three times the standard deviation of the blank divided by the slope of the calibration curve. For comparison purposes, the detection limits of rare-earth elements estimated by Winge et al. [19] with ICP-AES using a pneumatic cross-flow nebulizer without desolvation were also listed in Table 2. Although a direct comparison may not be proper among these two systems, because an ultrasonic nebulizer was used in the present work, we can say that MPT-AES system gives fairly good results. Since the analytical wavelengths used are recommended for ICP-AES and actually MPT has a different excitation mechanism and different emission spectra (see Figs. 6 and 7), a more detailed search on selection of analytical wavelengths may, to some extent, improve the detection limits. It was found that several rare-earth elements have different maximum emission lines (see Table 2 and Table 3). For example, the most intense spectral line of La in the ICP source is 379.478 nm. However, in the MPT source, the maximum line for La is 408.67 nm rather than 379.478 nm. Actually, the 379.478 nm line is only about 57% of the 408.67 nm line in the MPT spectrum. Therefore, the detection limits of MPT-AES are improved when these very intense lines are used in the MPT system (see Table 2).

Table 1
Experimental facilities and operational conditions

Monochromator	WDG 500-II, 1200 grooves/mm, entrance and exit slits: 10–30 mm
Plasma	
Microwave generator	As supplied by Wen-Zhou Co., rated at 200 W at 2450 MHz.
MPT	Laboratory built, as described in the literature [13].
Incident power	70 W
Reflected power	ca. 0 W
Carrier gas flow rate	500–550 ml/min.
Support gas flow rate	500–550 ml/min.
Vertical observation zone	Zone height of 2 mm, centered at crossing point of the plasma.
Plasma viewing mode	Side-on
Nebulizer	Self-assembled ultrasonic nebulizer based on commercial humidifier operated at 1.4 MHz.
Sample uptake rate	0.38 ml/min.
Desolvation system	As described in the literature [17]. It consists of a heating device, a water-cooling system and a concentrated sulfuric acid desiccator.

3.4. Some comparisons of MPT and ICP systems

To highlight the different excitation mechanisms for MPT and ICP, a relatively systematic comparison was made for different rare-earth elements with the emphasis on the relative spectral line intensity and background complexity. Analyte scans for eleven elements were performed in the wavelength range from 250 to 550 nm. The concentrations used for these scans are usually 200 times higher than the detection limits. The scan speed is fixed at 67 A/min. Other operational conditions are identical to those listed in Table 1 except for microwave power in which 80 W was used to robust the plasma. Table 3 gives the normalized S/B values for both MPT and ICP. Please note that the S/B values were separately normalized for individual elements and individual sources. For example, all spectral lines were normalized by using S/B values of 379.48 nm as 100% for the ICP system; while for MPT, the normalization was performed with an S/B value of 408.67 nm since this line gives the maxi-

Table 2
Analytical figures of merit for MPT-AES in the determination of rare-earth elements

Element	Wavelength (nm)	Detection limit (ng/ml)		Precision (R.S.D. %)
		MPT	ICP [a]	
La(II)	379.48	11	10	4.3
	480.67	6.3	10	
Ce(II)	413.77	83	48	4.8
Pr(II)	390.84	51	37	4.5
Nd(II)	401.23	23	50	4.1
	410.95	22	115	
Sm(II)	359.26	29	43	4.2
Eu(II)	381.97	0.8	2.7	2.2
	420.51	0.6	4.3	
Gd(II)	342.25	5	14	3.2
Tb(II)	384.87	65	55	4.9
Dy(II)	364.54	4.2	23	3.7
Ho(II)	345.60	1.5	5.7	3.3
	389.10	0.4	16	
Er(II)	323.06	6.1	18	3.3
Tm(II)	346.22	1.2	8.1	2.7
	384.80	0.2	9.7	
Yb(II)	328.94	0.7	1.8	2.3
Lu(II)	261.54	0.5	1.0	3.4
Y(II)	371.03	0.3	3.5	2.0

[a] Cited from [19].

mum S/B value for the MPT system. It can be seen from the Table that the maximum signal to background ratio of spectral lines in MPT and ICP is not identical. In most cases, a maximum red shift was observed in the MPT plasma. This is probably caused by the different excitation mechanisms in the different plasmas. In microwave plasmas, free electrons are probably the most active species in energy transfer processes. The electrons efficiently absorb energy from the electric field of the microwave and then transfer their kinetic energy to other species by elastic and/or inelastic collisions. The most efficient way for electrons to transfer energy to heavy particles, such as the analyte, is through inelastic collisions, including collisional excitation and ionization. Although the direct excitation of analyte by electron collision is not dominant in the MIP plasma for non-metals, however, for some analytes with relatively low ionization potentials, direct excitation by electron collision should play a role. In this point of view, it seems that electron impact and metastable species play more important roles in the excitation process in MPT than in ICP, and thermal excitation plays a less important role. Because a low resolution monochromator (1200 grooves/mm) was used in this work, only in some cases the spectral line overlap was observed. For example, the 492.098 and 492.179 lines of La can not be resolved with this monochromator system. Figs. 6 and 7 show the typical spectra of La and Nd obtained by MPT. Compared with the atlas of those elements reported from ICP system [21], the MPT source gives relatively simple spectra and much lighter background emission. Those characteristics make the MPT source even more attractive in the determination of rare-earth elements considering their complex spectral lines.

3.5. Matrix effects

Spectral interferences from Fe on almost all analytes examined are obvious in this particular monochromator system since Fe has many spectral lines. Usually, an equal amount of Fe in the analyte gives a significant contribution to the emission intensity of rare-earth element analytical lines. Because rare-earth elements also have many emission lines, the mutual spectral interfer-

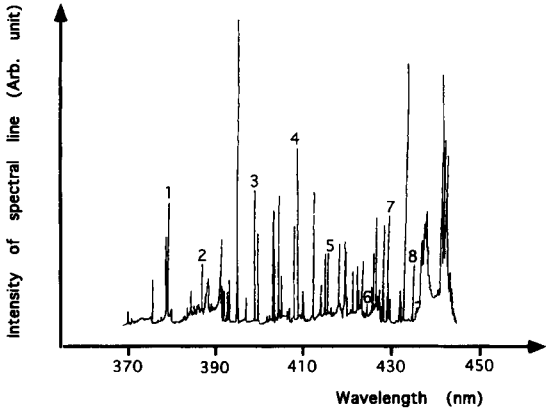

1. La (II) 379.478 2. La (II) 387.164 3. La (II) 398.852
4. La (II) 408.672 5. La (II) 415.197 6. La (II) 423.838
7. La (II) 429.605 8. La (II) 435.440

Fig. 6. Lanthanum emission spectrum obtained by MPT. Working solution: 2 μg/ml La; microwave power: 80 W; scan speed: 67 A/min. Other experimental conditions as in Table 1.

Table 3
Spectral lines of some RE elements in MPT and ICP sources [a]

Element	Wavelength (nm)	Normalized signal/background (%)	
		ICP [b]	MPT
La			
	333.749 II	98	20
	338.091 II	67	4
	364.542 II	42	6
	371.354 II	29	3
	379.478 II	100	57
	387.164 II	74	24
	398.852 II	91	58
	408.672 II	95	100
	415.197 II	41	18
	423.838 II	52	20
	429.605 II	70	46
	435.440 II	28	24
	442.990 II	52	27
	455.846 II	23	5
	465.550 II	30	7
	474.028 II	27	5
	482.406 II	17	0
	492.098 II	50	31
	492.179 II		
	499.947 II	28	11
	512.299 II	30	10
Nd			
	378.425 II	52	16
	386.333 II	69	35
	386.340 II		
	394.151 II	56	24
	401.225 II	100	96
	410.946 II	64	100
	417.732 II	56	37
	424.738 II	52	31
	430.358 II	69	100
	435.817 II	39	35
	445.157 II	50	49
	464.110 II	23	15
	470.654 II	48	20
	492.453 II	36	55
	509.280 II	32	12
	513.060 II	47	21
Ho			
	339.898 II	59	7
	345.600 II	100	25
	351.559 II	41	5
	359.877 II	19	3
	374.817 II	27	13
	381.073 II	47	49
	389.102 II	57	100
Tm			
	336.261 II	87	8
	346.220 II	100	13
	353.552 II	37	4
	360.877 II	50	5
	370.026 II	67	31
	376.133 II	85	61
	384.802 II	96	100
	395.810 II	46	10
	424.215 II	57	31
Eu			
	368.842 II	36	3
	372.494 II	61	17
	381.967 II	100	82
	390.710 II	63	42
	397.196 II	59	47
	412.970 II	79	73
	420.505 II	83	100
	443.556 II	51	34

[a] S/B values were normalized separately for individual element and individual source.
[b] Cited from [21] with a conversion from log to normal scales.

ences among these elements are considerable. A detailed research on these spectral interferences has not been carried out because of limitations of our low resolution monochromator system. However, some non-spectroscopic interferences, such as matrix effects, which influence both detection

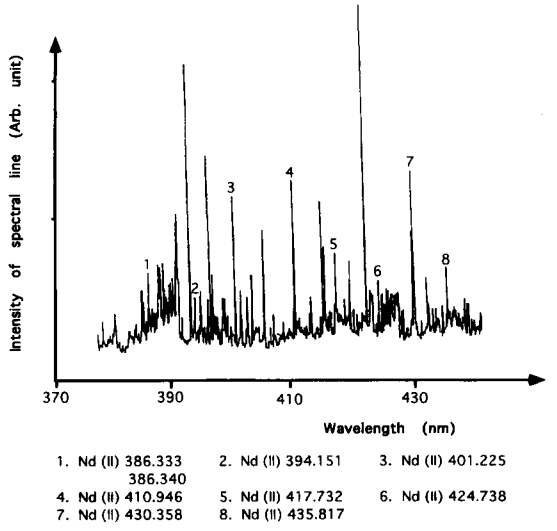

Fig. 7. Neodymium emission spectrum obtained by MPT. Working solution: 4 μg/ml Nd. Microwave power: 80 W. Other experimental conditions as in Fig. 6.

limits and accuracy of the spectrochemical analysis and vary with different excitation sources, were examined in relatively more detail. The work described here provides information on matrix effects under the operating conditions recommended above. No attempt was made to obtain spatial resolution of the effects, so the results presented here refer to overall effects throughout the observation zone at a fixed viewing height in the plasma and with 0.1 M HCl as a blank solution. Four analytes, Eu, Y, Yb and Tm were chosen to examine the matrix effects. A series of elements, Co, Ni, Zn and Al was used as common matrices and K and Ca were used as easily ionized elements (EIE). The effect of the matrix concentration was investigated for the rare-earth elements being examined. Solutions which contain 30 ng/ml of an analyte and varying concentrations of a matrix element were used. The sensitivity obtained at zero matrix concentration was taken as the reference level for each analyte. For several common matrices (Co, Ni and Zn) there are no remarkable matrix effects on the emission intensities of analytes in the matrix concentration range from 30 ng/ml to 10 μg/ml. However, for EIE matrices, the emission enhancement of rare-earth elements was observed for all the analytes examined. As ion lines were used throughout this research on rare-earth elements, these results may be helpful for understanding the mechanism of EIE effects. Figs. 8 and 9 show

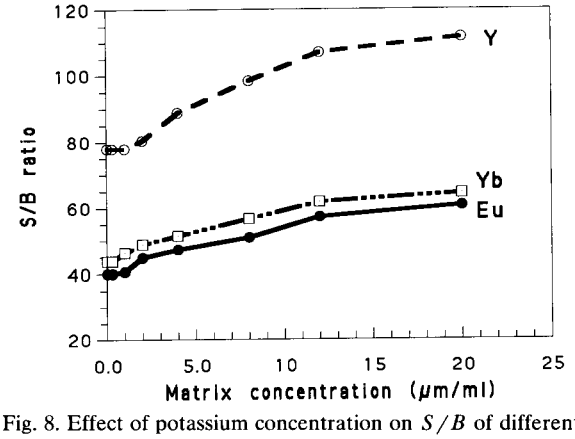

Fig. 8. Effect of potassium concentration on S/B of different rare-earth elements. See text for more details.

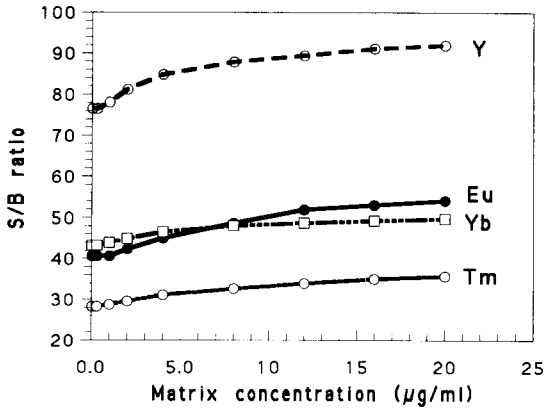

Fig. 9. Effect of calcium concentration on S/B of different rare earth elements. See text for more details.

both K and Ca influences on rare-earth element signal to background ratios. As is shown, the enhancement in the K matrix is nearly approaching 50% at the matrix concentration of 20 μg/ml (Fig. 8), which is approximately 700 times the analyte value; while for Ca the enhancement observed is usually around 20% at the same matrix concentration. This difference is probably correlated with the matrix ionization potential. It can be concluded that K has a much lower ionization potential than Ca. One can expect that a lower ionization potential matrix should give higher signal enhancement according to the ionization equilibrium which occurred in the plasma. Aluminium is another typical matrix element which has been examined several times by ICP-AES [3,22], and it is also examined in this work. Influence from Al on several aspects of analytical performance for the determination of rare-earth elements were observed. First of all, rare-earth element signals were suppressed even at low aluminum concentration. Fig. 10 shows the details of this influence at varied matrix concentration and for different rare-earth elements. Yttrium was most severely suppressed among these analytes. The emission signals decreased significantly with increasing matrix concentration. Moreover, the addition of Al is not only affecting on analyte signal intensity, but, to a considerable extent, also degrades the precision and even signal peak shape. In most cases, the R.S.D. values with the

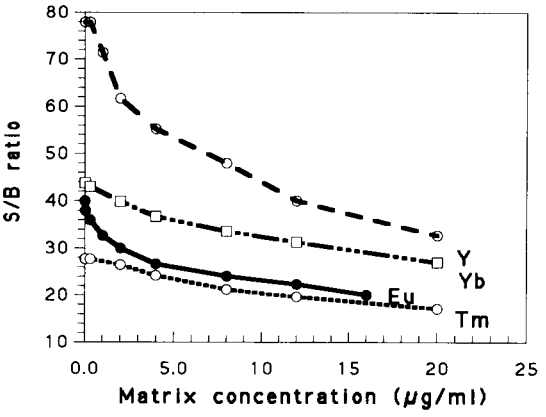

Fig. 10. Effect of aluminum concentration on S/B of different rare earth elements. See text for details.

Al matrix are around 15% or even worse. Besides, the existence of Al in solution also affects the blank (0.1 M HCl) spectrum. The molecular emission band from water was significantly suppressed by adding Al in the solution. This demonstrates that Al has serious influence on the determination of rare-earth elements with MPT-AES. In this point of view, a preliminary separation of aluminum from rare-earth elements is desirable.

4. Conclusion

The microwave plasma torch (MPT) is used to examine the analytical performance on the determination of rare-earth elements with optical emission spectroscopy. Fairly good detection limits were obtained by MPT-AES with a low microwave power and an ultrasonic nebulizer. Compared to the ICP source, the MPT source gives relatively simple spectra and lower background emission. Moreover, most of the sensitivity lines of some of the rare-earth elements observed in MPT and ICP analyses are not identical. A preliminary examination of matrix effects shows that easily ionizable elements definitely enhance the rare-earth signal intensities, and aluminum suppresses them. There are no remarkable matrix effects observed for some general matrix elements at relatively low concentration levels. Further modifications of this MPT-AES system for rare-earth elements determination include use of a high resolution monochromator to cut down spectral interferences, and selection of the most sensitive lines in the MPT system to improve the analytical performance.

Acknowledgments

This work was supported by National Natural Science Foundation of China.

References

[1] W. Ooghe and F. Verbeek, Anal. Chim. Acta, 73 (1974) 87.
[2] J.A.C. Broekaert, F. Leis and K. Laqua, Spectrochim. Acta, 34B (1979) 73.
[3] Y. Nakamura, K. Takahashi, O. Kujirai and H. Kochi, J. Anal. At. Spectrom., 5 (1990) 501.
[4] S. Nikdel, A. Massoumi and J.D. Winefordner, Microchim. J., 24 (1979) 1.
[5] J.N. Walsh, F. Buckly and T. Barker, Chem. Geol., 33 (1981) 143.
[6] A. Bolton, J. Hwang and V.A. Vander, ICP Inf. Newsl., 7 (1982) 498.
[7] J.G. Crock and F.E. Lichte, Anal. Chem., 54 (1982) 1329.
[8] F.E. Lichte, A.L. Meier and J.G. Crock, Anal. Chem., 59, (1987) 1150.
[9] A.R. Date and D. Hutchison, J. Anal. At. Spectrom., 2, (1987) 269.
[10] K.E. Jarvis, J. Anal. At. Spectrom., 4, (1989) 563.
[11] A.T. Zander and G.M. Hieftje, Appl. Spectrosc., 35 (1981) 357.
[12] J.P. Matousek, J. Orr and M. Selby, Prog. Atom. Spectrosc., 7 (1984) 275.
[13] Q. Jin, C. Zhu, M.W. Borer and G.M. Hieftje, Spectrochim. Acta, 46B (1991) 417.
[14] Y. Duan, G. Li, M. Wu, Q. Jin and G.M. Hieftje, in preparation.
[15] Y. Duan, X. Du and Q. Jin, J. Anal. At. Spectrom., in press.
[16] Y. Duan, M. Huo, Z. Du and Q. Jin, Appl. Spectrosc., 47 (1993) 1871.
[17] Y. Duan, H. Zhang, M. Huo and Q. Jin, Spectrochim. Acta, in press.
[18] Y. Duan, X. Kong, H. Zhang, J. Liu and Q. Jin, J. Anal. At. Spectrom., 7 (1992) 7.

[19] R.K. Winge, V.J. Peterson and V.A. Fassel, Appl. Spectrosc., 33 (1979) 206.
[20] P.W.J.M. Boumans, Line Coincidence Tables for Inductively Coupled Plasma Atomic Emission Spectrometry, Vols. 1 and 2, Pergamon, Oxford, 1980.
[21] R.K. Winge, V.A. Fassel, V.J. Peterson and M.A. Floyd, Inductively Coupled Plasma Atomic Emission Spectroscopy: An Atlas of Spectral Information, Elsevier, Amsterdam, 1985.
[22] H.S. Mahanti and R.M. Barnes, Appl. Spectrosc., 37 (1983) 261.

ELSEVIER

Analytica Chimica Acta 295 (1994) 325–330

ANALYTICA CHIMICA ACTA

Rapid chromite dissolution using a manganese dioxide–lithium sulphate–sulphuric acid mixture for matrix-independent determination of chromium

P. Chattopadhyay [a,*], M. Mistry [b]

[a] *Regional Research Laboratory, Bhubaneswar-751013, Orissa, India*
[b] *Geological Survey of India, Bhubaneswar, Orissa, India*

(Received 7th December 1993)

Abstract

A mixture of manganese dioxide–lithium sulphate–sulphuric acid has been used for accurate and precise estimation of chromium in various chromite matrices. Inter-method comparison studies show that the proposed procedure can be used for a quality control programme and in the evaluation of reference materials. The method is very simple and easily adaptable and involves no separation of the analyte from the matrix elements. Sample decomposition is straight forward (0.2 g of sample + 0.3 g of MnO_2 + 1.0 g of Li_2SO_4 + 10 ml of H_2O + 20 ml of 36 M H_2SO_4).

Keywords: Atomic absorption spectrometry; Spectrophotometry; Titrimetry; Chromite dissolution; Chromium; Quality control

1. Introduction

Chromite or chrome ore is the sole commercial source of chromium metal, its alloys and compounds. It is also the major ingredient of an entire group of refractories. The mineral chromite is a spinel with theoretical formula $FeCr_2O_4$, and general formula $(Fe^{2+}, Mg)(Cr, Al, Fe^{3+})_2O_4$. There are wide variations in the composition of chromite because of this isomorphous replacement. Commercial ores fall into three major classes: metallurgical ores, having a Cr_2O_3 content of about 48% with Cr : Fe = 3 : 1 and Cr : Mg > 1; refractory ores, used in making chrome brick, chrome–magnesite brick, plastic cement, and other refractory products, having a high Al_2O_3–Cr_2O_3 content and relatively low iron and silica content; chemical ores, which do not meet the other requirements but contain about 43–47% Cr_2O_3 and are as low in iron and silica as possible.

A characteristic of the analytical requirement at the incoming inspection stage is the accuracy of the results, because these are frequently exchanged between the vendor and the purchaser, and become the subject of financial negotiation.

* Corresponding author.

SSDI 0003-2670(94)00184-N

The precision expected in the analysis of chrome is high because complete analysis of the ore is required to study mineral exploration, deposit evaluation, mill processing development, product impurity specifications (mineral concentrates, metals and alloys) and commodity evaluation. The complexities of mineralogical and metallurgical materials frequently present interferences.

The analysis of chrome ores and chrome-bearing refractories has become a subject of considerable study. The most important step is sample decomposition. The proper dissolution procedure is one which yields no residue or precipitate. It is one of the most refractory minerals with respect to chemical dissolution. It can be fused with alkali metal borate but dissolution of the cooled melt in mineral acid is slow (and impossible if boron trioxide is used as the fusion flux [1]). The methods based on peroxide fusion are tedious and proper care has to be taken to get reproducible results. The time-consuming acid attack involves decomposition of the ore with a mixture of H_2SO_4 and $HClO_4$ [2] and H_3PO_4 [3]. $HClO_4$ decomposition is mainly chosen for determination of Fe, Ca, Al and Mg rather than Cr [4]. Mandal et al [5] utilized a MnO_2–H_2SO_4 mixture in an open vessel which is faster than other acid decompositions and the conventional Na_2O_2 fusion route but lacks the desired speed and simplicity.

Yoshikuni [6] has studied extensively a number of oxidizing agents, such as MnO_2, $Ce(SO_4)_2$, $KMnO_4$ and KIO_4 for the decomposition of refractory oxides (Hf, Ti, Zr) and developed a method involving absorbance measurement of the less sensitive Cr(III) [7]. Of course, x-ray emission spectrometry can be employed for chromite analysis provided known standards of comparable matrices are available.

In a continuation of our previous reports [8–13] on decomposition procedures for accurate analysis of different elements in complex geological matrices, this paper describes a rapid and simple method for estimation of Cr in chromite matrices involving Li_2SO_4–MnO_2–H_2SO_4 decomposition. Further, the selection of an interference-free Cr spectral line is a prerequisite for accurate determination by flame atomic absorption spectrometry (FAAS). The aim of this work, therefore, is also to establish an appropriate matrix/ionization suppression buffer for FAAS.

2. Experimental

2.1. Materials

All chemicals were of analytical-reagent grade unless otherwise specified. Distilled water was used throughout.

2.2. Instrumentation

The analyses were carried out using a Varian Techtron AA-1475 spectrometer, equipped with a deuterium arc background correction system, coupled with an Epson LX-800 printer and Varian DS-15 data station. The instrumental parameters were as follows: wavelength, 357.9 nm; slit width, 0.2 nm; lamp current, 7 mA; integration time, 2 s; flame, air–acetylene (reducing); and double beam ON. A Varian (DMS 100) double-beam UV–vis spectrophotometer with a 10-mm quartz cell was used for absorbance measurements.

2.3. Procedure

Weigh accurately 0.2 g of sample (dried at 105°C for 2 h), 0.3 g of MnO_2 and 1.0 g of Li_2SO_4 and place them in a 250-ml borosilicate glass beaker. Add 10 ml of water and 20 ml of H_2SO_4 (36 M). Cover the mouth of the beaker with a watch glass and heat strongly at about 250°C with occasional stirring with beaker tongs for about 1 h. Observe the bottom of the beaker (the solution becomes brown at this stage and no black/brown particles should be seen). Cool, add 30 ml of water and boil for 5 min. Transfer the solution into a 100-ml volumetric flask and make up to volume with water.

Transfer an aliquot (50 ml) into a 250-ml beaker and add 50 ml of water, warm (ca. 70°C), add sequentially 5 ml of 1% $AgNO_3$ (aqueous, w/v), 20 ml of potassium peroxodisulphate ($K_2S_2O_8$) solution (aqueous, 10% w/v, Pronalysi,

E-Merck, India). Boil for about 10 min. A brown/black precipitate appears at this stage. Add 10 ml of (1 + 1) HCl and boil for another 5 min. Finally, add another 5 ml of (1 + 1) HCl and 5 ml of H_3PO_4 (15 M). Make up to 250 ml with water. (soln. A). Transfer a 100-ml aliquot from this solution and add 5 ml of H_3PO_4 (15 M) and 25 ml of Fe(II) [prepared from ammonium iron(II) sulphate $(NH_4)_2Fe(SO_4)_2 \cdot 6H_2O$ in 5% H_2SO_4]. Titrate against 0.01667 M $K_2Cr_2O_7$ using sodium diphenylaminesulphonate as indicator equation

$$\% \ Cr_2O_3 = Fe(II) \text{ consumed} \times 0.01667 \times 0.02532 \times 100/0.04 \times 3$$

$$1 \text{ ml (M)Fe(II)} = 1 \text{ ml (M/3)}K_2Cr_2O_7 = 0.02532 \text{ g } Cr_2O_3$$

Solution A (containing 400 μg sample ml^{-1}) can also be used directly for absorbance measurement at 445 nm against an appropriate reagent blank prepared under identical conditions:

Take 5-ml aliquot from solution A in a 100-ml volumetric flask, add 10 ml (1 + 1) HCl and 10 ml of 2% Li_2SO_4 solution and make up to volume with water. This solution (containing 20 μg sample ml^{-1} and ca. 270 μg Li ml^{-1}) can be directly aspirated for FAAS using the most sensitive Cr resonance line (357.9 nm).

2.4. Reference samples

In surveying the range of geological reference materials currently available, samples bearing chromite matrices are under-represented. Two chromite samples, CHR-Pt + and CHR-BKg have been introduced [14] after cooperative analysis by 35 laboratories world wide. IGS-30 chromite (re-evaluated 1985) has been issued by the British Geological Survey [15] and BCS No. 308 is a Grecian chrome ore.

All these standard reference materials along with the samples generated from our recently concluded project entitled "Mineralogical and liberation study on low grade chromite ore and overburdens of chromite mines at Nausaki, Bhadrak, Orissa" have been analysed in order to check the validity of the recommended procedure.

3. Results and discussion

Typical results for the determination of chromium in chrome ore are presented in Table 1. In the proposed method, MnO_2 acts as an oxidising agent and facilitates the quantitative decomposition of chrome spinel. MnO_2 reacts with H_2SO_4 to produce soluble Mn(IV), which is a strong oxidising agent. The standard potential of the systems:

$$Mn(IV) + 2e \rightleftharpoons Mn(II);$$

$$Mn(IV) + e \rightleftharpoons Mn(III);$$

$$Mn(III) + e \rightleftharpoons Mn(II)$$

are 1.577, 1.62 and 1.511 V, respectively [16], whereas the formal potential of Cr(VI)/Cr(III) in 8 M H_2SO_4 is 1.35 V. Mn(IV) sulphate, therefore, oxidises Cr(III) to Cr(IV). In the presence of H_3PO_4, Mn(IV) is unstable and the Mn(III) phosphate complex cannot oxidise Cr(III). Hence, the H_3PO_4 decomposition route, as advocated elsewhere [17], is more time-consuming and is not adaptable to routine analysis where speed and accuracy are required. The H_2SO_4–H_2O–MnO_2 mixture gives a similar reaction, but in the presence of Li_2SO_4 the oxidation of Cr(III) takes place much faster. Lithium has no adverse effect on the titrimetric and spectrophotometric methods.

Cr has been widely determined in a variety of materials by FAAS. Difficulties are experienced when the determination is made in an air–acetylene flame. Sensitivity for Cr is best when the flame is fuel-rich; however, iron and nickel both significantly suppress Cr absorption in such a flame. This suppression can be compensated for in a variety of ways, including the use of a hot lean air–acetylene flame, the use of the hotter and more oxidising N_2O–acetylene flame, and the method of standard additions. Comparison of the analytical results with the certified values for standard reference material showed an acceptable agreement for all methods. The extremely poor sensitivity of the lean air–acetylene flame measurement nonetheless makes its use undesirable [18]. However, Cr determination in a fuel-rich air–acetylene flame in the presence of a suitable

interference suppressor such as La^{3+} [19] or K^+ [20] has been found to be an attractive solution for samples containing sufficient alkali metals. A comparison of results using La^{3+} (4000 μg ml^{-1}), K^+ (1000 μg ml^{-1}) and Li (400 μg ml^{-1}), as indicated in Fig. 1, clearly shows that Li^+ minimises the effects of the matrix upon analyte (Cr) sensitivity by modifying the volatility of the analyte or the matrix. It also enables the formation of a more thermally stable, uniform analyte/modifier compound which allows the matrix to be separated from the analyte and helps it to be atomized without interference. Li^+ has been found to be the best ionization suppressor/matrix modifier for Cr.

When chromium was determined by spectrophotometry at 445 nm, Beer's law was obeyed within the range 14–280 μg Cr ml^{-1} (molar absorptivity = 186 l mol^{-1} cm^{-1}). Sensitive methods [21–23] cannot be adapted because the samples must be extensively diluted. A less sensitive method (linear range 10–500 μg Cr ml^{-1}) as proposed earlier [7] requires more analytical manipulations.

3.1. Test of reliability of statistical data

The Student's t test value has been calculated using the data obtained from different methods on the basis of the formula described elsewhere [24] to test whether one set of data has a high probability of belonging to the population of a given mean value (recommended value) within a specified confidence limit. It has been found (see

Table 1
Determination of chromium in various chromite samples (wt.% Cr_2O_3) by different methods

Sample	Titrimetry [a]	Spectrophotometry [a]	FAAS [a]	Literature value
CHR-BKg	28.46–29.11 (28.72, 0.21; 0.73; 4.9)	28.55–29.76 (29.31; 0.35; 1.19; 2.35)	28.55–29.32 (28.85; 0.31; 1.07; 2.03)	29.05
CHR-Pt +	19.25–19.97 (19.76; 0.22; 1.11; 8.19)	19.97–21.05 (20.57; 0.32; 1.55; 2.37)	19.31–20.22 (19.81; 0.33; 1.66; 4.98)	20.33
IGS-30	34.78–35.28 (35.06; 0.17; 0.48; 1.11)	34.83–35.92 (35.29; 0.32; 0.91; 2.86)	34.55–35.18 (35.01; 0.30; 0.86; 0.105)	35.00
BCS (No. 308)	41.05–41.70 (41.28; 0.25; 0.60; 2.78)	40.96–41.89 (41.38; 0.29; 0.70; 1.31)	40.50–41.39 (40.94; 0.29 0.71; 6.10)	41.50
Nausahi ore concentrate	40.10–40.35 (40.22; 0.10; 0.26; 40.22 ± 0.08)	40.20–40.58 (40.42; 0.13; 0.32; 40.42 ± 0.11)	40.25–40.74 (40.50; 0.15 0.37; 40.50 ± 0.12)	40.05
Middling	8.60–8.75 (8.67; 0.06; 0.69; 8.67 ± 0.05)	8.72–8.90 (8.81; 0.07 0.79; 8.81 ± 0.06)	8.80–8.99 (8.87; 0.07 0.79; 8.87 ± 0.06)	8.45
Tailing	3.65–3.78 (3.72; 0.05; 1.34; 3.72 ± 0.04)	3.72–3.85 (3.77; 0.04; 1.06; 3.77 ± 0.03)	3.73–8.88 (3.81; 0.05 3.81 ± 0.04)	3.61

[a] Range of 10 determinations; (mean; standard deviation; relative standard deviation; t value). Literature values: for CHR-BKg and CHR-Pt +, Ref. 14; for IGS-30 and BCS (308) Ref. 15 and BCS Certificate, respectively. For Nausahi samples values are compared with those obtained by the Na_2O_2 fusion method. For the samples, concentrate, middling and tailings the Student's t tests have been used to calculate the error limits about the data-set mean ($\bar{x}$) within which the population mean (μ) must lie for a given confidence level (when $n = 10$, t value = 2.262 at 95% confidence level has been used for all samples). $\mu = x \pm ts/n$ where s is the standard deviation of the data set, n is the number of measurements. The fourth value within the brackets for the last 3 samples was calculated on the basis of the above equation at the 95% confidence level.

Table 1) that in most of the experiments, particularly for samples whose recommended values are available, t values are close to 95–99% confidence (for 9 degrees of freedom, t values for 95% and 99% confidence are 2.262 and 3.250, respectively) [25].

Inter-method comparison studies are necessary in the development and evaluation of methods. They are critical in the development of a quality control programme and in the evaluation of reference materials. Also, there are situations in which it may become important to compare analytical performance for individual analyst performing the same method. The Student's t test is used to compare the data obtained.t Values obtained [26] by comparing the result the three methods are presented in Table 2. t_c (99%) = 2.878 for 18 degrees of freedom.Those comparisons where the experimental t values are < 2.878 have at least a 99% probability of not being significantly different. Slight deviations are noticed in case of samples CHR-BKg and CHR-Pt +, for which proposed values are only available

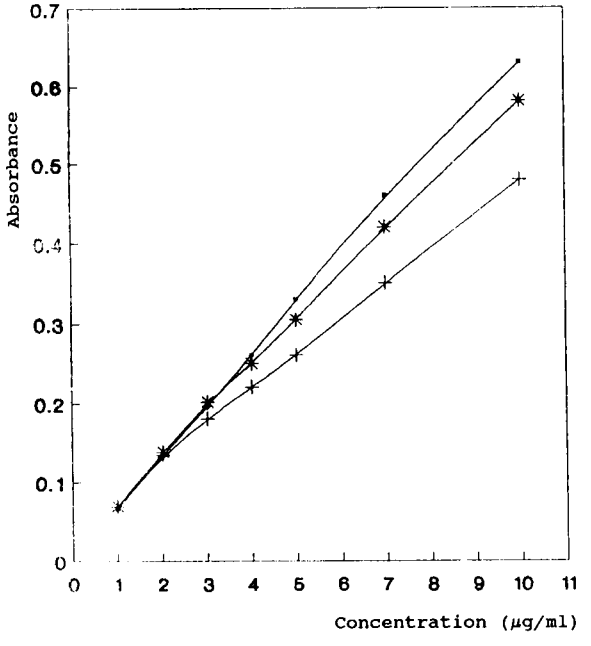

Fig. 1. Absorbance vs. concentration (ppm) using various interference suppressors: (·) Lithium; (+) potassium; (*) lanthanum.

Table 2
Experimental t values comparing results from the titrimetric–spectrophotometric (T–S) and titrimetric (T)–FAAS methods

Sample	T–S	T–FAAS
CHR-BKg	4.57	1.098
CHR-Pt+	6.59	0.399
IGS-30	0.2562	0.4586
BCS (308)	0.8257	2.809

[14] indicating some more data are still required before assigning certified or recommended values for them. Because of the growing requirements for accurate analytical results, it is sensible to work with at least two different techniques.

The results of the analyses of reference samples indicate that the proposed method provides accurate results for % Cr_2O_3 in diverse chromite matrices. The most effective matrix modifier/ionization suppressor for FAAS determination of chromium is Li^+ (270 μg ml^{-1}) rather than K^+ and La^{3+} as attempted earlier. Geological, metallurgical and mineral beneficiation laboratories require an accurate and rapid method for chromium analyses, and this method would fulfill their requirements.

Acknowledgements

We thank the Director, Regional Research Laboratory, Bhubaneswar, for granting permission to publish the results of this work. Dr. P.J. Potts, The Open University, UK, is thanked for providing the opportunity to participate in the cooperative analysis for CHR-BKg and CHR-Pt +. Mr. P.N. Sethi is thanked for very useful secretarial assistance.

References

[1] E. Kiss, Anal. Chim. Acta, 193 (1987) 315.
[2] T.R. Cunninghan and T.R. McNeill, Ind. Eng. Chem. Anal. Ed., 1 (1927) 70.
[3] G.F. Smith and C.A. Getz, Ind. Eng. Chem. Anal. Ed., 9 (1937) 518.
[4] S.K. Mandal, S.B. Rao and B.R. Sant, Talanta, 26 (1979) 135.

[5] S.K. Mandal, S.B. Rao and B.R. Sant, Talanta, 28 (1981) 771.
[6] N. Yoshikuni, Talanta, 36 (1989) 706.
[7] N. Yoshikuni, Talanta, 38 (1991) 515.
[8] P. Chattopadhyay and S.S. Nathan, Analyst, 116 (1991) 1145.
[9] P. Chattopadhyay, T.K. Sinha and T.S. Basu Baul, Anal. Sci., 7 (1991) 931.
[10] P. Chattopadhyay and B.N. Sahoo, Analyst, 117 (1992) 1481.
[11] P. Chattopadhyay and B.N. Sahoo, Talanta, 40 (1993) 701.
[12] P. Chattopadhyay, Geostand. Newsl., 17 (1993) 219.
[13] P. Chattopadhyay and M. Mistry, Microchem. J., (1993) in press.
[14] P.J. Potts, C.J.B. Gowing and K. Govindaraju, Geostand. Newsl., 16 (1992) 81.
[15] B. Lister, Geostand Newsl., 2 (1978) 157.
[16] G. Grube and K. Huberich, Z. Elektrochem., 29 (1923) 8.
[17] P. Dippel, Silikattechnik, 13 (1962) 51
[18] J.S. Kane and H. Smith, USGS Open-file Report 81-991, 1991.
[19] S. Terashima, Bull. Geol. Surv. Jpn., 37 (1986) 373.
[20] Staff of the Geoscience Laboratories, Ontario Geological Survey, The Analysis of Geological Materials, Vol. II: A Manual of Methods, 1990.
[21] E.B. Sandell, Colorimetric Determination of Trace of Metal, Interscience, New York, 1959.
[22] E.M. Donaldson, Methods for The Analysis of Ores, Rocks, and Related Materials, CANMET, Monograph 881, 2nd ed., 1982.
[23] D.P.S. Rathore and P.K. Tarafdar, Anal. Chim. Acta, 257 (1992) 129.
[24] P.J. Potts, A Handbook of Silicate Rock Analysis, Blackie, London, 1992.
[25] B. Lister, Geostand. Newsl., 6 (1982) 175.
[26] A.H.M. Vander Voet and C. Riddle, The Analysis of Geological Materials, Vol. 1, A Practical Guide, Ontario Geological Survey, Paper No. 149, 1993, p. 19.

ELSEVIER

Analytica Chimica Acta 295 (1994) 331–333

ANALYTICA CHIMICA ACTA

Author Index

PUBLICATION SCHEDULE FOR 1994

	J	F	M	A	M	J	J	A	S	O	N	D
Anal. Chim. Acta	284/3 285/1–2 285/3	286/1 286/2 286/3	287/1–2 287/3 288/1–2	288/3 289/1 289/2	289/3 290/1–2 290/3	291/1–2 291/3 292/1–2	292/3 293/1–2 293/3	294/1 294/2 294/3	295/1–2 295/3 296/1	296/2 296/3 297/1–2	297/3 298/1 298/2	298/3 299/1 299/2
Vib. Spec.	6/2		6/3		7/1		7/2		7/3		8/1	

INFORMATION FOR AUTHORS

Detailed "Instructions to Authors" for *Analytica Chimica Acta* was published in Volume 289, No. 3, pp. 381–384. Free reprints of the "Instructions to Authors" of *Analytica Chimica Acta* and *Vibrational Spectroscopy* are available from the Editors or from: Elsevier Science B.V., P.O. Box 330, 1000 AH Amsterdam, The Netherlands. Telefax: (+31-20) 5862 459.

Manuscripts. The language of the journal is English. English linguistic improvement is provided as part of the normal editorial processing. Authors should submit three copies of the manuscript in clear double-spaced typing on one side of the paper only. *Vibrational Spectroscopy* also accepts papers in English only.

Rapid publication letters. *Letters* are short papers that describe innovative research. Criteria for letters are novelty, quality, significance, urgency and brevity. Submission data: max. of 2 printed pages (incl. Figs., Tables, Abstr., Refs.); short abstract (e.g., 3 lines); *no* proofs will be sent to the authors; submission on floppy disc; *no* revision will be possible.

Abstract. All papers, reviews and letters begin with an Abstract (50–250 words) which should comprise a factual account of the contents of the paper, with emphasis on new information.

Figures. Figures should be suitable for direct reproduction and as rich in contrast as possible. One original (or sharp glossy print) and two photostat (or other) copies are required. Attention should be given to line thickness, lettering (which should be kept to a minimum) and spacing on axes of graphs, to ensure suitability for reduction in size on printing. Axes of a graph should be clearly labelled, along the axes, outside the graph itself.

All figures should be numbered with Arabic numerals, and require descriptive legends which should be typed on a separate sheet of paper. Simple straight-line graphs are not acceptable, because they can readily be described in the text by means of an equation or a sentence. Claims of linearity should be supported by regression data that include slope, intercept, standard deviations of the slope and intercept, standard error and the number of data points; correlation coefficients are optional.

Photographs should be glossy prints and be as rich in contrast as possible; colour photographs cannot be accepted. Line diagrams are generally preferred to photographs of equipment. Computer outputs for reproduction as figures must be good quality on blank paper, and should preferably be submitted as glossy prints.

Nomenclature, abbreviations and symbols. In general, the recommendations of IUPAC should be followed, and attention should be given to the recommendations of the Analytical Chemistry Division in the journal *Pure and Applied Chemistry* (see also *IUPAC Compendium of Analytical Nomenclature, Definitive Rules*, 1987).

References. The references should be collected at the end of the paper, numbered in the order of their appearance in the text (*not* alphabetically) and typed on a separate sheet.

Reprints. Fifty reprints will be supplied free of charge. Additional reprints (minimum 100) can be ordered. An order form containing price quotations will be sent to the authors together with the proofs of their article.

Papers dealing with vibrational spectroscopy should be sent to: Dr J.G. Grasselli, 150 Greentree Road, Chagrin Falls, OH 44022, U.S.A. Telefax: (+1-216) 2473360 (Americas, Canada, Australia and New Zealand) or Dr J.H. van der Maas, Department of Analytical Molecular Spectrometry, Faculty of Chemistry, University of Utrecht, P.O. Box 80083, 3508 TB Utrecht, The Netherlands. Telefax: (+31-30) 518219 (all other countries).

0003-2670/94/$07.00

Dynamics of Excited Molecules

Edited by **Kozo Kuchitsu**

Studies in Physical and Theoretical Chemistry Volume 82

The physical and chemical properties of the molecular species reviewed in this book, and sometimes the species themselves, had been postulated or predicted but their exact details remained essentially unexplored for decades. The recent advances in chemical physics (such as laser spectroscopy and quantum-theoretical calculations) have provided techniques for their unambiguous identification. Accurate data on their structures and dynamics are now available. Such information is indispensable for detailed discussion on the various properties of molecules and the mechanisms of intermolecular interactions and chemical interactions.

Information on the dynamics of excited molecules constitutes a firm basis of modern chemistry and physics. Moreover, it is of paramount importance in various fields of basic and applied sciences where chemical reactions play important roles: atomic and molecular physics, atmospheric and environmental science, space science, materials science, and biology.

This book contains 13 review articles on
(1) the techniques for production and identification of excited molecules in the gas phase, condensed phases, and intermediate phases (intermolecular complexes and atomic or molecular microclusters)
(2) their structures and dynamics (internal reactions) observed mainly by spectroscopic experiments
(3) their important roles in chemical processes. The target chemical species range from diatomics to relatively complicated aromatics in a variety of electronic and vibrational excited states, many of them being nonrigid or short-lived molecules, radicals, and positive or negative ions.

Contents:

© 1994 620 pages Hardbound
Price: Dfl. 495.00 (US$282.75)
ISBN 0-444-81796-4

ELSEVIER SCIENCE B.V.

ORDER INFORMATION

For USA and Canada
ELSEVIER SCIENCE INC.
P.O. Box 945
Madison Square Station
New York, NY 10160-0757
Fax: (212) 633 3880

In all other countries
ELSEVIER SCIENCE B.V.
P.O. Box 330
1000 AH Amsterdam
The Netherlands
Fax: (+31-20) 5862 845

US$ prices are valid only for the USA & Canada and are subject to exchange rate fluctuations; in all other countries the Dutch guilder price (Dfl.) is definitive. Customers in the European Union should add the appropriate VAT rate applicable in their country to the price(s). Books are sent postfree if prepaid.